



<https://theses.gla.ac.uk/>

Theses Digitisation:

<https://www.gla.ac.uk/myglasgow/research/enlighten/theses/digitisation/>

This is a digitised version of the original print thesis.

Copyright and moral rights for this work are retained by the author

A copy can be downloaded for personal non-commercial research or study,  
without prior permission or charge

This work cannot be reproduced or quoted extensively from without first  
obtaining permission in writing from the author

The content must not be changed in any way or sold commercially in any  
format or medium without the formal permission of the author

When referring to this work, full bibliographic details including the author,  
title, awarding institution and date of the thesis must be given

Enlighten: Theses

<https://theses.gla.ac.uk/>  
[research-enlighten@glasgow.ac.uk](mailto:research-enlighten@glasgow.ac.uk)

Micro-wave Delayed Echoes in Insulating  
Ferrimagnetic Single Crystals.

Submitted by J.D. Adam, B.Sc.  
for the degree of M.Sc. from  
the University of Glasgow.

1967.

ProQuest Number: 10647843

All rights reserved

INFORMATION TO ALL USERS

The quality of this reproduction is dependent upon the quality of the copy submitted.

In the unlikely event that the author did not send a complete manuscript and there are missing pages, these will be noted. Also, if material had to be removed, a note will indicate the deletion.



ProQuest 10647843

Published by ProQuest LLC (2017). Copyright of the Dissertation is held by the Author.

All rights reserved.

This work is protected against unauthorized copying under Title 17, United States Code  
Microform Edition © ProQuest LLC.

ProQuest LLC.  
789 East Eisenhower Parkway  
P.O. Box 1346  
Ann Arbor, MI 48106 – 1346

Summary :-

This thesis describes experimental observations on the parametric amplification, in single crystal Yttrium Iron Garnet of elastic, magnetoelastic and magnetostatic modes, by application of a pump pulse of twice the frequency of the L - band micro-wave signal pulse, and on the excitation of a delayed pulse by the application of two time separated microwave pulses of the same frequency. Details of experiments performed to determine the internal magnetostatic field profile of a magnetised rectangular cross-section Yttrium Iron Garnet rod are given. The experimental internal fields are compared with those derived theoretically.

It was found to be possible to reduce the attenuation of elastic echoes by parametric amplification. Details are given of saturation levels, attenuation and timing of the pump pulse. In the magnetoelastic regime details are given of the variation of gain with, timing of the pump pulse, pump power, signal power and orientation of the rod to the external field.

Magnetostatic propagating mode, the amplitude of the parametrically excited echo is plotted against, time of application of the pump pulse, pump power and signal power.

Magnetostatic standing wave mode, the amplitude of the parametrically excited echo is plotted against, time of application of the pump pulse, pump power and signal power.

Magnetostatic wave mode echo, parametrically excited by the application of two time separated pulses of the same frequency, plots

are shown of gain relative to the first pulse with variation of, second pulse amplitude, the first pulse amplitude and time between the application of the two pulses.

Parametric amplification of magnetostatic modes due to subsidiary absorption of the pump frequency. Plots of attenuation of the delayed pulse against signal power, pump power and time of application of the pump pulse are given. This is found to be a two port phenomenon. At L - band the subsidiary absorption is coincident with the main absorption, due to the low signal frequency used, 12KMc/s, the ends of the rod were not saturated.

## Index.

Page	Section	Content.
1		Acknowledgements.
2		Summary.
3	1.0.0.	Introduction.
8	1.1.0.	Experimental Arrangement.
12	2.1.0.	Field inside a Non-Ellipsoidal Ferrimagnetic.
13	2.2.1.	First order demagnetising field in a square Y.I.G. rod.
17	2.2.2.	Anisotropy Field.
18	2.3.0.	Magneto-elastic waves and Internal Field Analysis.
	2.3.1.	Theory.
22	2.3.2.	Experiment.
26	2.3.3.	Plots of Magneto elastic delay versus field.
33	3.0.0.	Parametric Amplification.
	3.1.0.	Parametric Amplification of Magneto- Static Wave.
	3.1.1.	Theory.
35	3.1.2.	Experiment.

38	3.2.0.	Parametric amplification of Elastic Waves.
	3.2.1.	Theory of elastic wave excitation.
	3.2.2.	Experiment.
46	3.3.0.	Parametric Amplification of Magneto-elastic waves.
50	3.4.0.	Parametric excitation of a delayed pulse by application of two time separated pulses of the same frequency or $\omega.\omega$ . parametric amplification of magneto-static modes.
58	3.5.0.	Parametric excitation of magneto-static mode echo by Subsidiary Absorption.
64	4.0.0.	Conclusions.
68	Appendix	A summary of the properties of Yttrium Iron Garnet.

## Acknowledgements.

I express my appreciation to Professor J. Lamb for use of laboratory and other facilities, to Mr. J.H. Collins for invaluable supervision, to Mr. G.G. Neilson, Mr. I. Alexander, Mr. M.R.B. Dunsmore and Mr. J. Cochrane for advice on microwave measurements and other experimental techniques, and to other members of the Department of Electrical Engineering without whose help this thesis would not have been possible.

Summary:-

This thesis describes experimental observations on the parametric amplification, in single crystal Yttrium Iron Garnet, of elastic, magneto-elastic and magneto-static modes, by application of a pump pulse of twice the frequency of the L-band microwave signal pulse, and on the excitation of a delayed pulse by the application of two time separated microwave pulses of the same frequency. Details of experiments performed to determine the internal magneto-static field profile of a magnetised, rectangular Yttrium Iron Garnet rod are given. Conclusions are drawn from the experimental results.

### Introduction:-

In many electronic communications and radar systems there is a need for a variable delay line, operating in the micro-wave region, able to give delays of the order of micro-seconds. Yttrium Iron Garnet (YIG), (see appendix), delay lines could satisfy this need where high insertion loss of greater than 40db. can be tolerated. In addition, due to the increase of delay with frequency at a fixed field when the delay line is operated in the magneto-elastic mode, a device is available to provide pulse compression of a suitably frequency modulated micro-wave pulse. The above property also makes a YIG delay line suitable for frequency memory applications.

The magnetic and elastic properties of the ferri-magnetic single crystal YIG, allow a means of coupling electro-magnetic energy into the crystal, which can propagate as a spin wave in the magnetic system or as an elastic wave in the lattice due to coupling between the magnetic and elastic systems.

The internal field of an axially magnetised ferri-magnetic rod, in the direction of the applied external field, varies due to demagnetising effects from approxi-

mately half of the value of the external field at the end faces to a value slightly less than the external field at the centre. Spin waves are excited at the turning point in the rod, where  $\frac{\omega}{\gamma} = H_i$ ,  $\omega$  is the signal frequency in Mc/s,  $\gamma$  is the gyromagnetic ratio in Mc/s/oersted and  $H_i$  is the internal field in oersteds.

Spin waves excited at the turning point propagate with increasing wave number, in the direction of decreasing internal field. When the wave number of the spin wave is the same as that of an elastic wave of the same frequency, at the crossover point, coupling between the spin and elastic waves takes place, so that energy is transferred from the magnetic to elastic systems. The elastic wave travels towards and is reflected from the end face of the rod which is highly polished. The reflected elastic wave is converted back to a spin wave at the crossover point, and propagates towards the turning point where a delayed pulse is observed. The position of the turning point in the rod and hence the magneto-elastic path length is dependent on the external field, the magneto-elastic delay varies with the inverse of the external field. The upper and lower field limits of

the magneto-elastic mechanism are when at high field the turning point is very close to the end face and at low field when the turning point is at the centre of the rod. This latter condition gives rise to a magneto-static burst.

At lower fields where no turning point exists in the rod spin waves are generated very close to the end face, these can propagate over the high field region and be reconverted to electro-magnetic energy at the opposite end face. Since the group velocity of the spin or magneto-static waves is an inverse function of magnetic field, the two port magneto-static delay increases with the applied field. At very high fields where the turning point is very close to the end face, elastic waves are generated by a magneto-strictive mechanism at the rod end face. The delay of the elastic waves is invariant with field, being dependent only on the length of the rod and its elastic properties. In addition to the linear effects outlined above, there are second order terms in the magnetisation, coupling between different branches in the magneto-elastic dispersion and nonlinearities in the magneto-strictive mechanism, which

allow parametric amplification of magneto-static, magneto-elastic and elastic waves respectively.

Parametric amplification of the elastic waves by application of a pump at twice the signal frequency of 700 Mc/s., in YIG at room temperature with electronic gains of 30 db. was first reported by Matthews<sup>1</sup> in 1964. Subsequently, amplification of magneto-elastic waves in YIG at 8.7 Gc/s, at 1.5°K with a net gain of 35 db. and amplification of magneto-static waves at 8.7 Gc/s at 1.5°K were reported by Damon and Van de Vaart.<sup>2,3</sup> Amplification of magneto-elastic waves at L-band and C-band was reported by Van de Vaart, Grace and Damon.<sup>4</sup> CW-pumped and non-degenerate parametric amplification of elastic waves by Sparks and Higgins.<sup>5</sup> Parametric amplification of magneto-static, magneto-elastic and acoustic waves at L-band and room temperature has been reported by Donaghey and Olson.<sup>6</sup> All the above reports refer to amplification of a signal pulse by applying a pump pulse of twice the signal frequency and very much greater power at some later time. Kaplan<sup>7</sup> has reported the generation of a magneto-static echo, by the application of two pulses of the same frequency, time separated.

This, with an echo due to Subsidiary Absorption has been reported by Comstock and Raymond.<sup>8</sup>

The theory of magneto-elastic and magneto-static waves is well documented in the literature.<sup>9,10</sup> Only a brief summary of each is given in the appropriate sections.

In this thesis experiments performed at L-band on parametric amplification, by pumping at twice the signal frequency, of elastic, magneto-elastic and magneto-static waves, by the subsidiary absorption mechanism, and by applying a second pulse at the signal frequency are described. Measurements were taken to determine the internal field configuration of an axially and transversely magnetised square YIG rod.<sup>11</sup>

Original contributions are as follows. The observation of the incoherent content of a delayed signal frequency pulse produced by application of a pump pulse of twice the signal frequency with no signal applied. The delay against field characteristics of this signal pulse were also determined. Net gain was observed in the experiments with the pump and signal of the same frequency. This was also found to be a one port phenomenon.

### Experimental Arrangement:-

The YIG rod used in all the experiments performed, was of rectangular cross section, fig. 1.1.1 of dimension  $2a = 2.794$  mm,  $2b = 3.036$  mm,  $2c = 9.906$  mm. The two end faces flat to  $\frac{\lambda}{8}$  of sodium light, polished with  $0.1 \mu$  diamond paste and parallel to within 10 seconds of arc. One side face  $2b \times 2c$  was polished in the course of experiments to the above flatness and surface finish. The crystallographic orientation of the rod was such that the  $[100]$  and  $[110]$  directions lay along the 'y' and 'x' axes respectively.

The rod was mounted in a holder with fine wire couplers as shown in fig. 1.1.2, note coupler C is against the centre of the polished side. The holder was supported in an arrangement which allowed  $360^\circ$  rotation in a horizontal plane and  $\pm 2^\circ$  rotation in the other two vertical planes.

The fine wire couplers were normally used as follows, for longitudinal magnetisation, A signal input and output (one port), B pump input, C signal output (two port) and for the transversely magnetised rod, D signal input and output and pump input.

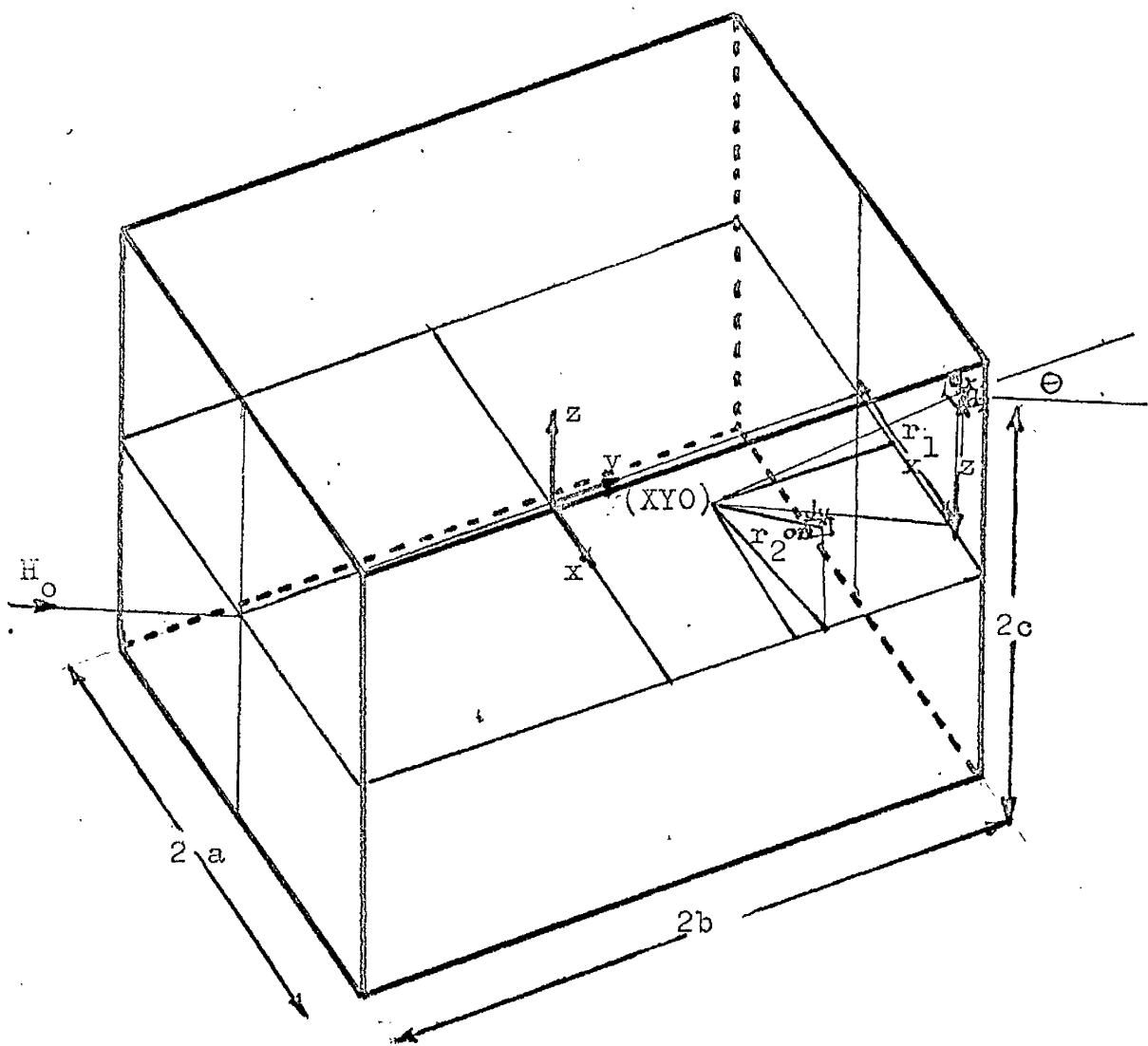


Figure 1.1.1. Showing YIG rod 'A' used in the experiments described in this thesis.  $(XYO)$  is any point on the  $x, y, 0$  plain,  $r_1$  and  $r_2$  are vectors from the point  $(XYO)$  to  $dx, dz$  and  $dy, dz$  respectively.  $\theta$  is the angle between the normal to  $dx, dz$  and the direction of the external field

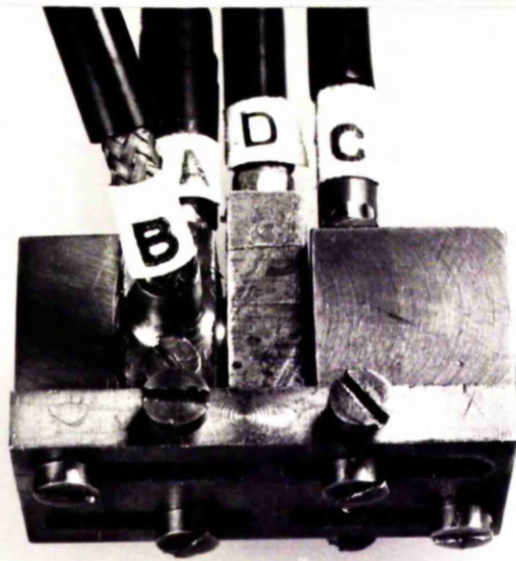
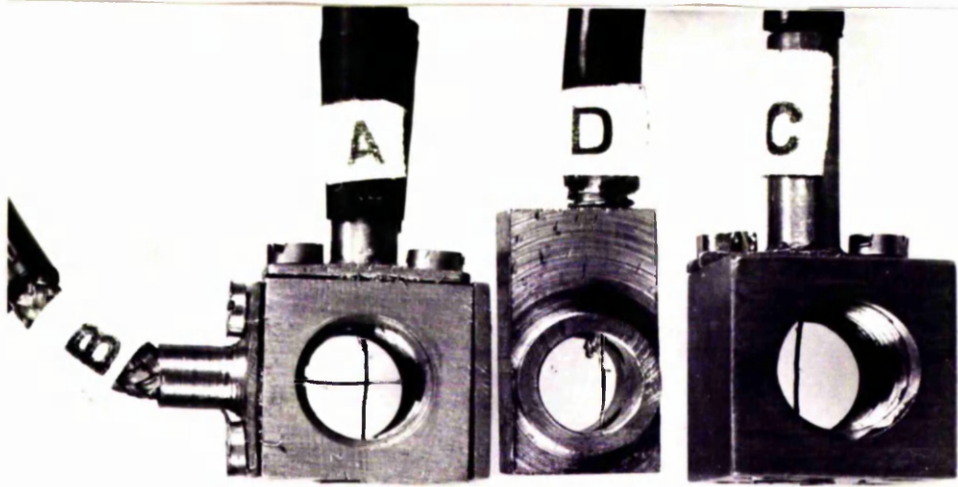
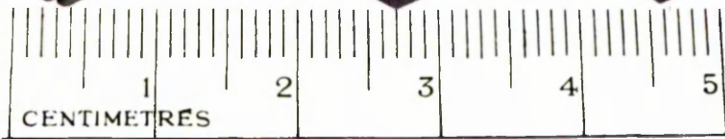
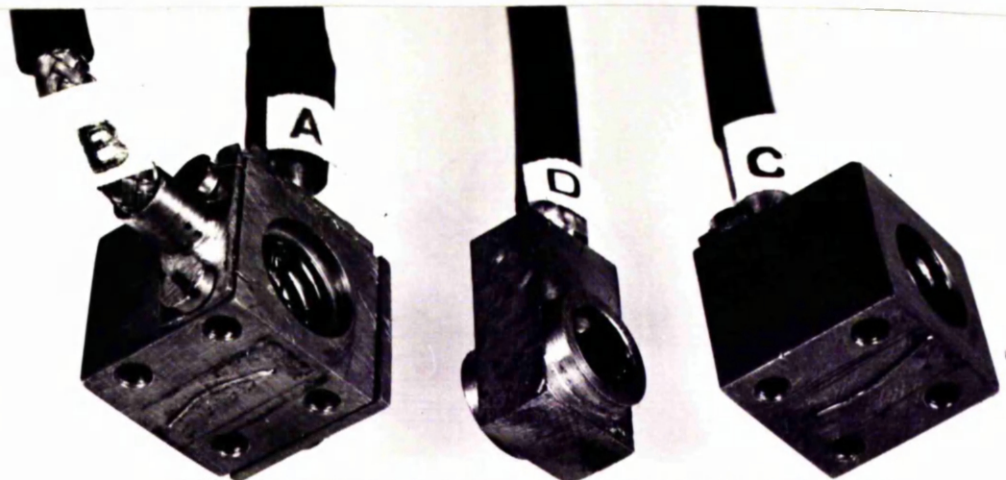


Figure 1.1.2

Showing Crystal holder  
and fine wire couplers.  
a) is an exploded view  
showing the wire couplers  
b) assembled unit.  
c) exploded view showing  
position of the crystal.



Figures 1.1.3 and 1.1.4 show the micro-wave circuitry and triggering arrangements.

The apparatus used was as follows, the numbers correspond to those in figures 1.1.3 and 1.1.4.

1. Stabilised power supply.
2. General Radio unit oscillator type 1218 - A, 900 - 1200 Mc/s. maximum power output 200 mw into 50 $\Omega$ .
- 3,5,11. Sage Laboratories, 10db directional coupler, model 782 - 10, frequency range 1 - 2 KMc/s.
- 2,44. Hewlett - Packard modulators, model 8714A.  
Frequency range 800 - 2400 Mc/s. Insertion loss  $1.2 \pm 0.5$ db. Attenuation more than 80db.
6. Weinschel Engineering Manual Stepattenuator, model 90 - 10, 0 - 10 db. Frequency range dc - 10KMc/s.
7. Hewlett Packard modulator drive unit, 8403A.
8. Hazeldine experimental test oscillator Type XT24.  
Frequency range 825 - 1375 Mc/s.
9. Four port L, band circulator.
10. Hewlett-Packard modulator unit 8731B. Frequency range 800 - 2400 Mc/s. Insertion loss  $1.2 \pm 0.5$ db. Attenuation more than 80db.
12. Sage balanced mixer and pre-amp type 2521. 1 - 2KMc/s. 30 Mc/s I.F. output. Pre-amp. band-width 8 Mc/s gain 21 db.

13. L.E.L. I.F. amplifier, gain  $\sim$  70db, band-width 8 Mc/s, centre frequency 30 Mc/s.
14. Tektronix 585A oscilloscope. Twin beam plug-in unit Type CA., maximum sensitivity 0.05 volts / cm.
15. R.F. Power Meter, Hewlett-Packard model G 245 maximum sensitivity -30dbm.
16. Crystal holder and associated fine wire couplers.
17. Sage micro-wave crystal detector.
- 18,19,26. Sage Laboratories 2 - 4 KMc/s. 10db directional couplers.
20. Solartron pulse generator G. O. 1101 - 2.
- 21 Travelling Wave Tube Amplifier, gain 20db, delivered  $>$  40dbm, unsaturated.
- 23,27. Arra T-T line variable attenuators. Type 4414-30.
24. Sanders Klystron CLC24, frequency range 2-4.5 KMc/sec.
25. Sanders Klystron Power supply, Mk IV.
26. M.E. Laboratories 3 port circulator, 1.7 - 2.3 KMc/sec.

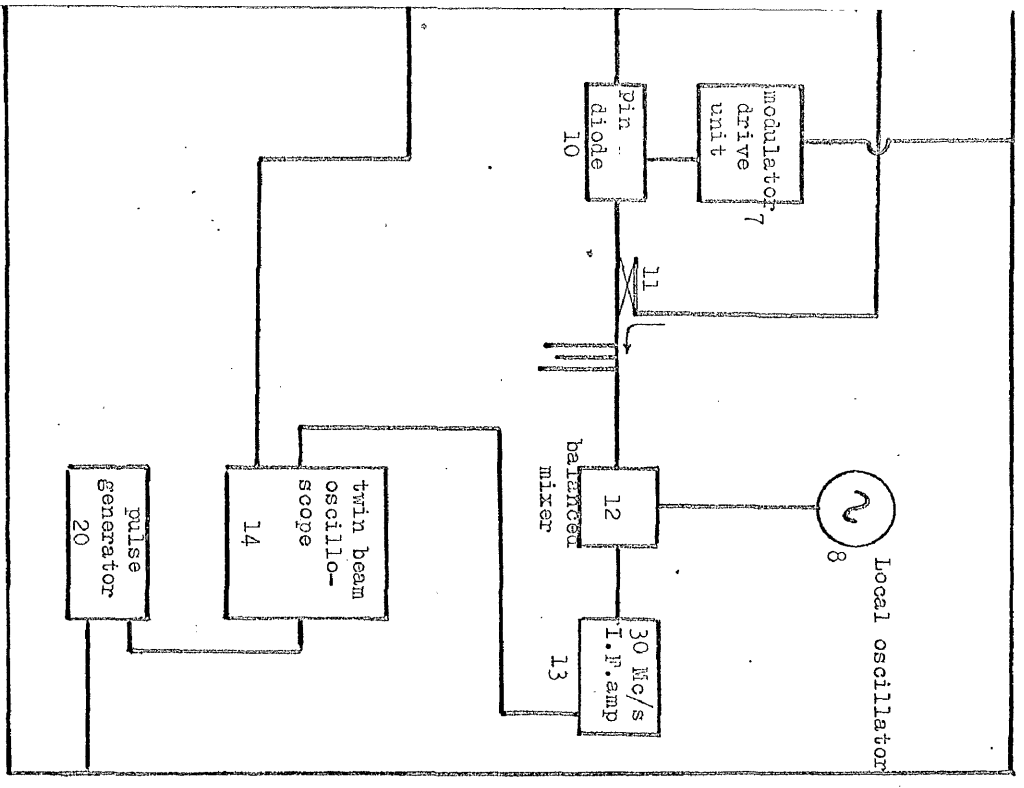
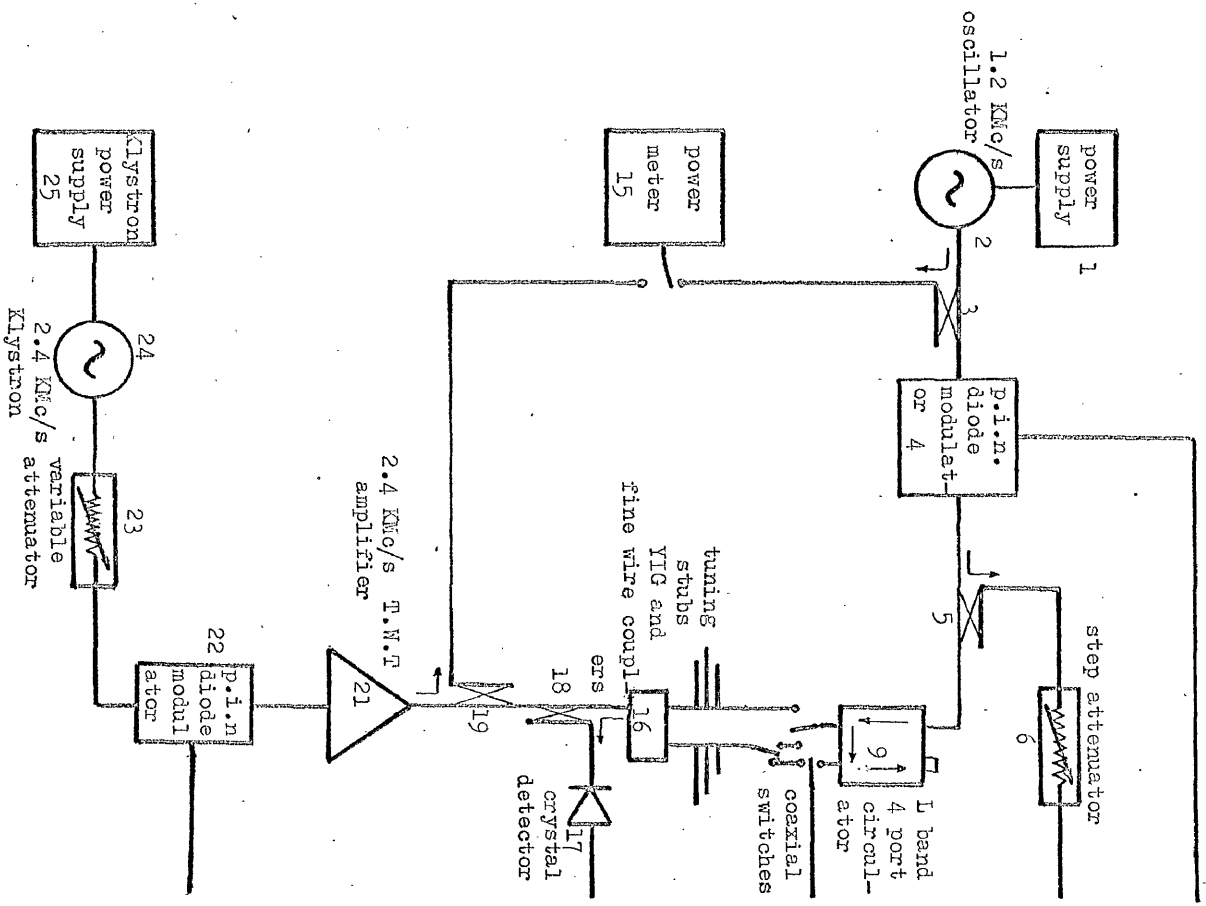


Figure. 1.1.3 Experimental arrangement for 1.2 KMc/s experiments.  
2.4 KMc/s. pump.

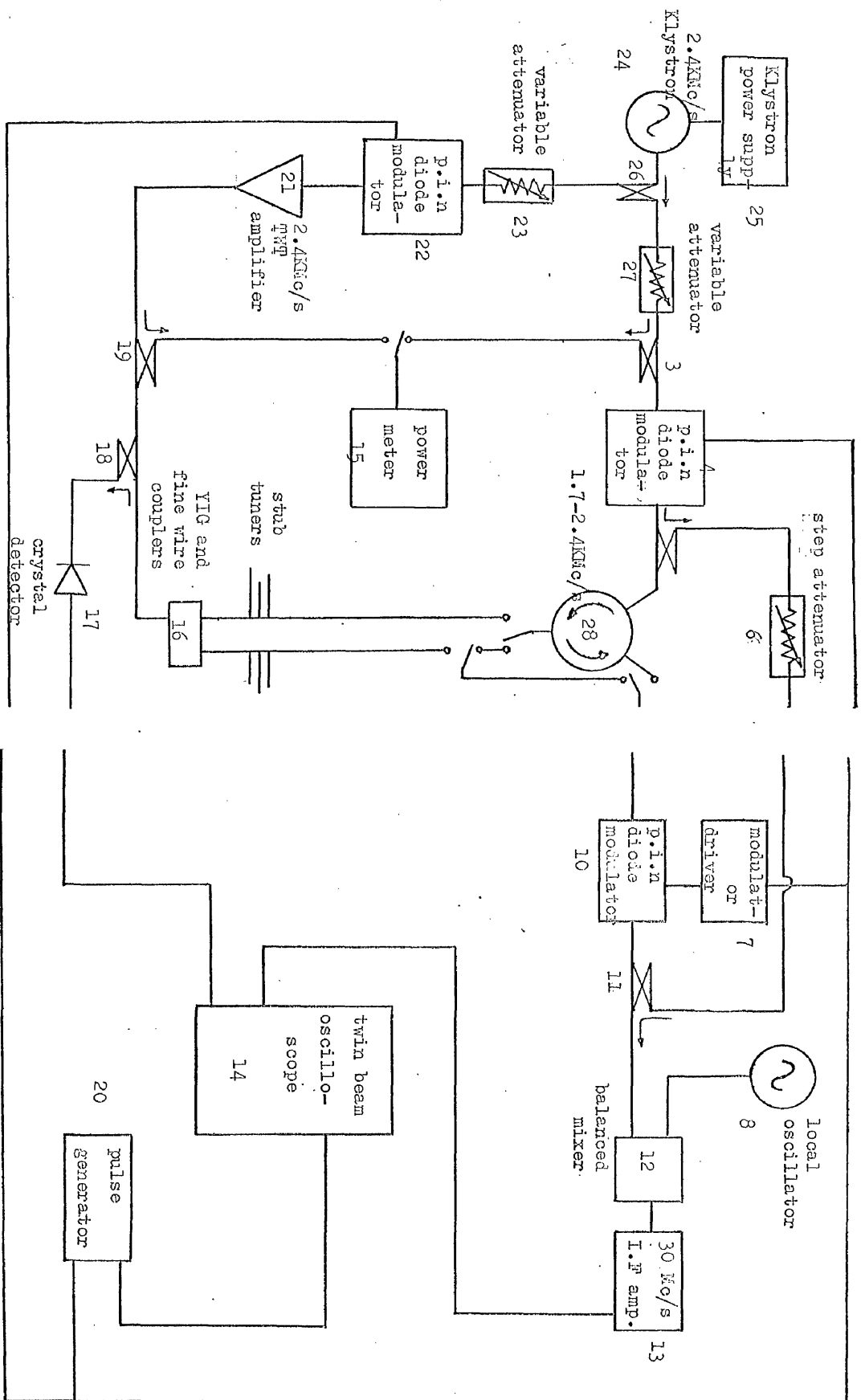


Figure 1.1.4. Apparatus arrangement for 2.4 KMc/s signal frequency experiments.

Note that in experiments using the fine wire coupler D, the pump power is coupled into the signal line before the tuning stubs, and a low pass filter which cuts off at 2.0 KMc/sec inserted between the directional coupler and the circulator.

Figure 1.1.5 shows the field generation and measuring apparatus.

1. Newport Instruments Type A, 4" electro-magnet.
2. Newport Instruments Type P, Mk II magnet power supply.
3. I.E. model DS50/5 stabilised power supply 0-50 volts.
4. Telequipment Serviscope Type S 43.
5. Newport Instruments magnetometer supply unit Type F.
6. Newport Instruments magnetometer head unit Type P.2. using modified coils with white petroleum jelly core to measure fields down to 200 oe.
7. Advance type TC 10/H 10 Mc/sec. Timer Counter.

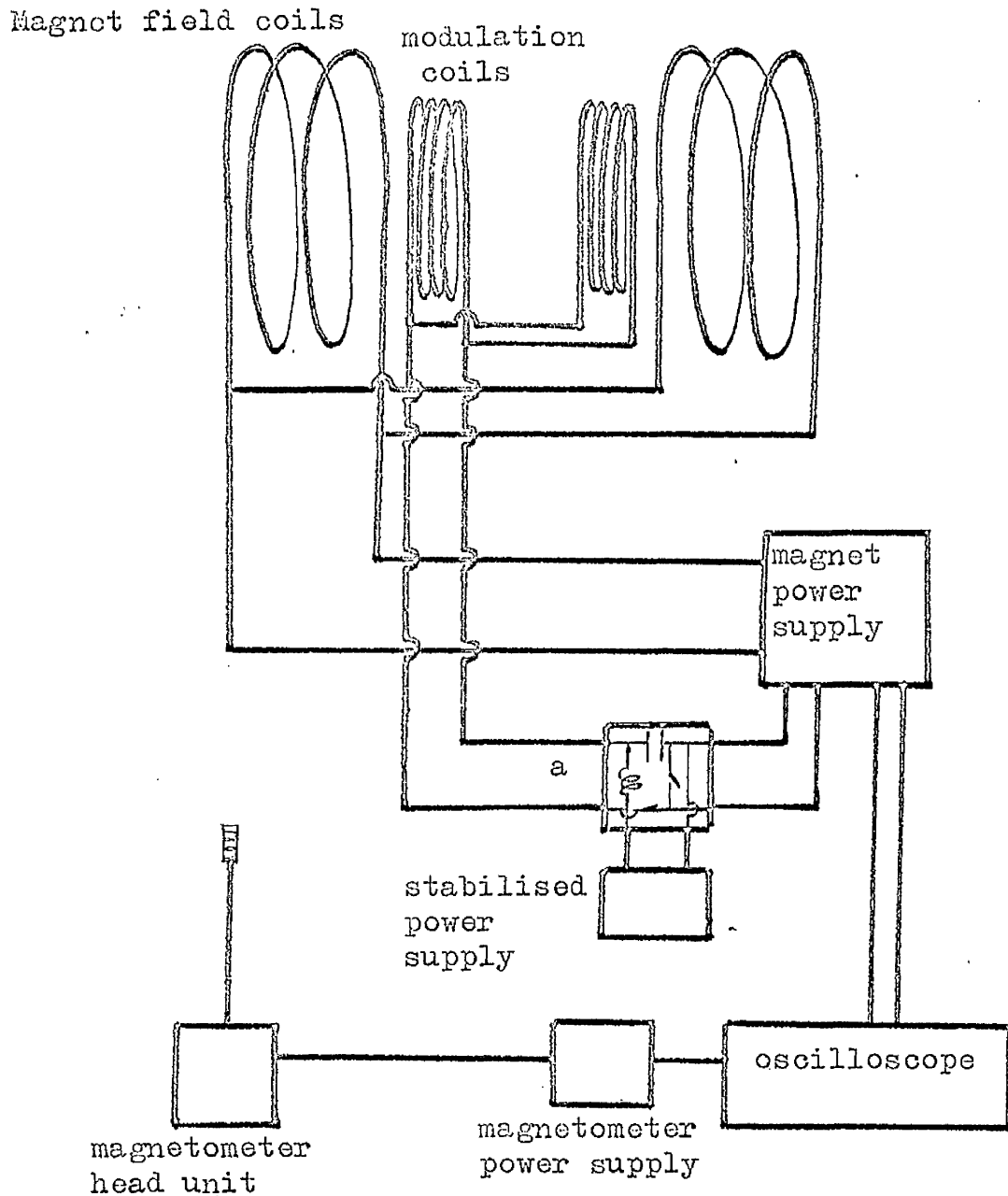


Figure 1.1.5. Magnet and field measurement arrangement, Box marked 'a' is to prevent 50 c/s modulation current from the magnet power supply interfering with the operation of the stabilised power supply.

Field inside a non-ellipsoidal ferrimagnet.

The internal field of a non-ellipsoidal ferrimagnet is given by

$$H_i(z) = H_{\text{ext}} - H_d(z) + H_A(z).$$

where  $H_i$  is the internal field at any point  $z$ .

$H_{\text{ext}}$  is the applied magnetic field.

$H_d$  is the demagnetising field at any point  $z$ .

$H_A$  is the anisotropy field at any point  $z$ .

First Order demagnetising field in a square YIG rod.

Assume that the magnetisation is constant everywhere in the rod and that the magnetisation is in the direction of the applied field, then from Schlomann<sup>12</sup> equation 6.

$$\psi(x', y', z') = \frac{1}{4\pi} \int_V \frac{\underline{m} \cdot \underline{r}}{|\underline{r}|^3} dV$$

$$\nabla \cdot \underline{m} = 0$$

$$4\pi\psi(x', y', z') = \int \frac{\underline{m} \cdot d\underline{s}}{r}$$

$$H = -(\nabla\psi)_{x', y', z'}$$

$$= -\frac{1}{4\pi} \int \underline{m} \cdot d\underline{s} \cdot \nabla \left( \frac{1}{r} \right)_{(x', y', z')}$$

Take applied field in the 'y' direction.

$$H_y(x', y', z') = -\frac{1}{4\pi} \int \underline{m} \cdot d\underline{s} \frac{(y' - y)}{r^3}$$

where  $\underline{H}$  is the demagnetising field,  $\underline{m}$  is the magnetisation,  $\underline{r}$  is a radius vector.

Consider, the diagram in Figure 1.1.1, only points in  $(x, y, 0)$  plane.

Then

$$r_1^2 = (b - Y)^2 + (x - X)^2 + z^2$$

$$r_1^2 = (a - X)^2 + (y - Y)^2 + z^2$$

$\theta$  is the angle between the direction of the field and the rod axis,

$$N_y(x, y, 0) = \frac{1}{4\pi} \int \frac{n \cdot ds}{r^3} \quad N \text{ is demagnetising factor.}$$

$$N_y = \frac{1}{4\pi} \left[ \int_{-a}^a \int_{-c}^c \frac{dx dz (b-Y) \cos \theta}{((b-Y)^2 + (x-X)^2 + z^2)^{3/2}} + \int_{-a}^a \int_{-c}^c \frac{dx dz (b+Y) \cos \theta}{((b+Y)^2 + (x-X)^2 + z^2)^{3/2}} \right. \\ \left. + \int_{-b}^b \int_{-c}^c \frac{dy dz (a-X) \sin \theta}{((a-X)^2 + (y-Y)^2 + z^2)^{3/2}} + \int_{-b}^b \int_{-c}^c \frac{dy dz (a+X) \sin \theta}{((a+X)^2 + (y-Y)^2 + z^2)^{3/2}} \right]$$

$$N_y = \frac{1}{4\pi} \left[ \int_{-a}^a (b-Y) dx \cos \theta \frac{2c}{((b-Y)^2 + (x-X)^2)((b-Y)^2 + (x-X)^2 + c^2)^{1/2}} \right. \\ + \int_{-a}^a (b+Y) dx \cos \theta \frac{2c}{((b+Y)^2 + (x-X)^2)((b+Y)^2 + (x-X)^2 + c^2)^{1/2}} \\ + \int_{-b}^b (a-X) dy \sin \theta \frac{2c}{((a-X)^2 + (y-Y)^2)((a-X)^2 + (y-Y)^2 + c^2)^{1/2}} \\ \left. + \int_{-b}^b (a+X) dy \sin \theta \frac{2c}{((a+X)^2 + (y-Y)^2)((a+X)^2 + (y-Y)^2 + c^2)^{1/2}} \right]$$

$$\begin{aligned}
N_y = \frac{1}{2\pi} & \left[ \cos\theta \left( \frac{\tan^{-1} \frac{c(a-X)}{(b-Y)((a-X)^2+(b-Y)^2+c^2)^{1/2}}}{\tan^{-1} \frac{c(a+X)}{(b-Y)((a+X)^2+(b-Y)^2+c^2)^{1/2}} \right. \right. \\
& + \frac{\tan^{-1} \frac{c(a-X)}{(b+Y)((a-X)^2+(b+Y)^2+c^2)^{1/2}}}{\tan^{-1} \frac{c(a+X)}{(b+Y)((a+X)^2+(b+Y)^2+c^2)^{1/2}} \left. \right) \\
& + \sin\theta \left( \frac{\tan^{-1} \frac{c(b-Y)}{(a-X)((a-X)^2+(b-Y)^2+c^2)^{1/2}}}{\tan^{-1} \frac{c(b+Y)}{(a-X)((a-X)^2+(b+Y)^2+c^2)^{1/2}} \right. \\
& \left. \left. + \frac{\tan^{-1} \frac{c(b-Y)}{(a+X)((a+X)^2+(b-Y)^2+c^2)^{1/2}}}{\tan^{-1} \frac{c(b+Y)}{(a+X)((a+X)^2+(b+Y)^2+c^2)^{1/2}} \right) \right]
\end{aligned}$$

Let  $p = \frac{X}{a}$ ,  $q = \frac{Y}{b}$ . normalise.

$$\begin{aligned}
N(x, y, 0) = \frac{1}{2\pi} & \left[ \cos\theta \left( \frac{\tan^{-1} \frac{ca(1-p)}{b(1-q)(a^2(1-p)^2+b^2(1-q)^2+c^2)^{1/2}}}{\tan^{-1} \frac{ca(1+p)}{b(1-q)(a^2(1+p)^2+b^2(1-q)^2+c^2)^{1/2}} \right. \right. \\
& + \frac{\tan^{-1} \frac{ca(1+p)}{b(1+q)(a^2(1+p)^2+b^2(1-q)^2+c^2)^{1/2}}}{\tan^{-1} \frac{ca(1-p)}{b(1+q)(a^2(1-p)^2+b^2(1+q)^2+c^2)^{1/2}} \left. \right) +
\end{aligned}$$

$$\begin{aligned}
& + \sin \theta \left( \tan^{-1} \frac{cb(1-q)}{a(1-p)(a^2(1-p)^2 + b^2(1-q)^2 + c^2)^{1/2}} \right. \\
& + \tan^{-1} \frac{cb(1+q)}{a(1-p)(a^2(1-p)^2 + b^2(1+q)^2 + c^2)^{1/2}} \\
& + \tan^{-1} \frac{cb(1-q)}{a(1+p)(a^2(1+p)^2 + b^2(1-q)^2 + c^2)^{1/2}} \\
& \left. + \tan^{-1} \frac{cb(1+q)}{a(1+p)(a^2(1+p)^2 + b^2(1+q)^2 + c^2)^{1/2}} \right) \text{-----} (1)
\end{aligned}$$

The variation of demagnetising factor, with  $q$ ,  $p = 0$  is shown in figure 2.2.1 for angles  $\theta$  from  $0^\circ \rightarrow 90^\circ$  and with  $p, q = 0$  in figure 2.2.2. Note that at 1400 oe the second order correction<sup>12</sup> to the demagnetising field for  $\theta = 0$  is of the order of 20%. This error decreases with increasing applied field.

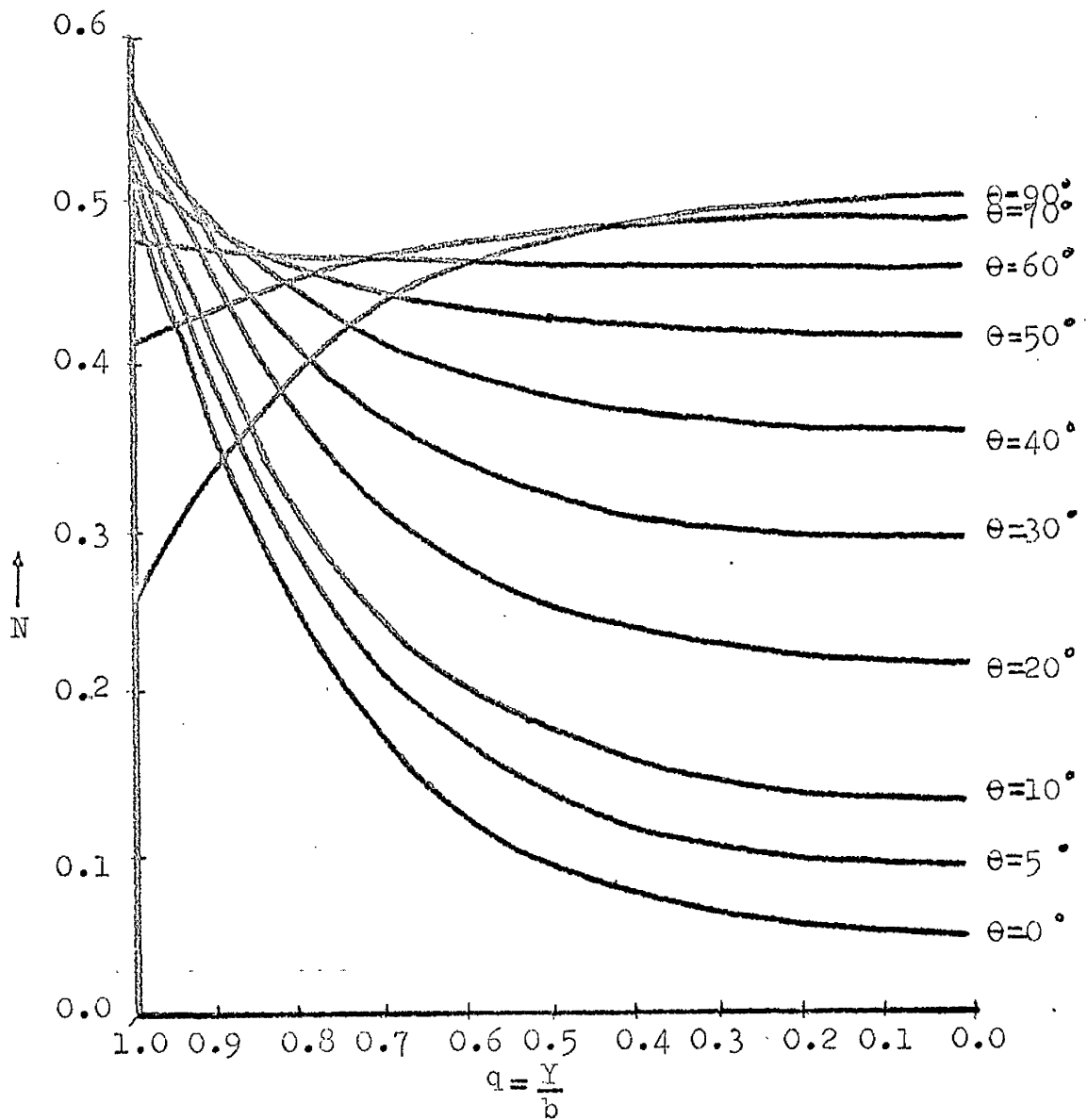


Figure 2.1.1. Demagnetising factor ~ Normalised distance into rod.  $\theta = 0^\circ$  when rod is longitudinally magnetised,  $N$  = Demagnetising factor along central axis.

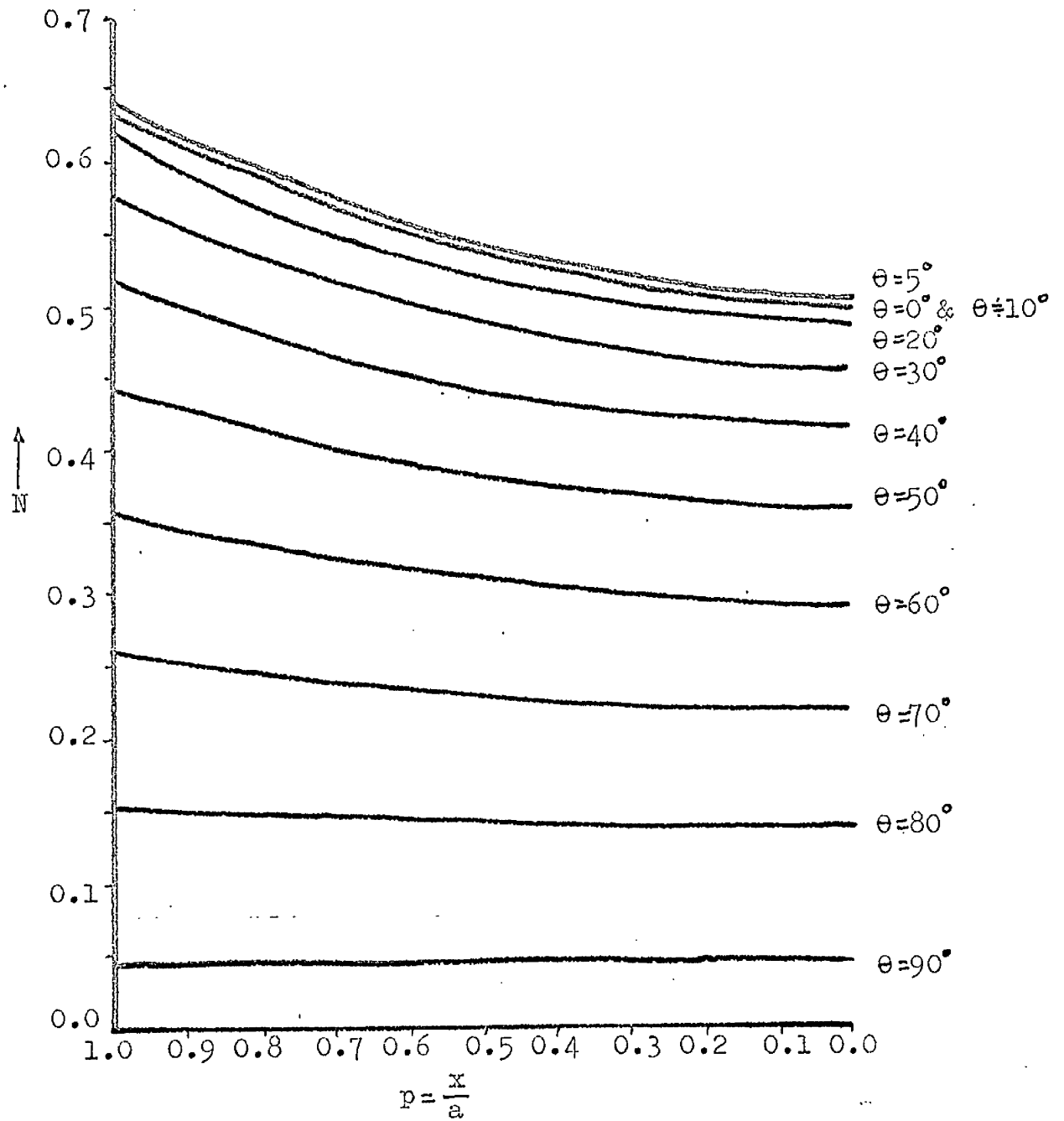


Figure 2.1.2. Demagnetising factor ~ Normalised distance across rod.  $\theta = 0^\circ$  when rod is transversely magnetised.  $N$  = Demagnetising factor across centre of the rod.

## Anisotropy Field.

Dillon et al.,<sup>13</sup> have derived relations relating the applied magnetic field to effective magnetic field in ellipsoidal magnetically anisotropic ferrimagnets. These relations are true for non-ellipsoidal specimens providing internal fields at a point are considered.

The effective field for [l, m, n] direction is given by,

$$[100] \quad H_{eff}^2 = (H_i + \frac{2K_1}{M_s})^2$$

$$[100] \quad H_{eff}^2 = (H_i - \frac{2K_1}{M_s})(H_i + \frac{K_1}{M_s} + \frac{1}{2}\frac{K_2}{M_s})$$

$$[111] \quad H_{eff}^2 = (H_i - \frac{4}{3}\frac{K_1}{M_s} - \frac{4}{9}\frac{K_2}{M_s})^2$$

In YIG  $K_1/M_s$  has a value of 41 oe  $K_2/M_s$  being approximately zero. In [100]  $H_{eff}^2 = (H_i - 82)^2$ .

$$\therefore H_{eff} = H_i - 82 \text{ oe.}$$

i.e., anisotropy field = - 82 oe.

In [110], the anisotropy field is a function of  $H_i$ .

We shall only calculate  $H_{anis}$  at the turning point for

1.2KMc/s i.e.,  $H_i = 419$  oe.

$$H_{eff}^2 = (H_i - \frac{2K_1}{M_s})(H_i + \frac{K_1}{M_s} + \frac{1}{2}\frac{K_2}{M_s})$$

$$= (H_i^2 - \frac{H_i K_1}{M_s} - \frac{2K_1^2}{M_s}) = 175,561 + 17,179 - 3360$$

$$H_{eff} = 435$$

$$\therefore H_{anis} = 435 - 419 = 16 \text{ oe.}$$

Magneto-elastic waves<sup>9</sup> and internal field analysis.<sup>11</sup>

## 2.3.1.

Theory:-

Consider the  $\theta = 0$  propagation of magneto-elastic waves in the direction of the applied field in a uniformly magnetised media. The spin wave is circularly polarised and coupling occurs to a circularly polarized shear wave. The coupled magneto-elastic equations are.

$$\frac{d^2 m^+}{dz^2} + k_m^2 m^+ - \frac{b_2}{D} \frac{dR^+}{dz} = \frac{m_0}{D} h^+$$

$$\frac{d^2 R^+}{dz^2} + k_e^2 R^+ + \frac{b_2}{cm_0} \frac{dm^+}{dz} = 0$$

where the + superscript refers to circular polarisation where m is the small signal time dependent magnetisation.

D is the exchange constant.

R is the transverse elastic displacement.

$\gamma$  is the gyromagnetic ratio.

$b_2$  is the magneto-elastic coupling constant.

$\rho$  is the material density.

c is the elastic constant of interest.

$\omega$  is the angular frequency.

$k_m$  is the spin wave number.

$k_e$  is the elastic wave number.

With no coupling between spin and elastic waves the dispersion relation for the two modes are,

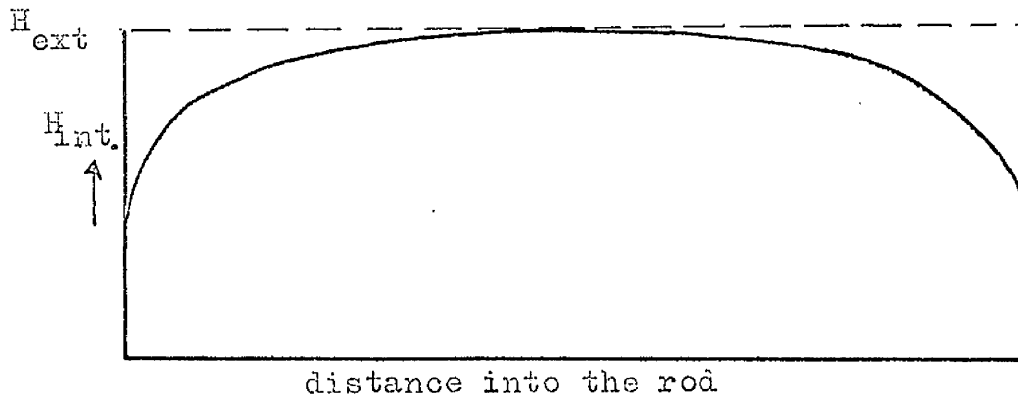
$$k_m^2 = \frac{1}{D} \left[ \frac{\omega}{\gamma} - H_i \right] \quad \text{for spin waves} \quad (2)$$

and  $k_e^2 = \omega^2 \rho / c$  for elastic waves (3)

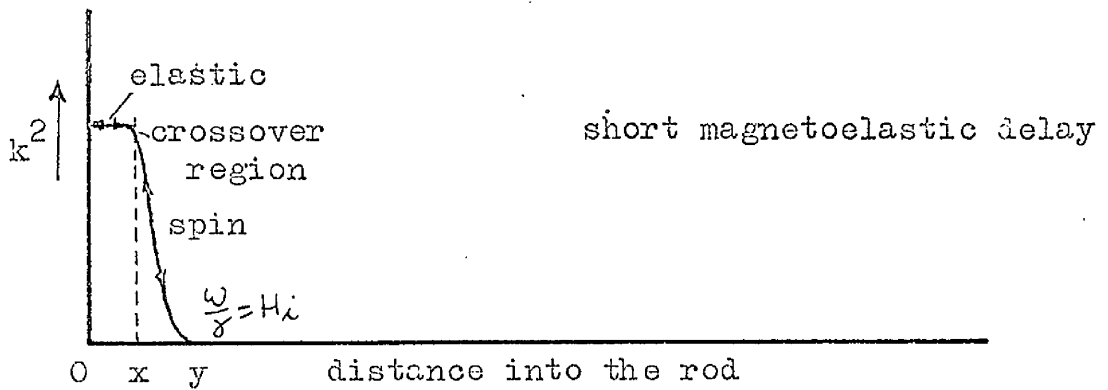
Coupling from electro-magnetic to spin waves occurs at the turning point when  $H_i = \frac{\omega}{\gamma}$  i.e., from equation (2), when the spin wave number is zero. Coupling from spin to elastic waves occurs in the region where  $k_e = k_m$ , the cross over point.

In figure 2.3.1. spin waves are excited at the turning point, propagate with increasing wave number towards the cross over point, where they couple with elastic waves, which propagate towards and are reflected from the end face, back along their path to the turning point. YIG possesses weak magneto-elastic coupling, i.e.,  $b_2$  is small, so that hybrid modes only exist in the vicinity of the cross over point.

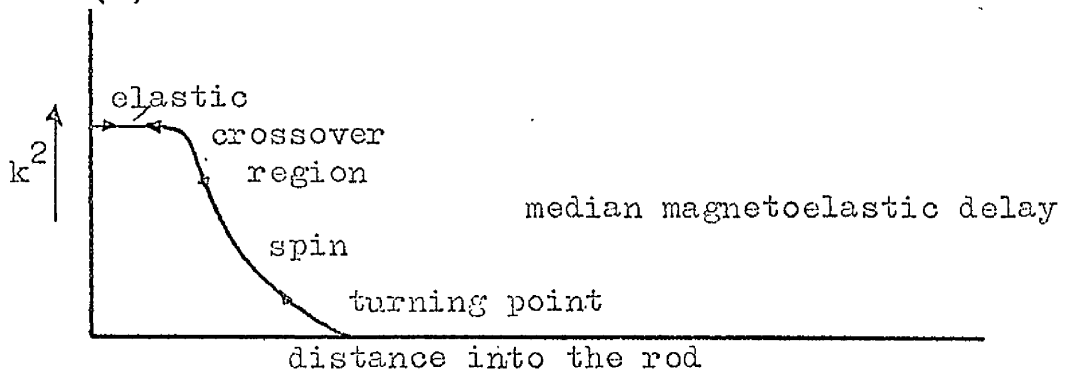
If the cross over region is regarded as being infinitely narrow then the round trip delay time  $T_r$ , required for the magneto-elastic wave packet to travel from  $z = y$  to  $z = 0$  and back, figure 2.3.1, is given approximately by



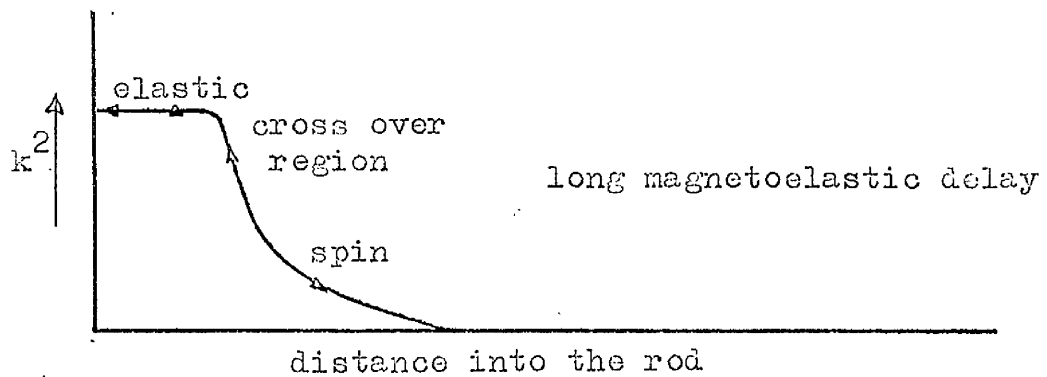
(a) Internal field variation with distance into the rod



(b) Variation of  $k^2$  with distance into the rod.



(c) Variation of  $k^2$  with distance into the rod.



(d) variation of  $k^2$  with distance into the rod.

Figure 2.3.1. External field decreasing from (b) to(d).

$$\frac{T_r}{2} = \int_0^x \frac{dz}{c} + \int_x^y \frac{dz}{v_s(z)} = \frac{x}{c} + \int_x^y \frac{dz}{2\{[\gamma D][\omega - \gamma H_i(z, H_{ext})]\}^{1/2}} \quad (4)$$

where  $c$  is the elastic shear wave velocity.

$v_s(z)$  is the spin wave velocity at any point  $z$ .

$H_i$  is the internal field at any point  $z$ , with external field  $H_{ext}$ .

When the magneto-elastic delay is short, the internal field gradient at the turning point is large and the spin path length short so that the distance  $y - z$  is small, and the first two terms of a Taylor expansion about a point at  $\bar{z} = y$  provide an approximate description of  $H_i$  in the region of spin wave propagation.

Substitution of

$$H_i(\bar{z}, H_{ext}) \doteq H_i(y, H_{ext}) + (\bar{z} - y) H_i' \quad \text{with. } H_i' = \left. \frac{\partial H_i(\bar{z}, H_{ext})}{\partial \bar{z}} \right|_{\bar{z}=y}$$

into equation (4) gives

$$T_r = \frac{2}{c} \left[ y + \frac{\omega}{\gamma H_i'} \left( 1 - \frac{D\gamma\omega}{c^2} \right) \right] \quad (5)$$

Spin-elastic resonances occur when the round trip phase change  $\phi = 2n\pi$  plus an arbitrary constant, where  $n$  is an integer.<sup>14</sup> An adjacent resonance, of mode number  $(n + 1)$ , can be set up by adjusting the applied field by

$\delta H$  at constant frequency so that the turning point moves by  $\delta y$ , equal to  $\delta H/H'_i(y)$ , the spin wave delay contribution, to the first order, is unchanged, and the one-way acoustic path is altered by half a wavelength, giving

$$\delta H = \pi H'_i(y)/k_e = \pi c \frac{H'_i}{\omega}$$

Then

$$y = \frac{1}{2} c T_r - \frac{2\pi}{\gamma \delta H} \left( 1 - \frac{D\Omega \gamma^2}{c^2} \right) \quad \text{where } \Omega = \frac{\omega}{\gamma} \text{ --- (6)}$$

### Experimental.

With an arrangement as shown in figure 1.1.5 whereby a stabilised current could be applied to the magnet modulation coils, causing a field change variable over 3 oe. A 1.2KMc/s signal pulse was applied and the field adjusted until a magneto-elastic pulse was observed on the oscilloscope, its delay noted and the externally applied magnetic field measured using the n.m.r. gauss meter. The oscilloscope time base was set at  $0.2 \mu\text{Secs}/\text{cm}$  so that individual cycles of the 30 Mc/s I.F. content of the delayed pulse could be seen. The current through the modulation coils was then increased and the number of cycles passing a point on the oscilloscope screen recorded. From this  $\delta H$  and  $H_i$  were calculated. This procedure was repeated at about 30 points over the range of delays observable. The results are shown in Table 1 and figures 2.3.2 and 2.3.3.

From figure 2.3.2 which is a plot of experimental demagnetising field and theoretical demagnetising field, including anisotropy field, against position in rod, for an axially magnetised rod, with magneto-elastic propagation along the axis. The agreement between theoretical

TABLE 1.

Measurement of internal field, rod axially magnetised.

Mean field change 2.64 gauss.

Mean field gauss.	Mean delay $\mu$ sec.	Number of cycles.	y mm.	Demagnetising field gauss.
615	9.8	56.0	4.61	195
620	8.57	52.6	3.09	200
631	6.9	38.0	3.62	211
639	5.925	31.4	3.42	219
649	5.26	26.4	3.41	229
678	3.775	19.3	2.36	258
708	3.03	15.2	1.97	288
716	2.81	14.0	1.86	296
727	2.60	12.4	1.86	307
752	2.17	10.0	1.64	332
772	1.93	9.0	1.43	352
778	1.845	8.3	1.44	358
784	1.755	8.0	1.34	364
790	1.685	7.6	1.31	370
831	1.375	6.0	1.12	411
855	1.25	4.8	1.18	435
886	1.11	4.5	0.99	466
905	0.99	4.1	0.86	485
929	0.92	3.4	0.909	509
950	0.875	3.6	0.77	530
988	0.79	3.3	0.677	568
1070	0.6	2.4	0.54	650
1124	0.51	2.0	0.48	704
1191	0.42	1.7	0.37	771
1252	0.37	1.5	0.33	832

Rod transversely magnetised, mean field change 3.6 gauss

1573	0.38	2.30	0.303	1154
1557	0.38	2.30	0.303	1138
1550	0.38	2.35	0.294	1130
1534	0.38	2.45	0.285	1114
1512	0.40	2.50	0.304	1093
1496	0.45	2.70	0.306	1077
1462	0.485	3.00	0.365	1042
1449	0.51	3.05	0.395	1030
1440	0.52	3.10	0.424	1021
1419	0.575	3.20	0.521	999
1399	0.705	3.50	0.581	979
1383	0.72	3.60	0.687	963
1378	0.73	3.65	0.688	958
1371	0.74	3.70	0.737	952
1360	0.755	3.90	0.728	941
1354	0.855	3.95	0.766	935

Mean field gauss.	Mean delay μ sec.	Number of cycles.	g. y. " mm.	Demagnetising field gauss.
1350	0.85	4.0	0.797	930
1337	0.875	4.2	0.855	917
1312	0.87	4.6	0.915	892
1298	0.915	5.0	0.937	878
1286	1.03	5.4	0.921	867
1275	1.065	5.5	0.995	855
1264	1.13	5.8	1.00	845
1261	1.175	6.0	1.02	841
1252	1.18	6.5	1.024	832
1243	1.23	6.75	1.113	823
1230	1.295	7.3	1.260	810
1226	1.365	7.5	1.281	806
1223	1.46	8.0	1.264	803
1194	1.90	11.0	1.571	774
1188	1.98	11.5	1.67	769
1167	2.70	18.3	1.014	747

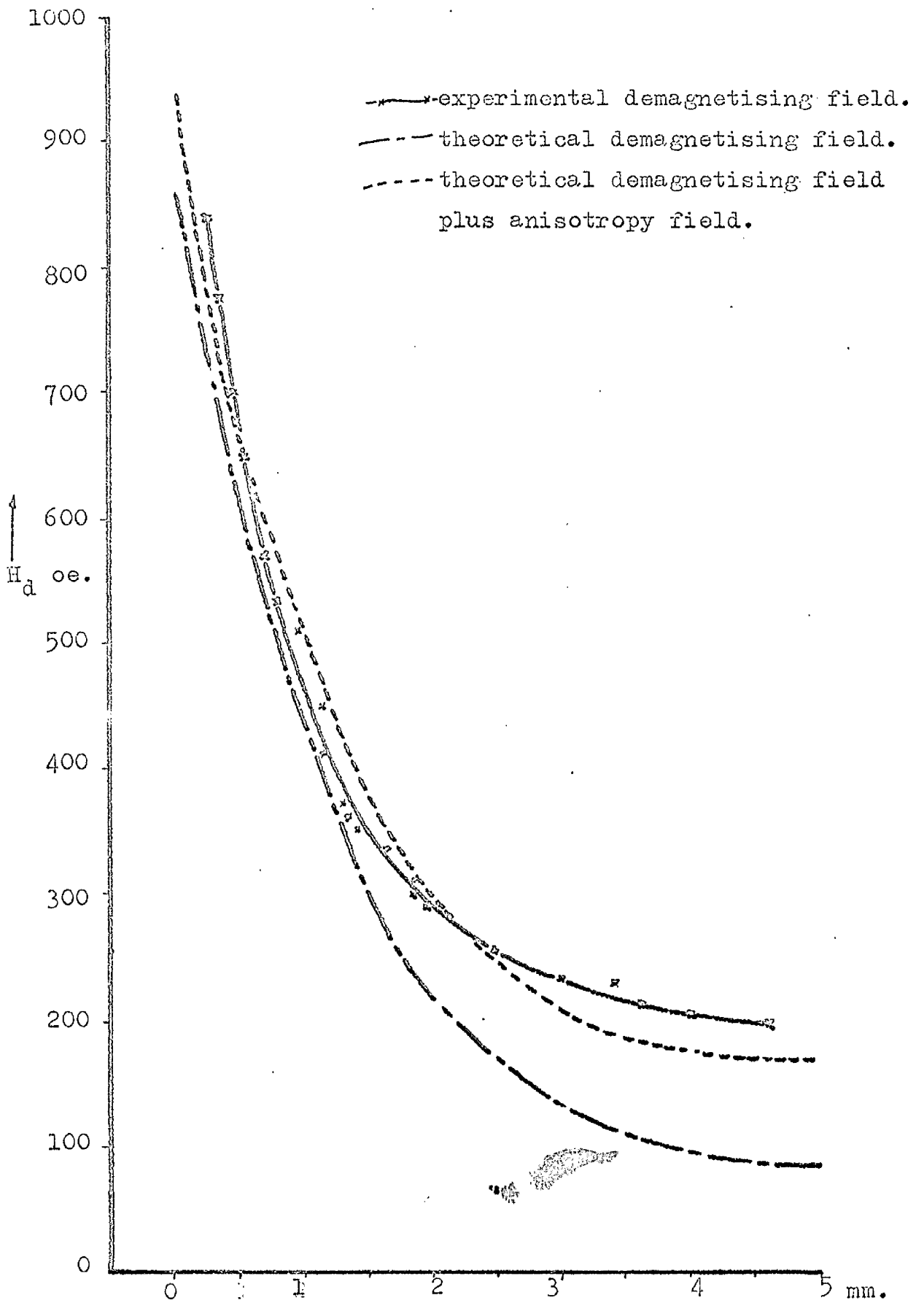


Figure 2.3.2. Demagnetising field ~ Position in axially magnetised rod.

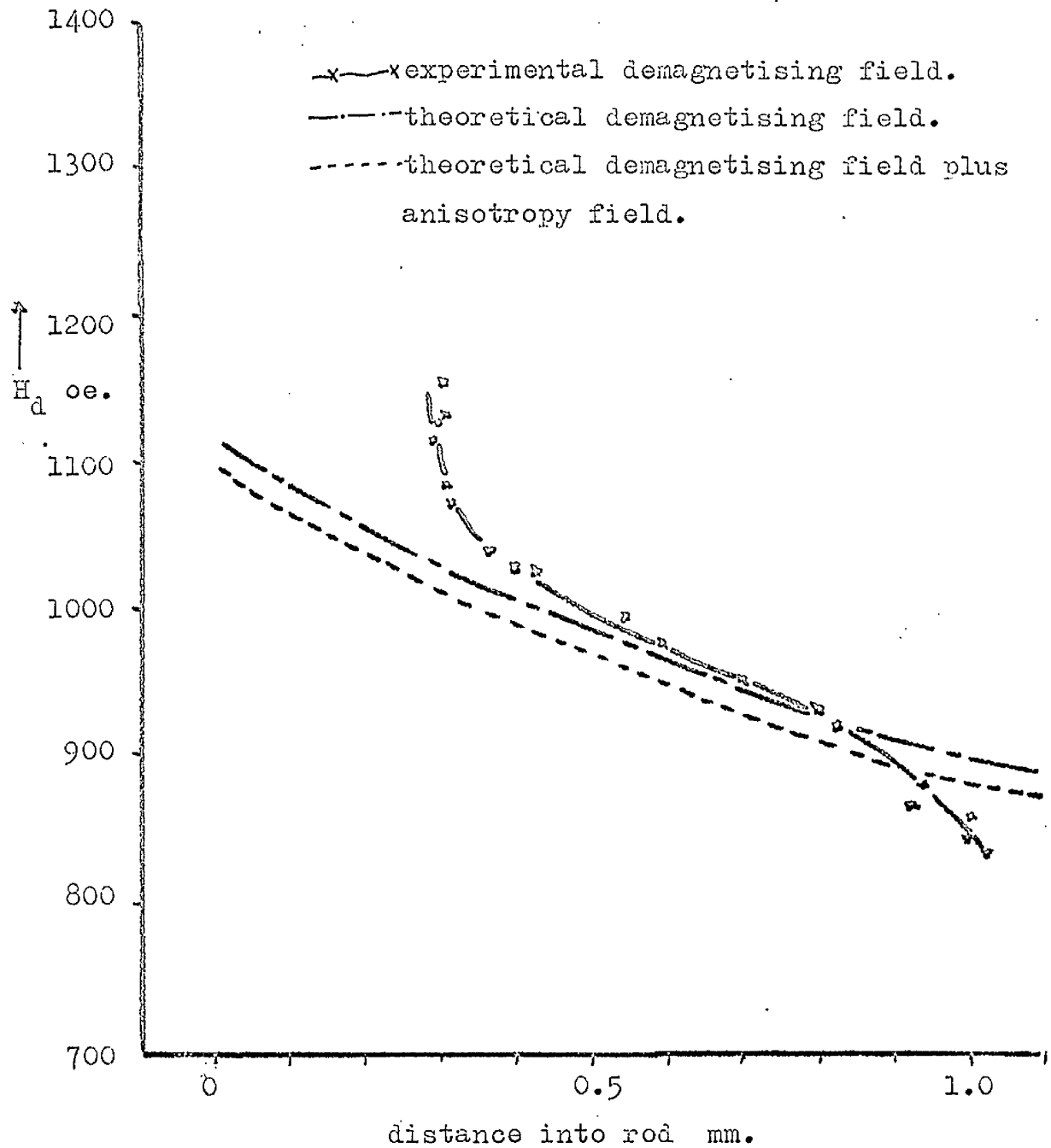


Figure 2.3.3. Demagnetising field ~ position in transversely magnetised rod.

results, taking into account anisotropy field, and the experimental results is very good. The maximum deviation of the experimental from the theoretical plot of demagnetising plus anisotropy field, is nowhere greater than 13% over the range of measurements. The deviation of experimental from theoretical results if the experimental curve is extrapolated to the end face is 9%.

Figure 2.3.3 shows a plot of theoretical, including anisotropy field, and experimental demagnetising field against position in the rod for a transversely magnetised rod, that is, with the external magnetic field applied normal to the polished side face. The agreement between theory and experiment is not as good, over the whole range as in the longitudinally magnetised case. Some deviation from theory is to be expected very close to the end face as predicted by Schlömann.<sup>12</sup> Although this correction, of the order of 10 or 20%, does not explain the large discrepancies between theoretical and experimental results, if the experimental plot is extrapolated to the end face. The experimental demagnetising field values are lower towards the centre than those expected theoretically. This may be accounted for by

propagation taking place in a direction not perpendicular to the polished side.

For these measurements of internal field it would be required, for good accuracy, to be able to measure field changes of 0.01 of an oersted and changes in delay of 10 nano-seconds. The field measurement technique was accurate to about 0.1%. Since the applied field change was of the order of 3 gauss, with a steady magnetic field of from 500 to 1000 oersteds, it was necessary to average all the field change readings. The term in equation (6)  $\frac{D\Omega\gamma^2}{c^2}$  was neglected since at 1.2 KMc/s this has a value of 0.006.

The technique used here<sup>15</sup> of counting the number of cycles of which pass for a given small field change is easier to use, and probably more accurate than the C.W. technique used by Auld and Strauss<sup>11</sup> or that of Kohane, Joseph and Schlomann<sup>16</sup> of obtaining interference cancellations between successive delayed pulses. By counting the number of cycles we are in effect counting the number of cancellations. Difficulty was met measuring delay time, very often on sweeping the field over a 3 gauss range the delay would be observed to increase with

increasing field. This is thought to be associated with ray bending of the magneto-elastic waves.<sup>17</sup>

This method of internal field measurement holds more accurately for long bare rods, axially magnetised.

Plots of Magneto-elastic Delay versus Field.

figures 2.3.4 - 2.3.7. Readings of delay against Magnetic field were taken for magneto-elastic pulses in YIG rod 'A' at 1.2KMc/s and at 2.4KMc/s with the rod axially in line with the external field and propagation along the axis, and with the rod transverse to the magnetic field, that is, with the magnetic field perpendicular to a polished side face of the rod, propagation is thought to be perpendicular to this side in the centre of the rod.

Figure 2.3.4. Shows the variation of delay with applied magnetic field. The magneto-static burst, when  $\frac{\omega}{\gamma} = H_i$  in the centre of the rod, occurs when the external field is 590 oe., but  $H_i = 420$  oe, giving a demagnetising factor, after considering anisotropy field of 0.051, which is in exact agreement with that obtained theoretically considering demagnetising field. The shape of this plot is typical of field delay characteristics in a bare YIG rod.

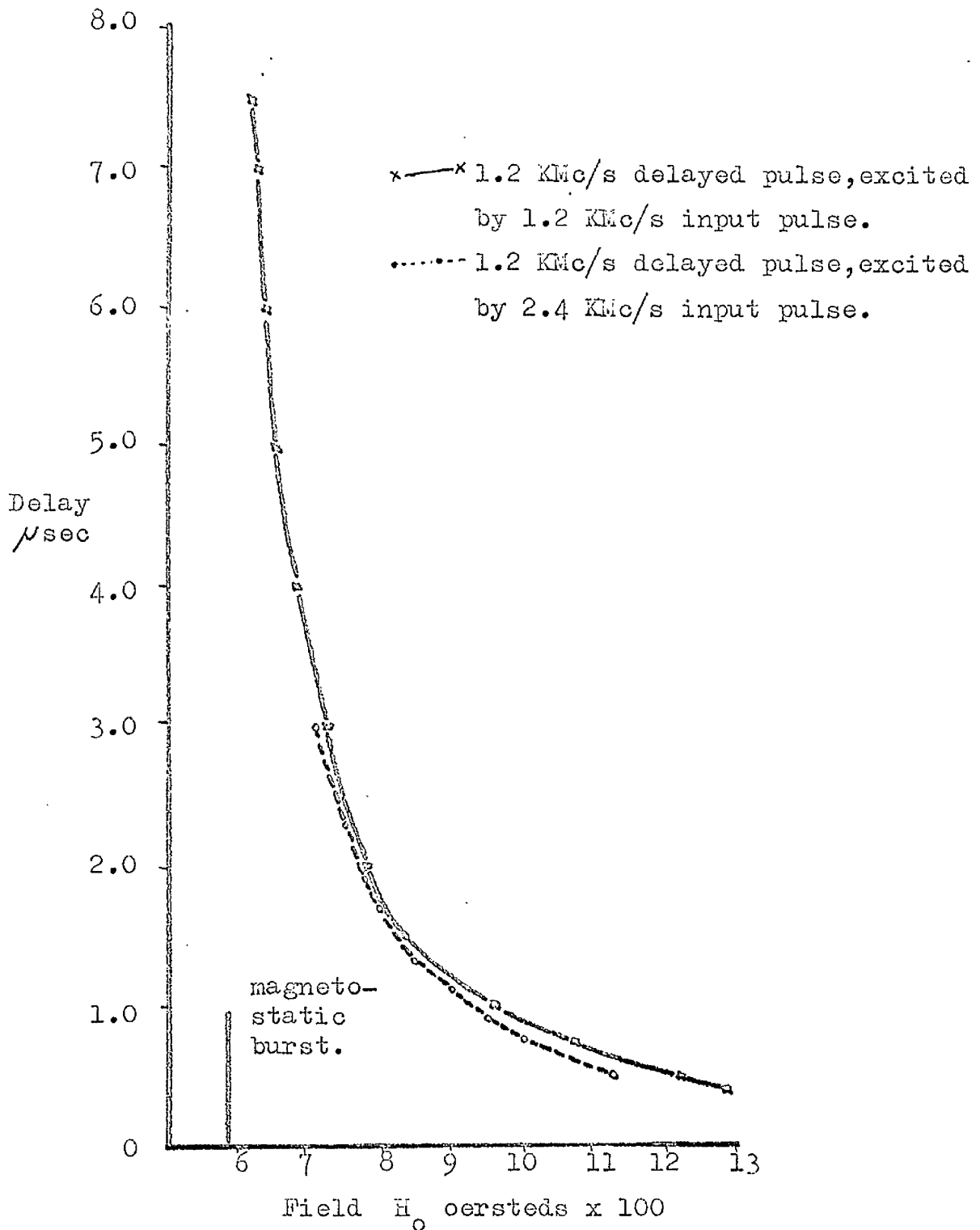


Figure 2.3.4. Plot of magnetoelastic delay  $\sim$  applied field for the axially magnetised rod.

Figure 2.3.5. Shows field against delay characteristics of the rod under the same conditions as above but at 2.4KMc/s. The magneto-static burst occurs with an external field of 1036 gauss, but  $H_i = \frac{\omega}{\gamma} = 840$  gauss hence the demagnetising factor =  $\frac{1035 - 840 - H_a}{1760}$  where  $H_a$  is the anisotropy field, 82 oe in the [100] direction, and 1760 is the  $4 \pi M$  of single crystal YIG. Giving a demagnetising factor = 0.058 which is in good agreement with the theoretical demagnetising factor. In experiments with the transversely magnetised rod. The square YIG rod as used in the axially magnetised case was rotated about its central axis through  $90^\circ$ , so that its axis was horizontal but perpendicular to the field direction. A fine wire coupler was used at one of the polished end faces. Magneto-elastic pulses were observed with delays of 1 - 2  $\mu$  seconds. These pulses were just discernable above the noise level being about 80db down on the input signal. One of the side faces which was normal to the field was polished optically flat. Stronger magneto-elastic pulses were observed about 60db down on the input signal. There was only a difference of  $\frac{1}{2}$ db observed in using a horizontal fine wire coupler,

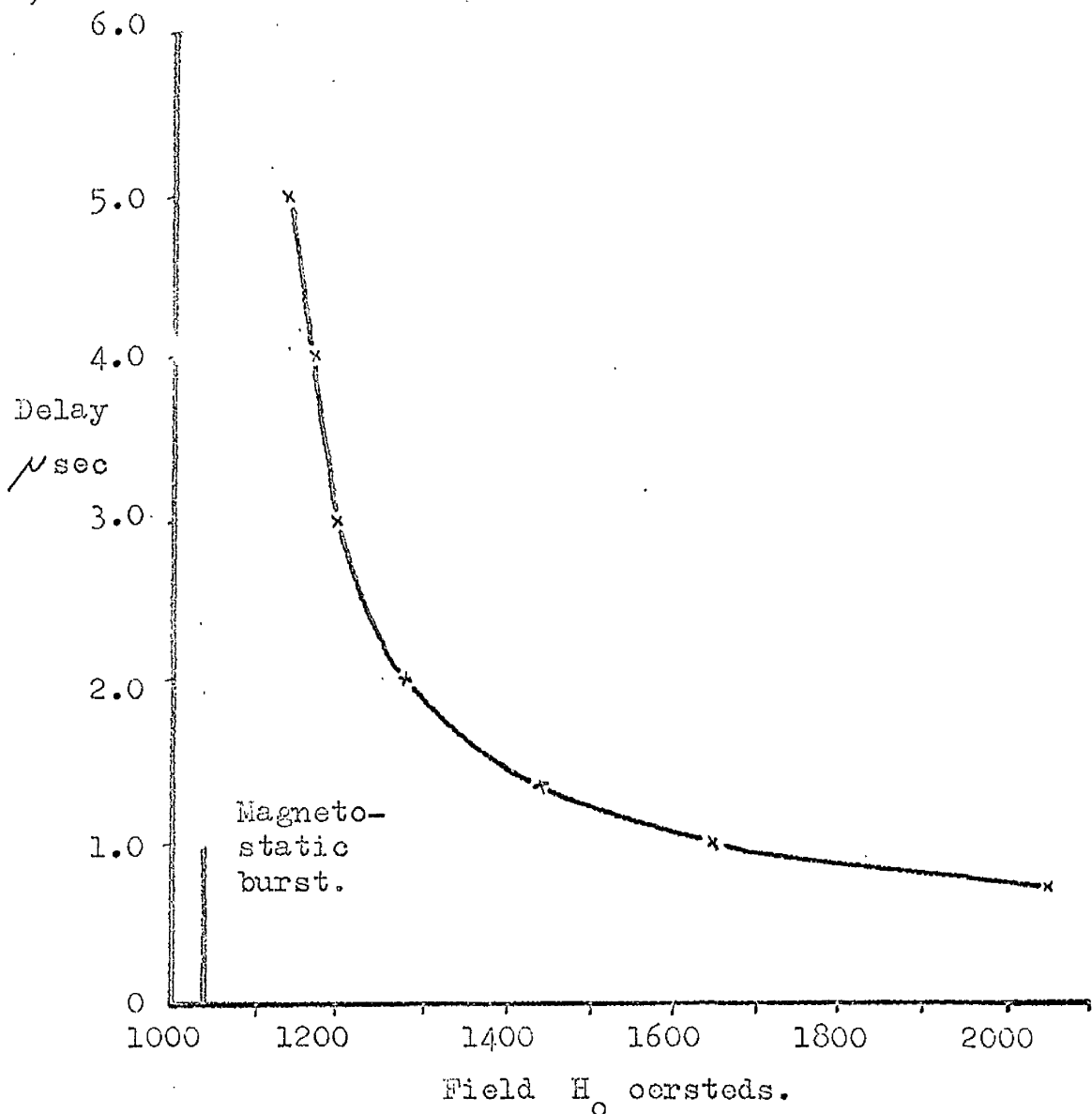


Figure 2.3.5. Plot of magnetoelastic delay ~ applied field for the axially magnetised rod. Signal and delayed pulse frequency 2.4 KMc/s.

which results in  $h_{r_f}$  being perpendicular to  $H_{dc}$  at the centre of rod, which is the theoretically ideal case, and a vertical wire coupler which results in  $h_{r_f}$  being parallel to  $H_{dc}$  at the centre of the rod. A fine wire coupler was arranged to be against the centre of the polished side face of the rod, and the rod arranged as before with the polished side face normal to the direction of external field.

Magneto-elastic pulses were observed, which at a delay of  $0.95\mu$ seconds had an amplitude referred to the input of -41db at 1.2KMc/s. The graph of delay against field is shown in Figure 2.3.6. The magneto-static burst occurs at 1146 oe giving an experimental demagnetising factor after considering anisotropy field of 0.423 compared with a theoretical value of 0.5. This curve has the same form as the corresponding curve for an axially magnetised rod, the main difference being, that in the transversely magnetised case, the range of fields over which magneto-elastic delays are observable is less than in the axially magnetised rod, due to the lower range of demagnetising factor.

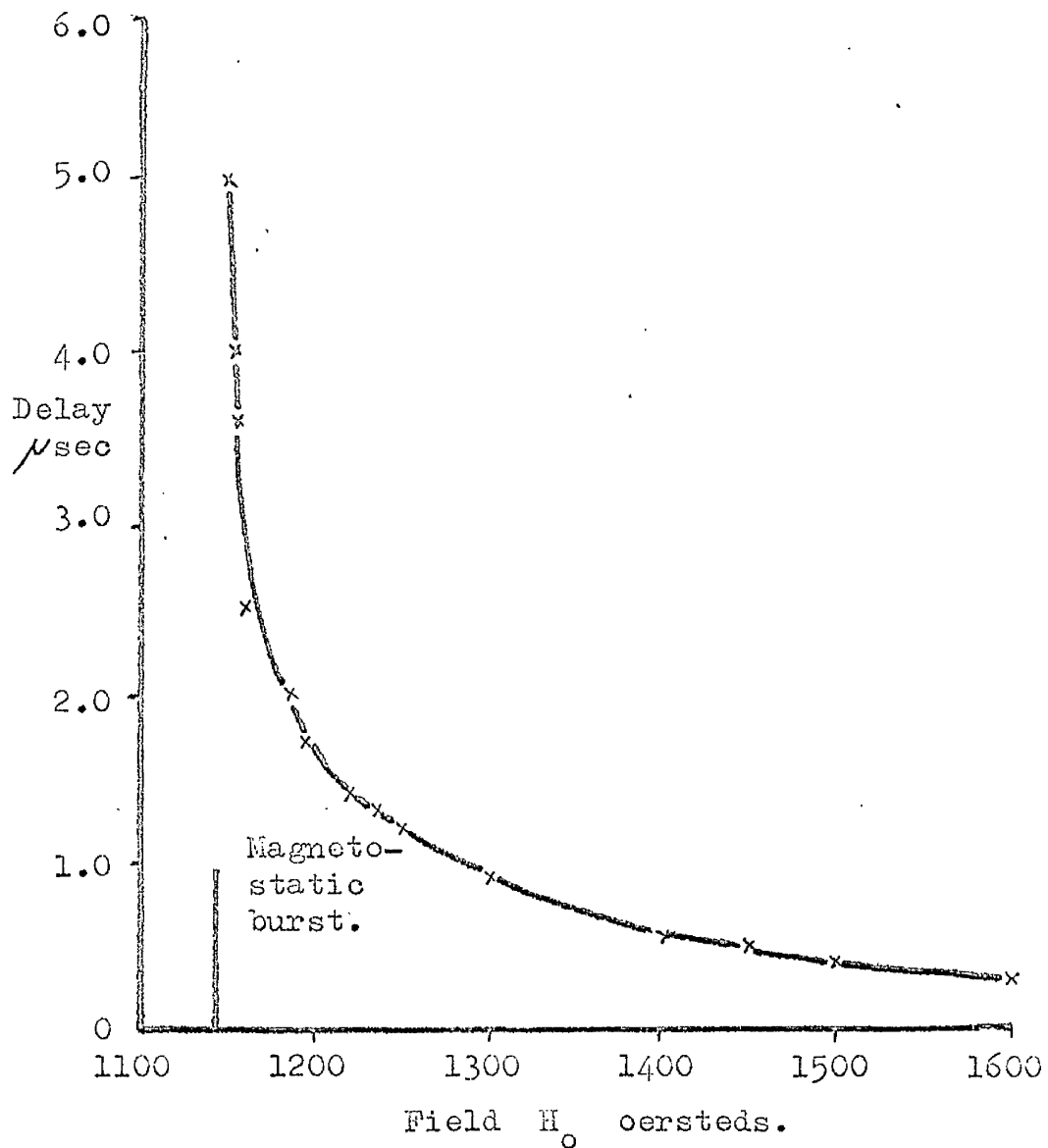


Figure 2.3.6. Plot of magnetoelastic delay ~ applied field, for transversely magnetised rod. Signal and delayed pulse frequency 1.2 Mc/s.

The plot of delay against field at 2.4KMc/s for a transversely magnetised rod is shown in figure 2.3.7. This is similar to those previously described above. The magneto-static burst occurs at a field of 1610 oersteds, resulting in an experimental demagnetising factor, in the centre of the rod of 0.446, compared with a first order theoretical demagnetising factor of 0.5. The error between theory and experiment in demagnetising fields close to the centre of the rod is not explained by anisotropy field. Also shown on this graph are the delay against field characteristics with the polished side face of the rod at an angle of  $88^\circ$  and at  $86^\circ$  to the external field. The median delay part of these curves are almost identical with the one at  $90^\circ$ , however at short delays the magneto-elastic pulses disappear into the signal pulse at a lower field for the  $86^\circ$  and  $88^\circ$  cases. At 1.2KMc/s with the same rod configuration the magneto-elastic pulses disappear into noise within  $\pm 1^\circ$  from the normal to the field.

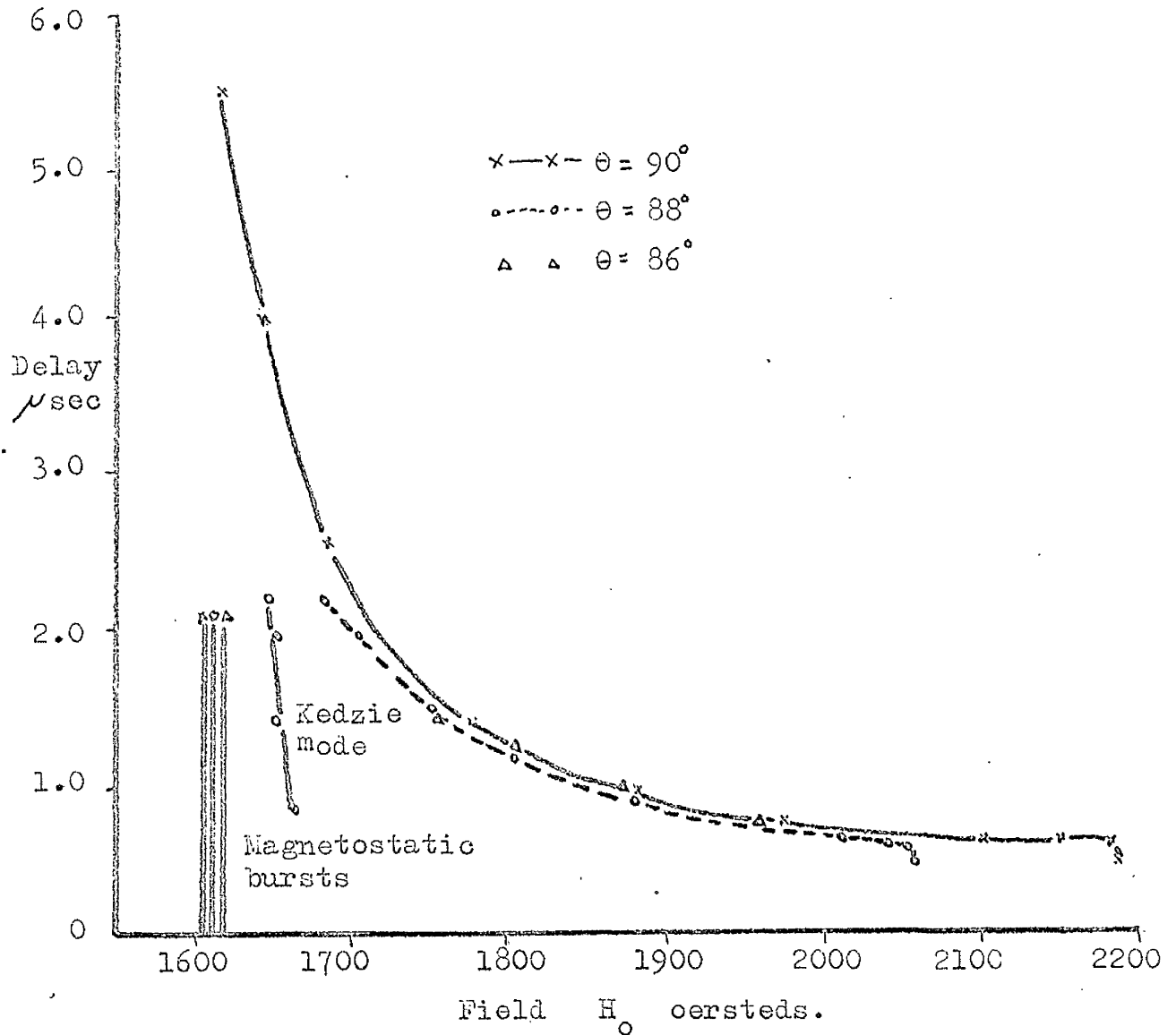


Figure 2.3.7. Plot of magnetoelastic delay  $\nu$  applied field for  $\theta = 90^\circ$  i.e. rod transversely magnetised,  $\theta = 88^\circ$  and  $\theta = 86^\circ$  Signal and delayed pulse frequency 2.4 KMc/s.

The linear plot on figure 2.3.7 at low fields is thought to be a Kedzie<sup>18</sup> mode. He has observed this mode at X-band and liquid helium temperature in both longitudinal and transversely magnetised circular YIG rods and reports on a linear dispersion  $\frac{dt}{dH} = -0.24 \mu$  Secs/oe for both axial and transverse magnetised rods. In these experiments at 2.4KMc/s a linear dispersion of  $\frac{dt}{dH} = -0.025 \mu$  Sec/oe was observed. The attenuation being of the order of 60 db, Kedzie reports on attenuation at 80°K of 80 db for 4  $\mu$  Sec. delay. This mode is thought to be produced as follows; consider magneto-static mode propagation cut off in the rod, due to a turning point being present fig. 2.3.8. The area under  $H_2$ , which is proportional to delay, is less than under  $H_1$  therefore the delay decreases as H increases, the mode occurs in the same field range as magneto-elastic propagation and is essentially one port.

During experiments on parametric amplification of magneto-elastic waves, 1.2KMc/s delayed pulse trains were observed with the 1.2KMc/s signal off and only the 2.4KMc/s pump frequency applied to the axially magnetised rod. The results of these observations are shown in

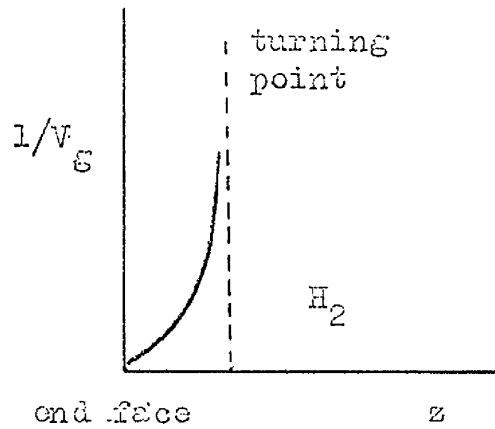
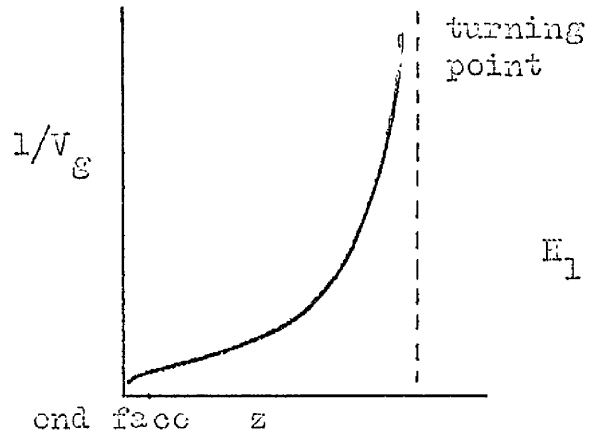


Figure 2.3.8. Kozie modes.  $H_2$  is greater than  $H_1$ ,  $z$  is the distance into the rod from the end face.

figures 2.3.9, 2.3.10 and in figure 2.3.4. The first pulse in figures 2.3.9, and 2.3.10 is coincident with the time of application of the pump. In figure 2.3.4 plots 1 and 2 are identical over the range of 2, within experimental error. A pulse train composed of first and second delay echoes is observable with the field along the axis of the rod, the first delayed pulse being attenuated by 110db with respect to the input pulse, which had a power of 3 watts. The first delayed pulse showed a maxima at an angle of  $9^\circ$  to the axis; the second and longer delayed pulse was not visible at this angle. This first delayed pulse was observable till  $H_{\text{ext}}$  was at an angle of  $16^\circ$  to the axis.

The fine detail of the pulse was not coherent, that is single cycles of intermediate frequency could not be observed, inside the pulse envelope the appearance was that of amplified noise. The excitation process is that due to Auld<sup>19</sup> of  $\frac{\omega p}{2}$  instabilities. This mechanism has its lowest threshold about  $9^\circ$  off axis. Once the  $\frac{\omega p}{2}$  spin waves have been excited they propagate as would spin waves generated by direct means.

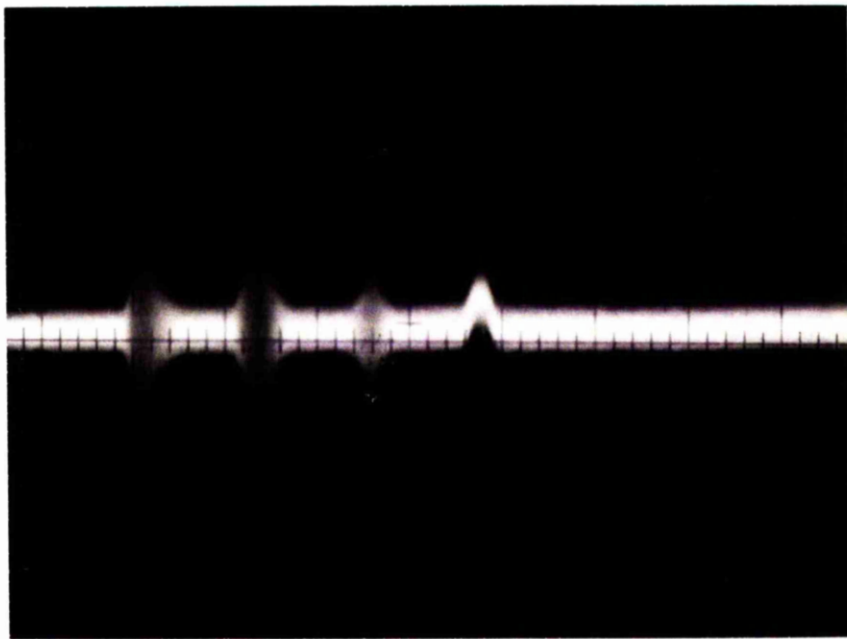


Figure 2.3.9.  $1\mu\text{sec}/\text{cm}$ . 0.5 volts/cm.  
Parametrically excited magnetoelastic noise pulse.  
Pump applied at time of first pulse. Field oriented  
at  $0^\circ$  to the rod axis. Pump frequency 2.4 KMc/s,  
delayed pulse frequency 1.2 KMc/s. Pump amplitude  
36 dbm. pulse width  $0.2\mu\text{sec}$ .

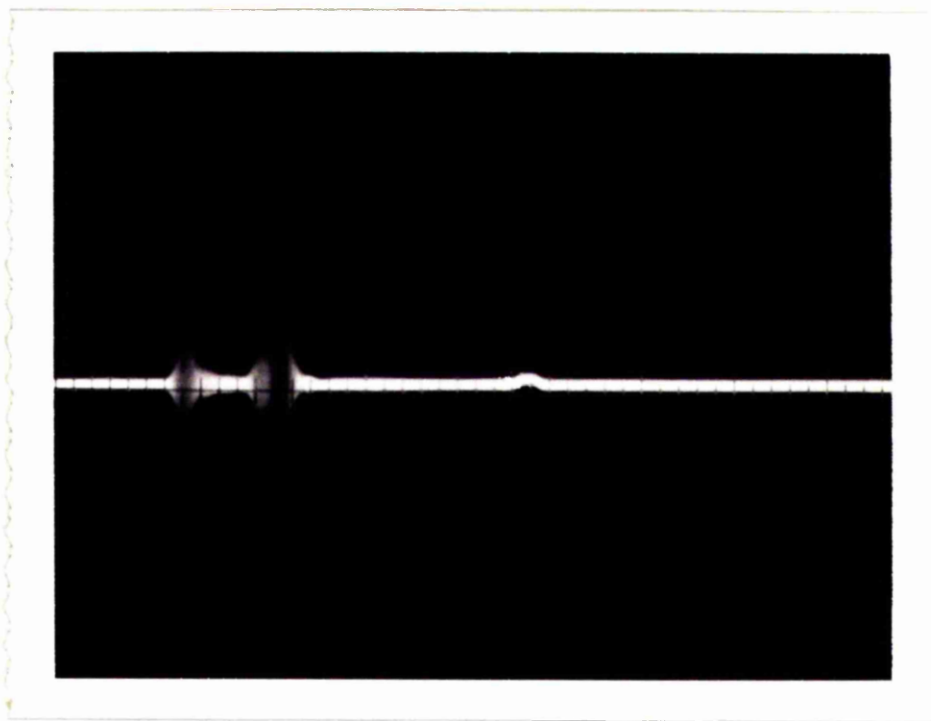


Figure 2.3.10. As in fig. 2.3.9., but rod axis oriented at  $9^\circ$  to the external field.

The variation of attenuation of magneto-elastic pulses is rather erratic.<sup>20</sup> The maxima of the pulse amplitudes decreases exponentially with delay. The largest maxima occurs normally at a delay of about  $1 \mu$  sec. The efficiency of conversion of electro-magnetic to spin and of spin to elastic waves is an inverse function of the gradient, the greatest part of the propagation loss for magneto-elastic waves is due to the spin wave losses. At some point in the rod a compromise occurs between spin loss and conversion efficiency, when this happens the magneto-elastic delayed pulse has a maximum amplitude.

## 3.1.0. Parametric Amplification of Magneto-Static Waves.

## 3.1.1. Theory:-

The phenomena discussed in this section, occur above the field required for the magneto-static burst and continue into the lower field region of the magneto-elastic regime. In an axially magnetised rod, the internal field is larger at the centre of the rod than at the ends, the operating conditions used here preclude the propagation of magneto-static waves through the centre of the rod, due to a turning point existing close to the centre of the rod. The magneto-static portion of the spin wave spectrum provides a mode with the longest wavelength at the end face of the rod and enables coupling to occur from electro magnetic to long wavelength spin waves.<sup>21</sup> The group velocity of the magneto-static waves, decreases with propagation along the increasing field profile, towards the turning point near the centre of the rod. The wave packet approaches the turning point asymptotically. Figure 3.1.1 which results in the spin wave energy being available, throughout its life time, for interaction with the pump field.

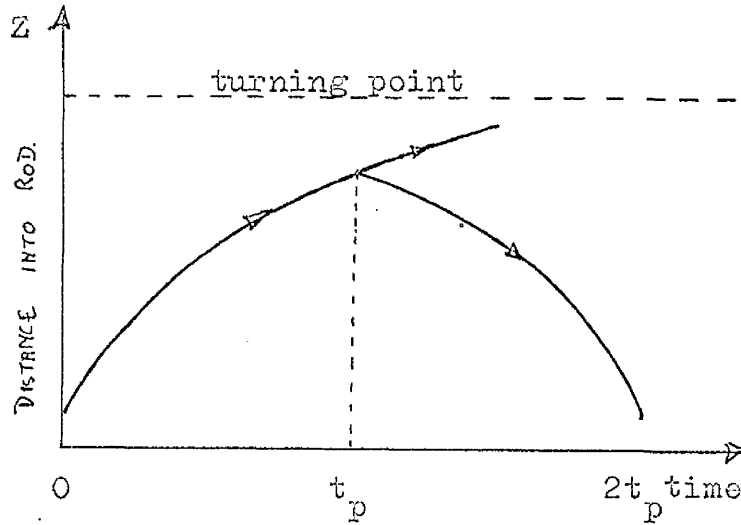


Figure 3.1.1. Explanatory time/distance diagram for the parametric amplification of magnetostatic waves. A signal frequency spin wave pulse is launched, close to the end face of the axially magnetised rod, at  $t=0$  and propagates towards the centre of the rod. A pump pulse, of twice the signal frequency, is applied at time  $t_p$  producing a forward and a backward travelling wave. The forward wave approaches the turning point asymptotically. The backward wave propagates back to the coupling structure along the input path, and is detected as a delayed pulse at time  $2t_p$ . The forward wave is lost in the cutoff region.

The parametric process as discussed by Damon<sup>3</sup> can be described by a model analogous to that used for non-linear effects in ferro-magnetic resonance.<sup>22</sup>

The input spin wave is of the form

$$b_k = b_k e^{j(k_z - \omega_k t)}$$

In the presence of the pump signal, this is coupled to its complex conjugate.

$$b_{-k}^* = b_{-k}^* e^{j(k_z + \omega_k t)}.$$

through the non-linear equation of motion.

$$-j \dot{b}_{-k}^* = \nu_k b_{-k}^* + \rho_k b_0 b_k$$

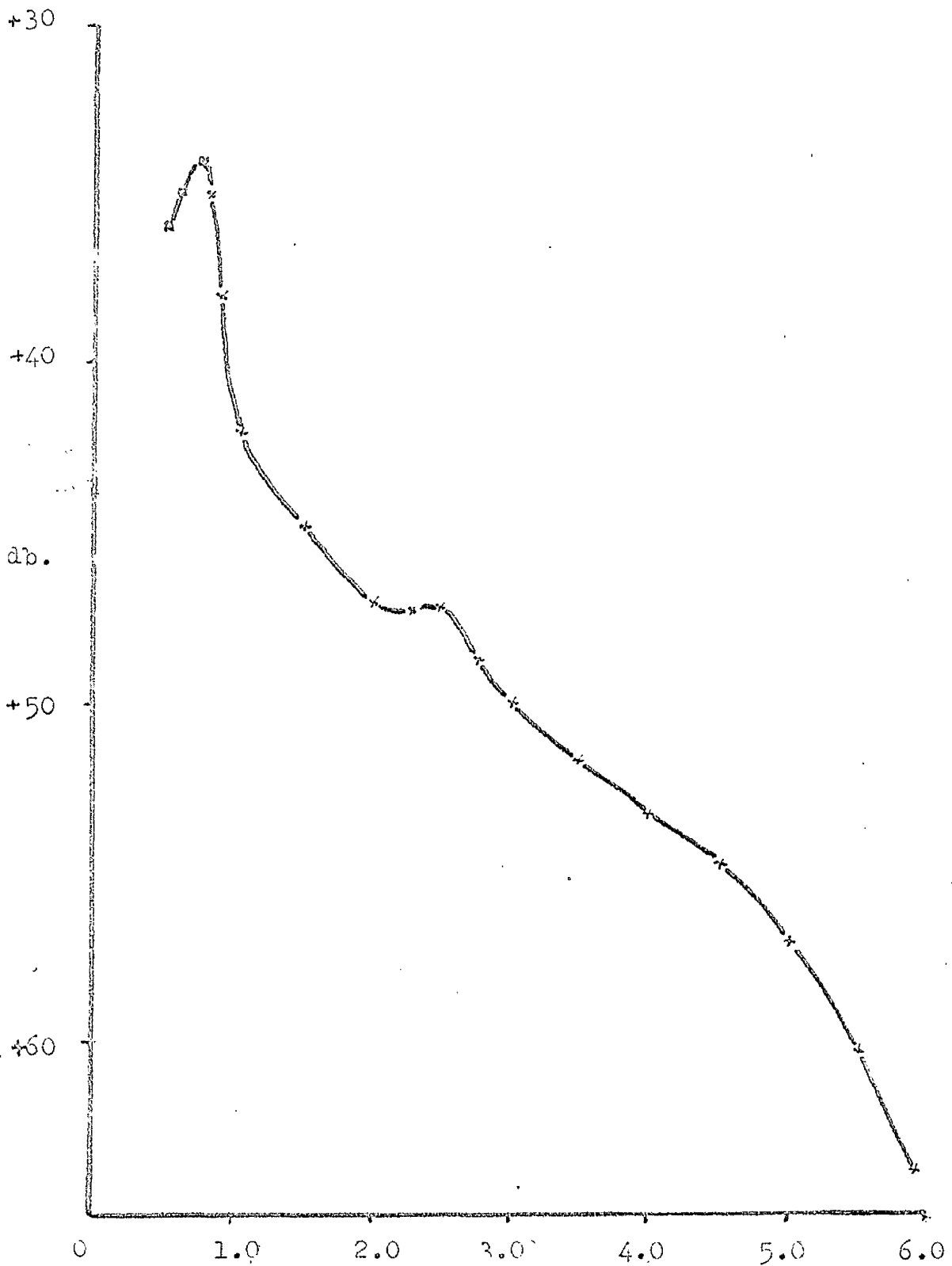
where  $b_0$  represents the uniform mode at frequency  $\omega_0$ ,  $\rho_k$  is a coupling parameter and  $k = \left[ \frac{1}{D} (\frac{\omega}{\gamma} - H_i) \right]^{\frac{1}{2}}$ . Thus providing  $\omega_0 = 2\omega_k$ , an oppositely directed wave-packet is generated at the time of pumping, that is the complex conjugate of the signal. This wave packet is the idler mode of the parametric process. The idler mode, with an amplitude proportional to the input wave, returns to the excitation point, with the same delay time as that required for the input pulse to reach the point at which the pump is applied. This process can be considered as the propagation of a wave through a time varying media, then due to the dependence of the wave on the direction and magnitude of the magnetisation, which the pump magnetic field varies, energy is transferred from the pump field to the spin waves.

**Experiment:-**

Experiments were performed on the parametric amplification of magneto-static waves in both longitudinally and transversely magnetised rods. Figures 3.1.2 and 3.1.3 show the variation of attenuation with delay of the parametrically excited pulse. In both cases the signal and pump pulse widths are  $0.2 \mu$  seconds. The signal frequency was  $1.2 \text{KMc/s}$  and the pump frequency  $2.4 \text{KMc/s}$ . Signal power  $2 \mu$  watts peak and pump power  $400 \text{m}$  watts peak.

The shape of these curves is typical of observations made in the field range considered. It would have been expected that the curves would decay monotonically. However there is a monotonic decay with additional terms superimposed. These are probably due to saturation effects since they occur in time when the spin waves have largest amplitude.

Disregarding saturation effects, the decay of amplitude of the parametrically excited pulse with time is not exponential suggesting that the efficiency of the parametric process is dependent on magnetic field gradient or spin wave number.



Delay of parametrically excited pulse  $\mu$ sec.

Figure 3.1.2. Plot of attenuation  $\sim$  delay of parametrically excited pulse. Signal frequency = 1.2 KMc/s, pump frequency = 2.4 KMc/s. Signal power - 30 dbm., pump power + 30 dbm.

$H_0 = 624$  oe. Rod axially magnetised. Parametric amplification of magnetostatic waves.

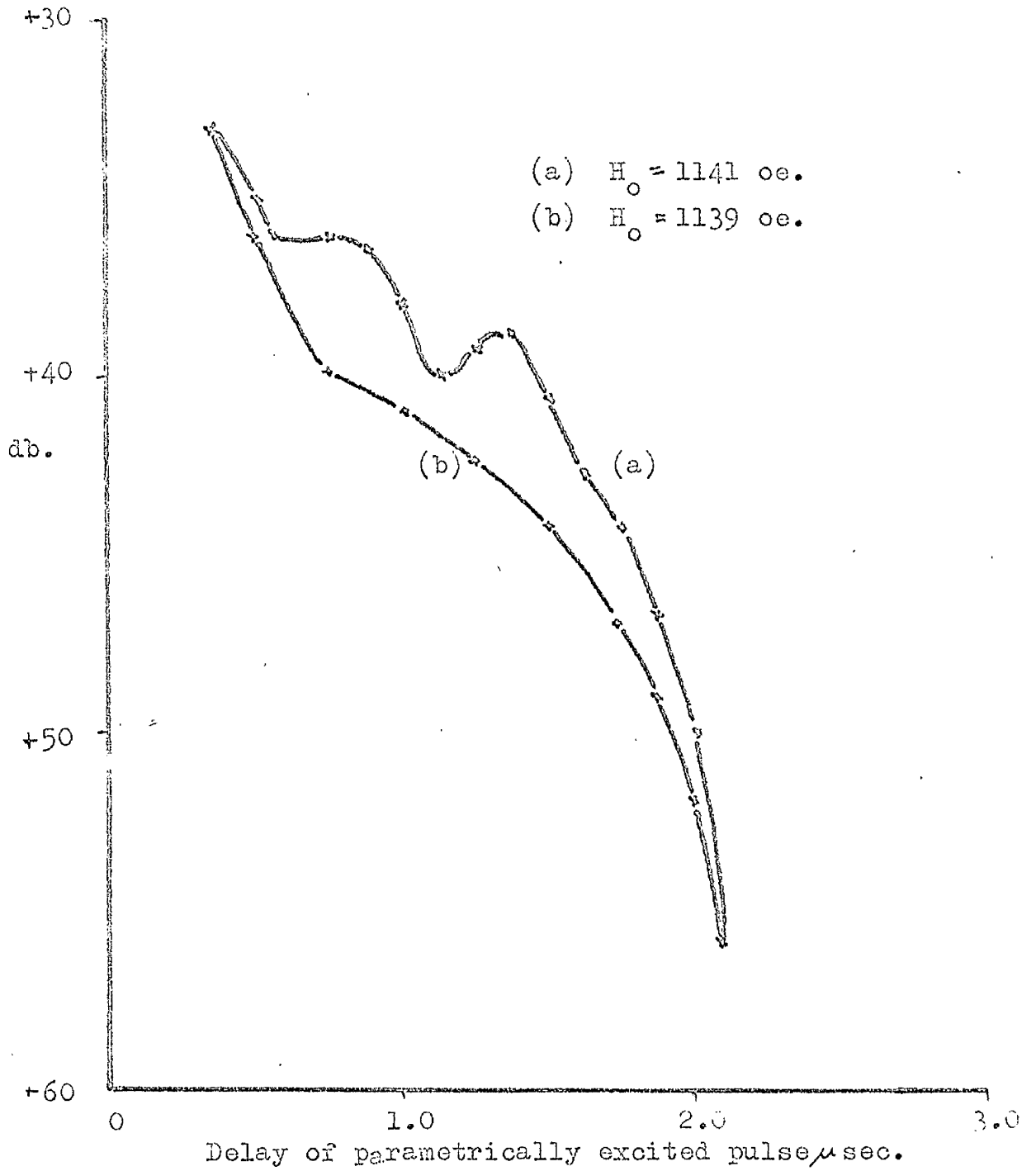


Figure 3.1.3. Plot of attenuation  $\sim$  delay of parametrically excited pulse. Signal frequency = 1.2 KMc/s, pump frequency = 2.4 KMc/s. Signal power -30 dbm, pump power +30 dbm. Parametric amplification of magnetostatic waves.

Figure 3.1.4 shows the results obtained by measuring the amplitude of the parametrically excited pulse and peak pump power. These measurements were performed with the signal power constant at  $-30$  dbm. The time of application of the pump was constant throughout at  $0.5$   $\mu$  seconds, corresponding to a parametrically excited pulse of  $1.0$   $\mu$  seconds delay. The pump and signal pulse widths were each  $0.2$   $\mu$  seconds and the signal and pump frequencies as before.

From figure 3.1.4 the gain increases linearly with Pump power above  $+15$ dbm. The rapid variation at low power is probably due to these being just above the threshold of the mechanism. There is no saturation observable with increases in available pump or signal power. It seems possible therefore that net gain will be attainable with high pump powers  $\sim 500$  watts. However saturation effects will almost certainly have their thresholds below this power level.

It was observed that as the width of the signal pulse was varied from  $0.2$   $\mu$  seconds to  $2.0$   $\mu$  seconds, with the pump pulse being applied at fixed time. The width of the echo pulse increases with increasing signal

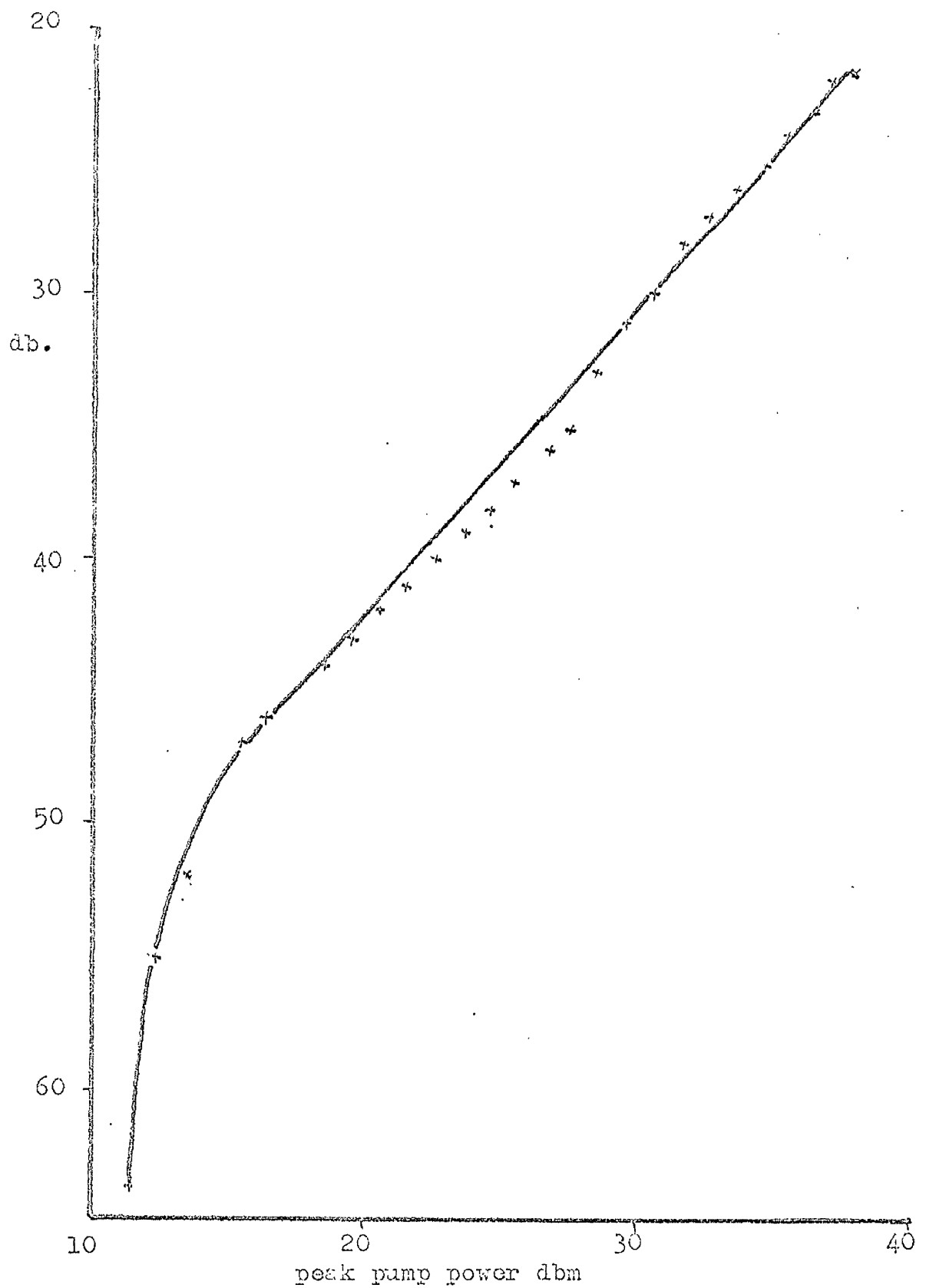


Figure 3.1.4. Plot of attenuation of parametrically amplified magnetostatic pulse  $\sim$  peak pump power. Rod axially magnetised, signal input power -30 dbm. Signal frequency 1.2KMc/s. Pump frequency 2.4 KMc/s.  $H_0 = 634$  oersteds.

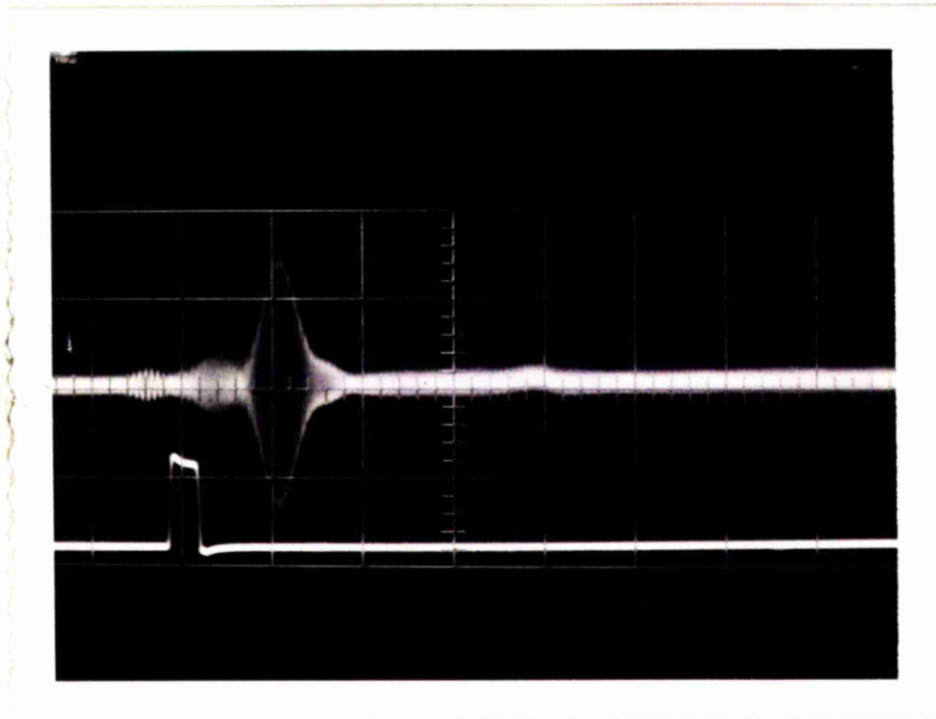


Figure 3.1.5. 1 volt/cm.  $0.5 \mu\text{sec/cm}$ . Parametric amplification of magnetostatic wave. Signal applied at first visible centimeter division. Bottom trace pump applied at  $0.5 \mu\text{sec}$  after the signal pulse. Upper trace, parametrically excited pulse received  $1.0 \mu\text{sec}$ . after the signal pulse. Signal frequency  $1.2 \text{ KMc/s}$  pulse width  $0.2 \mu\text{sec}$ . Pump frequency  $2.4 \text{ KMc/s}$  pulse width  $0.2 \mu\text{sec}$ .

input pulse width. Except for decay due to damping, the echo pulse was found to be symmetric with the input pulse about the pump pulse. If however the signal pulse is short compared with the duration of the pump pulse, then the echo pulses have the same width as the pump pulse. This is in full agreement with the theory presented. Echo pulses were observable at all angles between the longitudinally magnetised and transversely magnetised cases, adjustment of the field being necessary to ensure that a suitable condition existed in the rod, due to variations in demagnetising factor with angle to the external field. The optimum angle to the field in the longitudinally magnetised rod was  $\sim 10^\circ$  and in the transversely magnetised case  $\sim 5^\circ$ . Figure 3.1.5.

## Parametric Amplification of Elastic Waves.

## 3.2.1.

Theory:-<sup>23</sup>

In the range of fields above the field for shortest magneto-elastic delay. The magneto-elastic turning point is very close to the end face in an axially magnetised rod. On the application of a pulse of microwave energy, a uniform precession is set up at the turning point which couples over a very short distance to an elastic wave.

Consider an infinite YIG sheet of thickness  $2L$  buried in a infinite acoustic medium. Figure 3.2.1. Assume that acoustically the YIG is matched to the medium. Then we are required to solve.

$$C_{44} \frac{d^2 R^+}{dz^2} + \omega^2 \rho R^+ = - \frac{b_1}{M_0} \frac{dM^+}{dz}$$

where  $C_{44}$  is an elastic constant.

$R$  elastic displacement, (+) refers to a circular polarization

$\rho$  is the density.

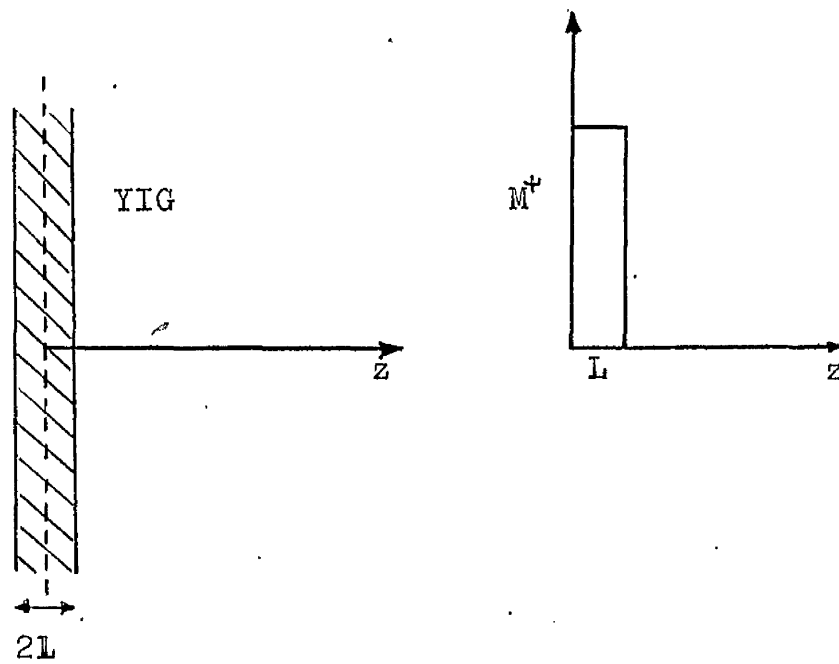


Figure 3:2.1 Consider a thin slice at the end face of an axially magnetised YIG rod. Dimensions of the rod, very much greater than the thickness of the slice.

$b_2$  is the magneto-elastic coupling constant.

$M_0$  is the d.c. magnetisation.

$M$  is the transverse r.f. magnetisation.

$$\left[ \frac{dM^+}{dz} \right] = S \bar{M}^+ - M^+ = M^+ [1 - e^{-SL}] - M^+ = -M^+ e^{-SL}.$$

$$\left[ \frac{d^2 R^+}{dz^2} \right] = S^2 \bar{R}^+ - S R^+(0) - R^+(0).$$

$$\therefore [C_{44} S^2 + \omega^2 \rho] \bar{R}^+ = S C_{44} R^+(0) - C_{44} R^+(0) = \frac{b_2}{M_0} M^+ e^{-SL}.$$

$$\text{i.e. } \bar{R}^+ = \frac{\frac{b_2}{M_0} M^+ e^{-SL} + C_{44} S R^+(0) + C_{44} R^+(0)}{(C_{44} S^2 + \omega^2 \rho)}$$

$$\therefore \bar{R}^+ = \frac{\left( \frac{b_2 M^+}{C_{44} M_0} e^{-SL} + S R^+(0) + R^+(0) \right)}{\left( S^2 + \omega^2 \rho / C_{44} \right)}.$$

There are poles at  $S = \pm j \omega \sqrt{\rho / C_{44}}$

We require only forward travelling wave,  $e^{-j \omega \sqrt{\rho / C_{44}} \cdot z}$

therefore must only consider pole at  $s = -j\omega\sqrt{\rho/c_{44}}$

$$\therefore R_{-}^{+} = e^{-j\omega\sqrt{\rho/c_{44}}z} \left[ \frac{b_2 M^{+}}{c_{44} M_0} e^{j\omega\sqrt{\rho/c_{44}}L} - j\omega\sqrt{\rho/c_{44}} R^{+}(0) + R^{+}(0) \right] - 2j\omega\sqrt{\rho/c_{44}}$$

Now at  $z = 0$ ,  $R^{+} = R^{+}(0)$ . Assume  $R^{+}(0)$  is zero (Symmetry of problem).

$$R^{+}(0) = \frac{b_2 M^{+} e^{j\omega\sqrt{\rho/c_{44}}L}}{c_{44} M_0 (-2j\omega\sqrt{\rho/c_{44}})} + \frac{1}{2} R^{+}(0).$$

$$\therefore R^{+}(0) = \frac{2 b_2 M^{+} e^{j\omega\sqrt{\rho/c_{44}}L}}{c_{44} M_0 (-2j\omega\sqrt{\rho/c_{44}})} = \frac{b_2 M^{+} e^{j\omega\sqrt{\rho/c_{44}}L}}{c_{44} M_0 (-j\omega\sqrt{\rho/c_{44}})}.$$

$$\text{i.e. } R^{+} = \frac{2 e^{-j\omega\sqrt{\rho/c_{44}}z} \cdot \frac{b_2 M^{+}}{c_{44} M_0} e^{j\omega\sqrt{\rho/c_{44}}L}}{-2j\omega\sqrt{\rho/c_{44}}}$$

$$\| \therefore R^{+} = \frac{j b_2 M^{+} e^{-j\omega\sqrt{\rho/c_{44}}(z-L)}}{c_{44} M_0 \omega \sqrt{\rho/c_{44}}}$$

$$= \frac{j b_2 M^{+}}{\omega M_0 \sqrt{\rho c_{44}}} e^{-j\omega\sqrt{\rho/c_{44}}(z-L)} \|$$

$$S = \frac{dR^+}{dz}$$

$$= \frac{b_2 M^+ \sqrt{\rho/c_{44}} \cdot \omega}{\omega M_0 \sqrt{\rho c_{44}}} e^{-j\omega \sqrt{\rho/c_{44}} (z-L)}$$

$$S = \frac{b_2 M^+}{c_{44} M_0} e^{j\omega [t - \sqrt{\rho/c_{44}} (z-L)]}$$

The process of amplification of elastic waves is not known but, may be due to non linear or second order terms in the magnetisation or magneto-elastic coupling.

Experimental:-<sup>1,6</sup>

The acoustic echoes were observed above 1330 oe. over a field range of a few hundred gauss due to the r.f. susceptibility decreasing. Elastic waves should still be observed above the range if enough power is available. The delayed pulses exhibited an erratic variation of amplitude with small variations in field.

The elastic signal echoes had a maximum amplitude with the rod oriented within  $2^{\circ}$  of the field direction, and a delay time of  $2.6 \mu$  seconds/cm. demonstrating that the elastic echoes are due to shear waves. Figure 3.2.2.

When the 2.4KMc/s pump is applied in the absence of a 1.2KMc/s signal input. Delayed incoherent elastic pulses, with the appearance of amplified noise are observed, on examination with filters etc., these pulses are found to have a frequency of 1.2KMc/s. With the signal pulses applied, and the application of the pump pulse, at the same end of the rod as the signal, timed to coincide with the first delayed elastic pulse. The second and longer delayed echoes are increased in amplitude figure 3.2.3.

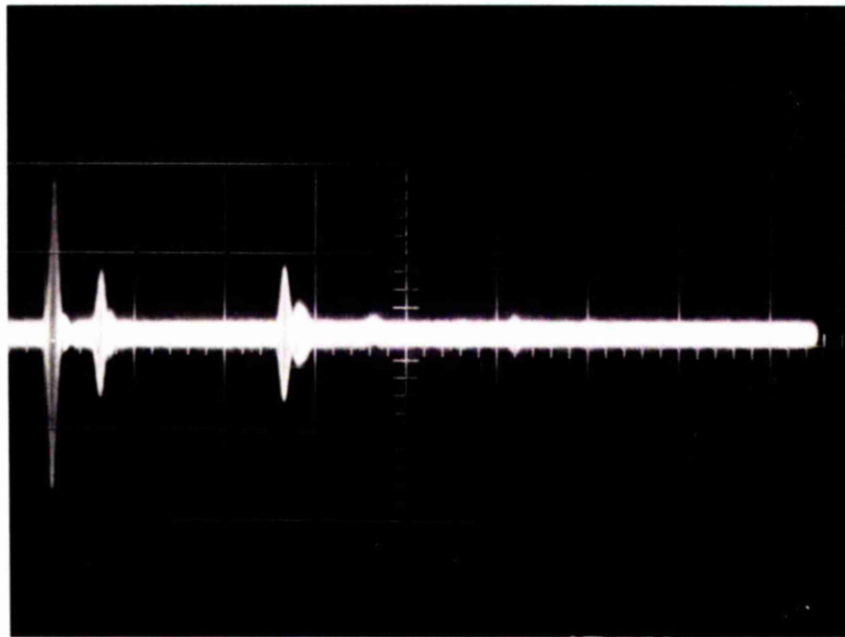


Figure 3.2.2. 1 volt/cm.  $2\mu\text{sec/cm}$ . Elastic echo train. First pulse, 1.2 KMc/s. signal applied,  $0.2\mu\text{sec}$  pulse width. Second pulse is an equipment peculiarity. The first and second elastic one port echoes are at 5.2 and  $10.4\mu\text{sec}$ . after the signal pulse respectively

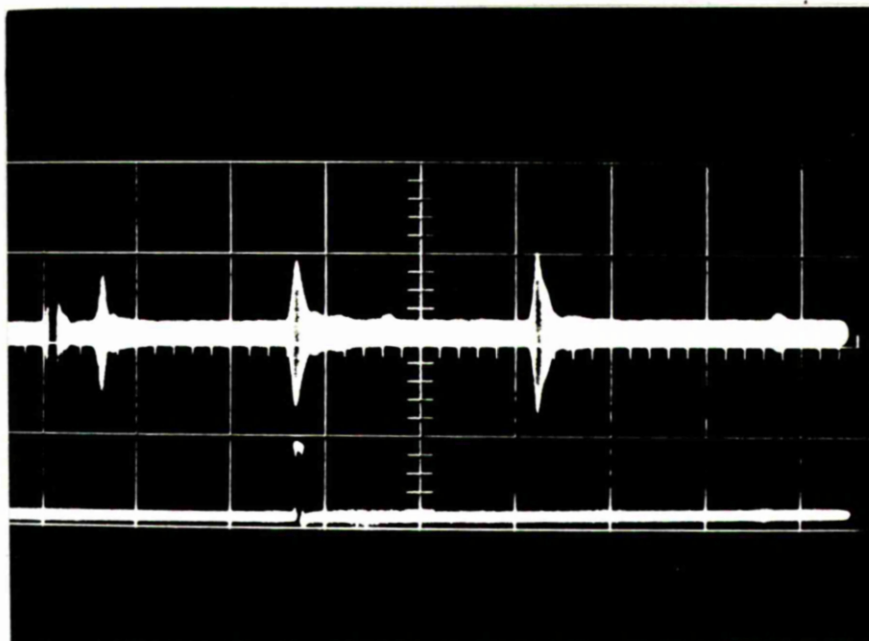


Figure 3.2.3.  $2 \mu$  sec/cm. 1 volt/cm. Parametric amplification of second elastic delayed echo, by applying the pump coincident with the first echo. One port observations, signal and pump applied from the same end. Signal frequency 1.2 KMc/s. pump frequency 2.4 KMc/s.

With the pump applied at the opposite end of the rod, and its time of application arranged to coincide with the arrival of the first elastic wave packet at the pump end of the rod, then amplification of all the delayed pulses is observed. The angle for maximum amplification being with the rod aligned to about  $3^{\circ}$  with respect to the field. Figure 3.2.4.

All the experimental measurements were performed at a magnetic field 1358 oe. Figure 3.2.5. Shows the variation of the amplitude of the first delayed elastic echo for increasing input power, with no pump applied. The signal frequency was 1.2KMc/s and pulse length 0.2  $\mu$  seconds. The plot is almost linear till the input exceeds -5 dbm., when saturation occurs. This power level is of the same order as that required to saturate one port magneto-elastic pulses. The insertion loss in the linear portion is  $\sim 70$  db compared with  $\sim 40$  db for magneto-elastic waves.

Figure 3.2.6. Shows a plot of attenuation or insertion loss of the first elastic echo with increasing pump power for different signal input levels. The pump being applied at the opposite end of the rod from

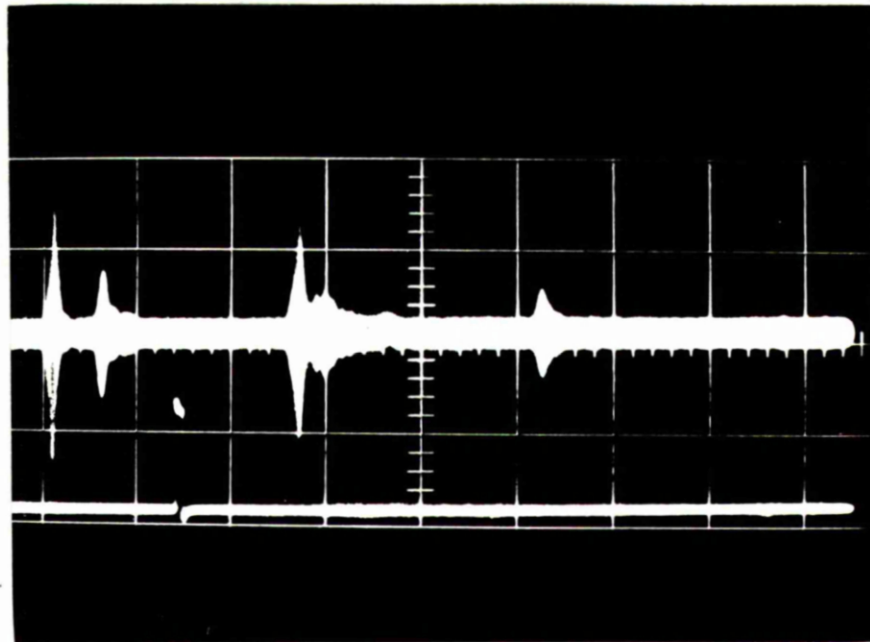


Figure 3.2.4.  $2 \mu\text{sec/cm}$ .  $1 \text{ volt/cm}$ . Parametric amplification of the first elastic echo, pump applied when the elastic pulse is at the opposite end of the rod from the signal coupler. Signal frequency  $1.2 \text{ KMc/s}$ , pump frequency  $2.4 \text{ KMc/s}$  One port observations.

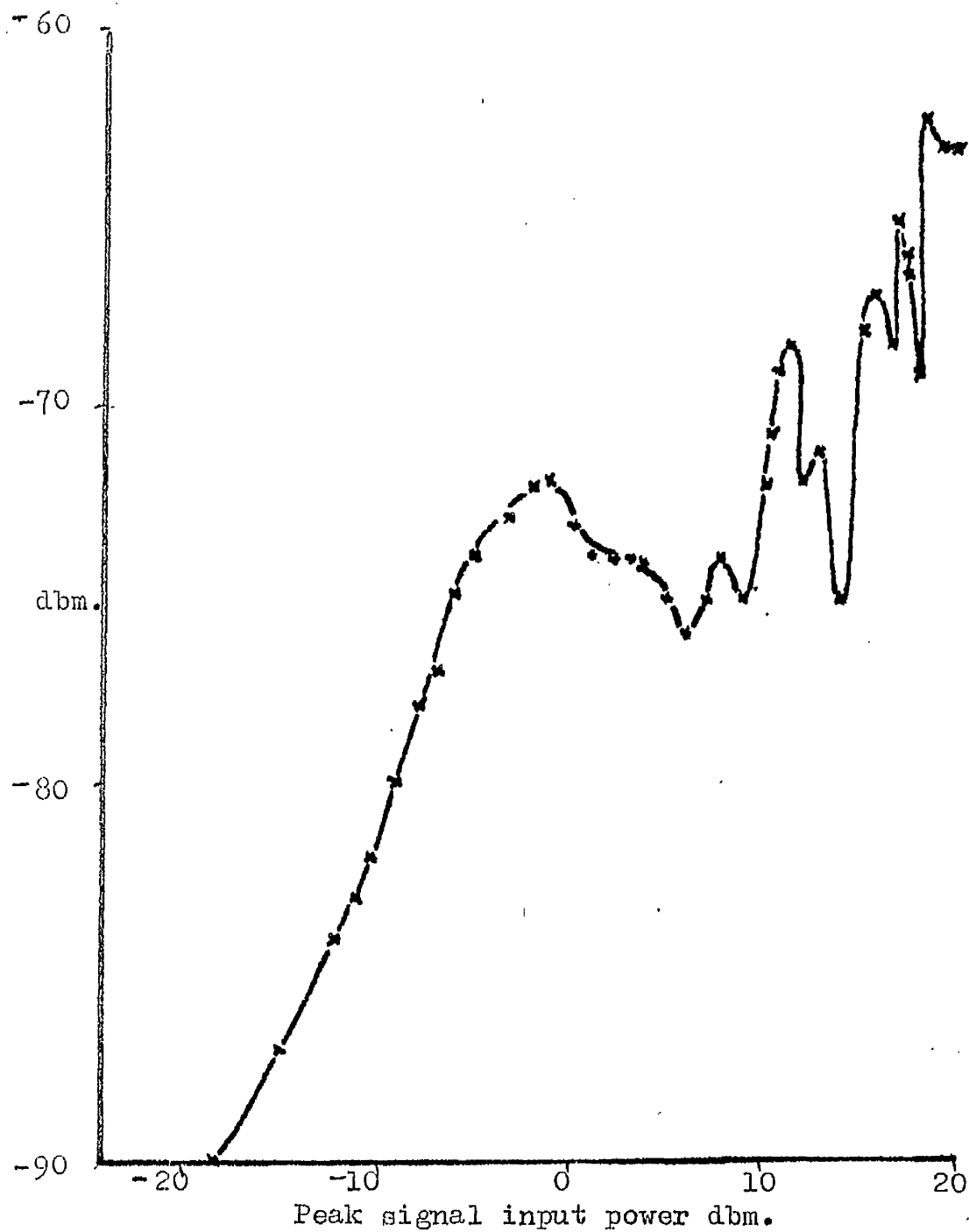


Figure 3.2.5. Plot of signal output power ~ Signal input power.  
For first delayed elastic echo. Signal frequency 1.2KMc/s.  
One port operation.

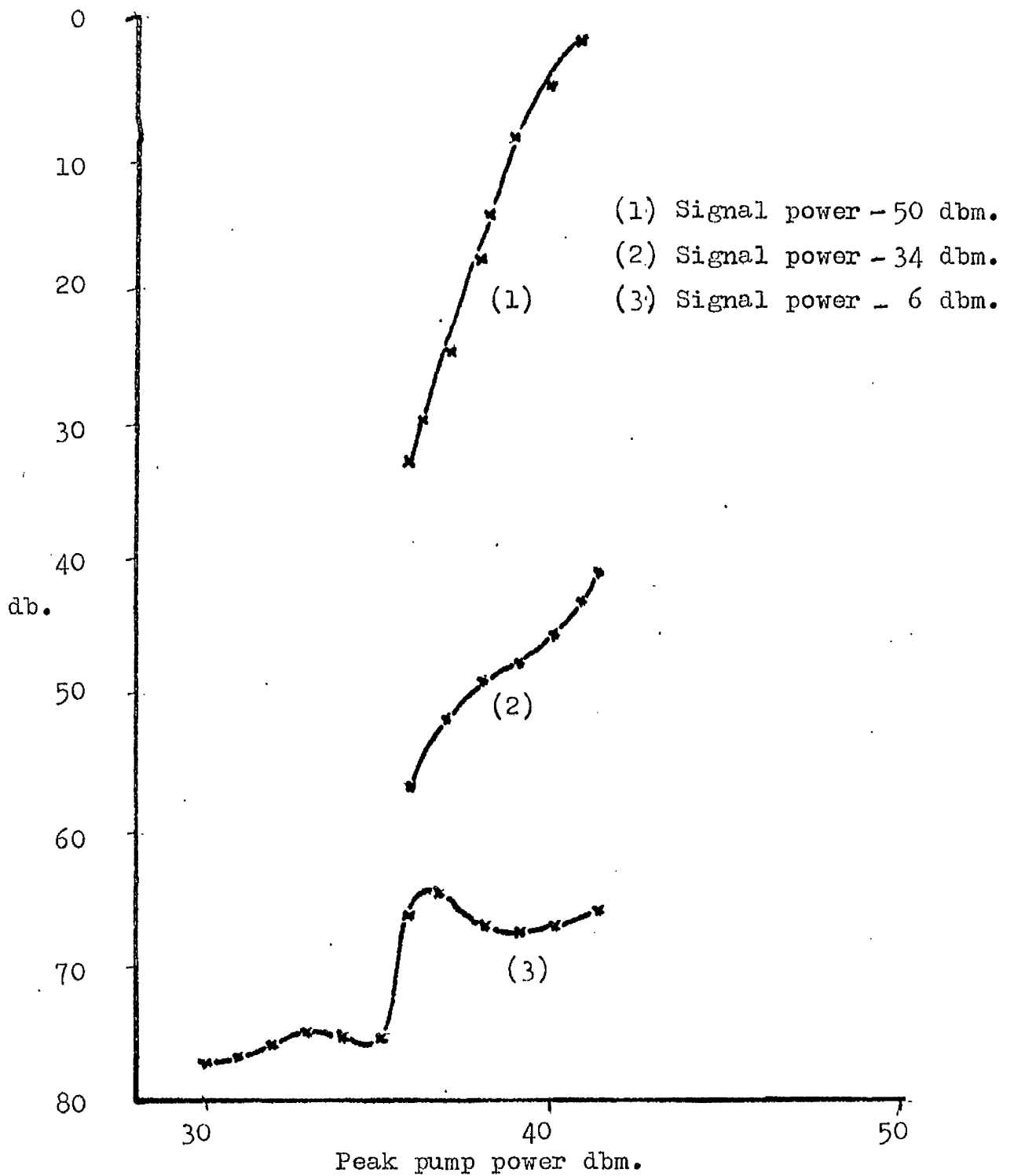


Figure 3.2.6. Plot of attenuation of first parametrically amplified elastic echo vs Peak pump power. Signal frequency 1.2 KMc/s. Pump frequency 2.4KMc/s. Rod axially magnetised. Pump and signal pulses applied at opposite ends of the rod.

the signal. Curve (1) saturates at a pump power of 40 dbm, (2) and (3) are saturated over the range in which observation was possible.

Figure 3.2.7. Shows a plot of attenuation or insertion loss of the 2nd elastic echo amplified by applying the pump at the same end of the rod as the signal and being timed to coincide with the return of the first elastic echo to the signal end of the rod. This exhibits the same saturation characteristics as those in the previous plot.

The attenuation is greater, due to the longer delay. The acoustic attenuation at 450 Mc/s has been measured as  $0.98 \text{ db}/\mu \text{ second}$  and at  $1.2 \text{ KMc/s}$  as  $2.47 \text{ db}/\mu \text{ second}$ . These values are rather large for YIG,  $1 \text{ db}/\mu \text{ sec.}$ , being typical at  $1.0 \text{ Gc/s}$ . Figure 3.2.8. shows a plot of signal power output against signal power input for the 1st elastic echo for two values of pump power. Figure 3.2.9. shows a plot of signal power output against signal power input for the amplified 2nd, elastic echo, excited by pumping the first delayed pulse.

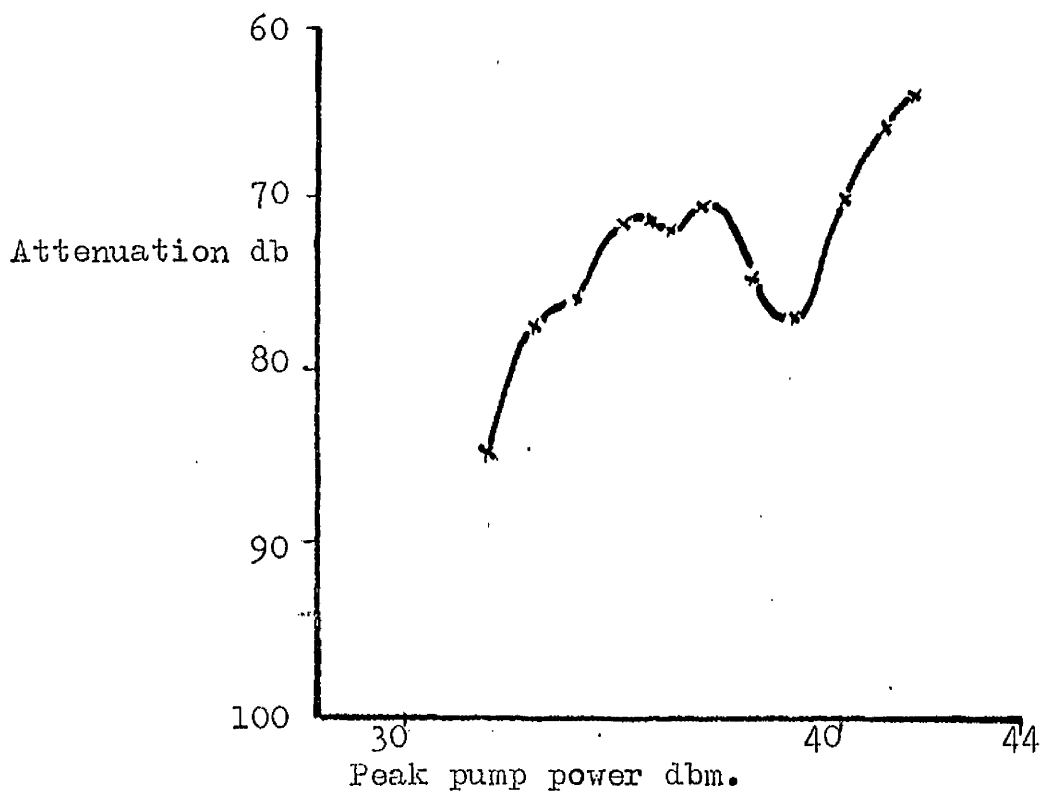


Figure 3.2.7. Plot of attenuation of parametrically amplified second elastic echo.  $\sim$  Peak pump power. Signal input level 1.3 dbm. Second echo amplified by applying pump at the signal input end of the rod at a time coincident with the first echo

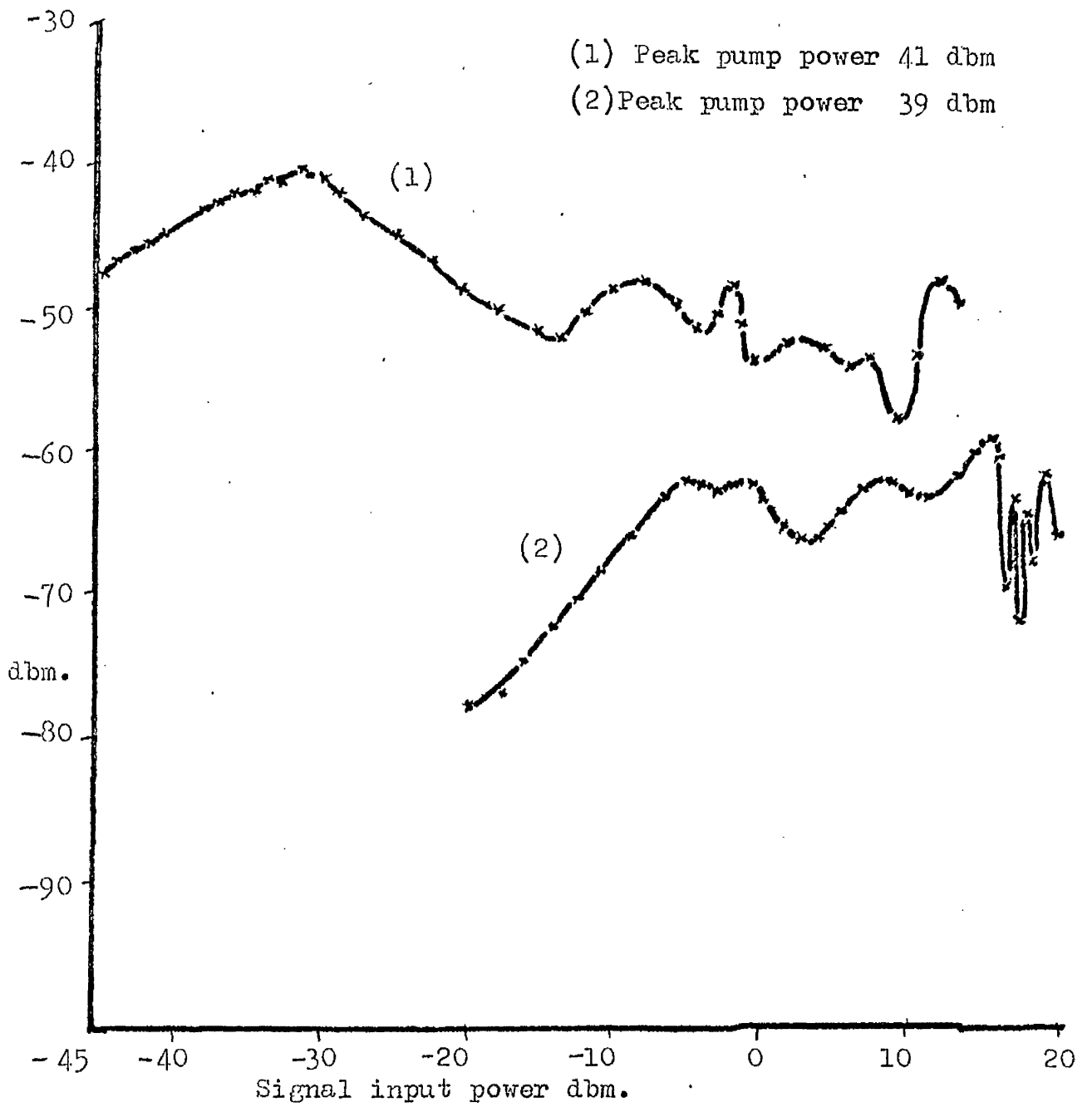


Figure 3.2.8. Plot of signal power output ~ signal power input for the parametrically amplified first elastic echo. Pump power constant.

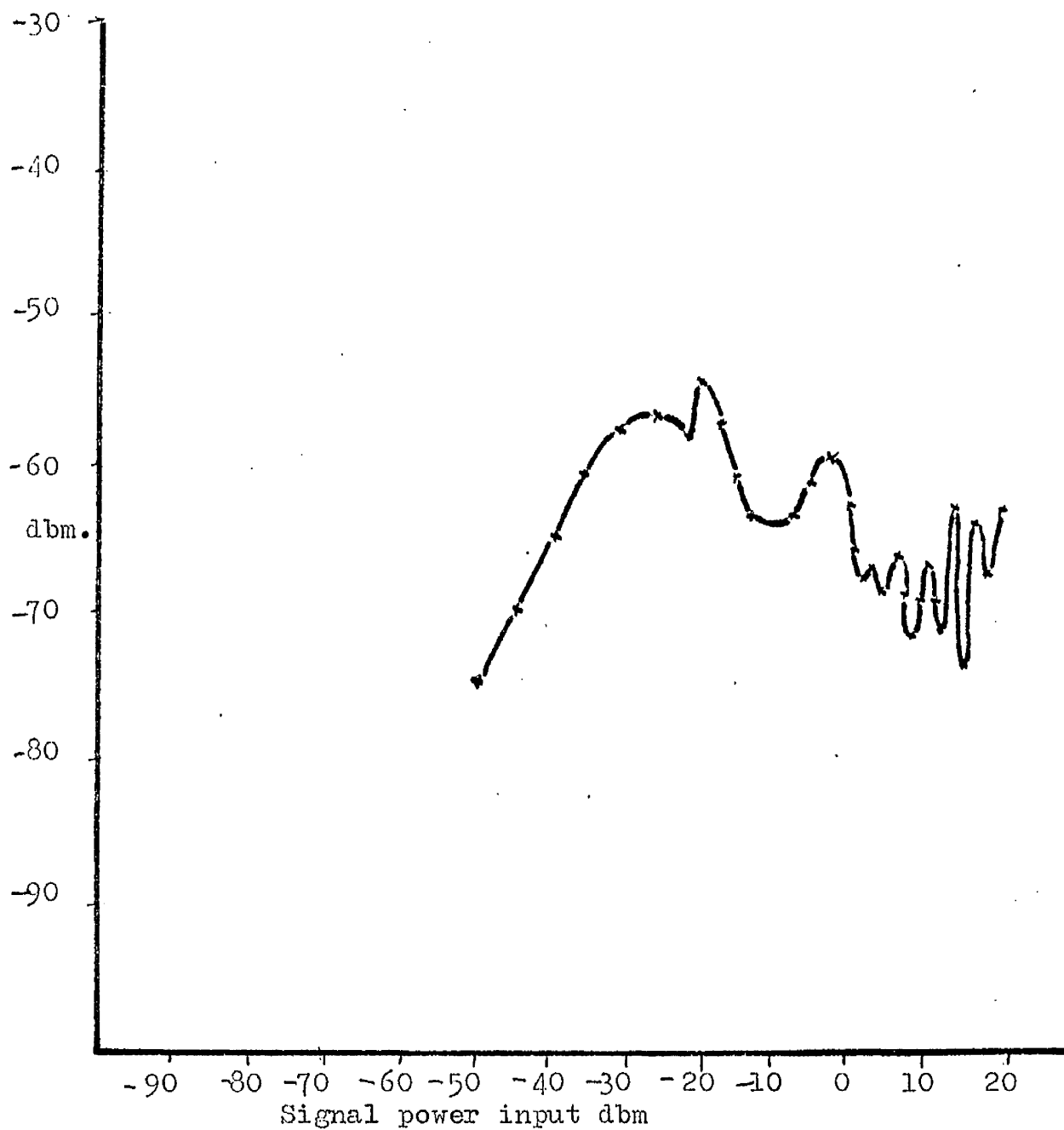


Figure 3.2.9. Plot of signal power output  $\sim$  signal power input, for the parametrically amplified second elastic echo. Peak pump power constant at 41 dbm,

The onset of saturation can be clearly seen in both graphs. The level at which saturation starts is dependent on the signal input power and the applied pump power. So that saturation occurs not only in the initial excitation of elastic waves but also in the pumping mechanism.

It was found with the arrangement used, to be impossible to amplify the delayed pulses whilst they were purely elastic, also the pulse with which the pump application is timed to coincide is not amplified.

**Parametric Amplification of Magneto-elastic Waves:-**

Magneto-elastic waves are excited as outlined in section 2.3.0. The experimental procedure was as follows, with the rod axis aligned with the external field and a 1.2KMc/s signal input, the external field was increased until magneto-elastic delayed pulses were observed. The 2.4KMc/s pump was then applied and parametrically amplified delayed pulses observed with delay of approximately  $2t_p$  figure 3.3.1. The angle of orientation of the rod was then changed with respect to the field, to give a maximum amplitude of the amplified pulse. With each change in the time of application of the pump the orientation was checked, to ensure that the parametrically amplified pulse had maximum amplitude. Figures 3.3.2, 3.3.3, and 3.3.4.

The results of a series of experiments performed with the rod aligned so as to give maximum amplitude of the parametrically amplified pulse, are shown in figures 3.3.5 - 3.3.12, for increasing values of field. The plots show the variation of amplitude of the parametric pulse with the time of application of the pump

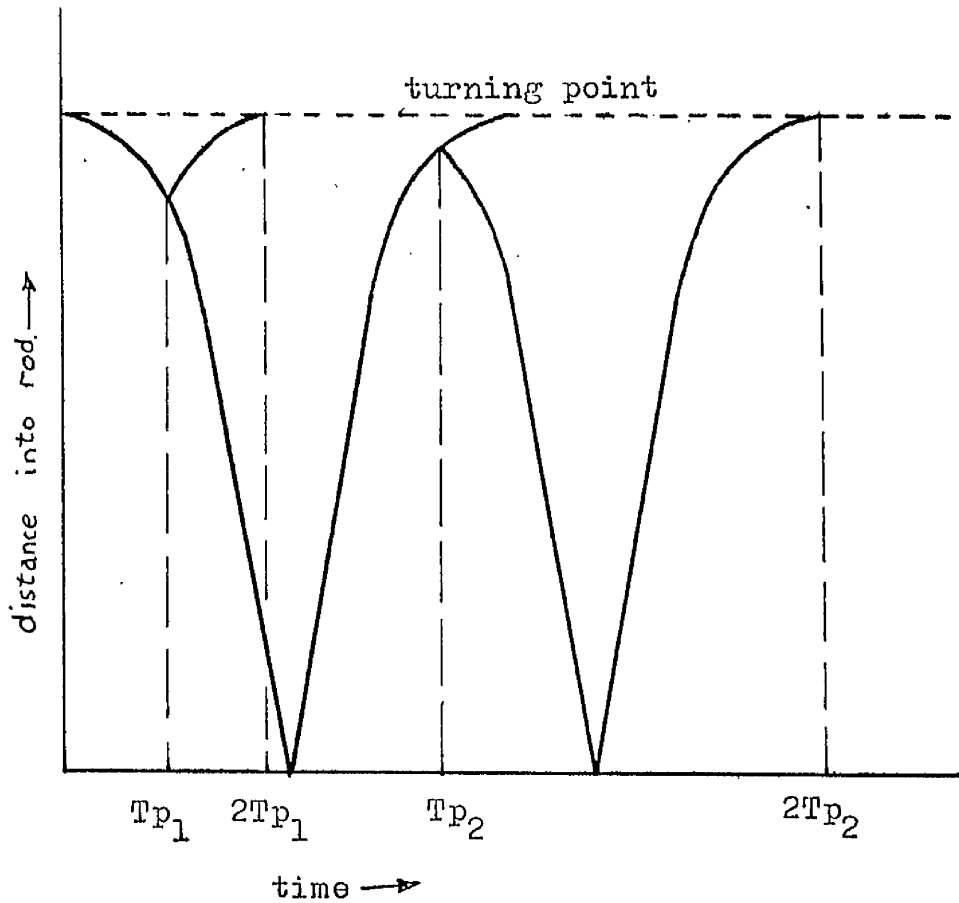


Figure 3.3.1. Parametric amplification of magnetoelastic waves.  $T_p$  is the time of application of the pump pulse. The signal is applied at  $T=0$ .

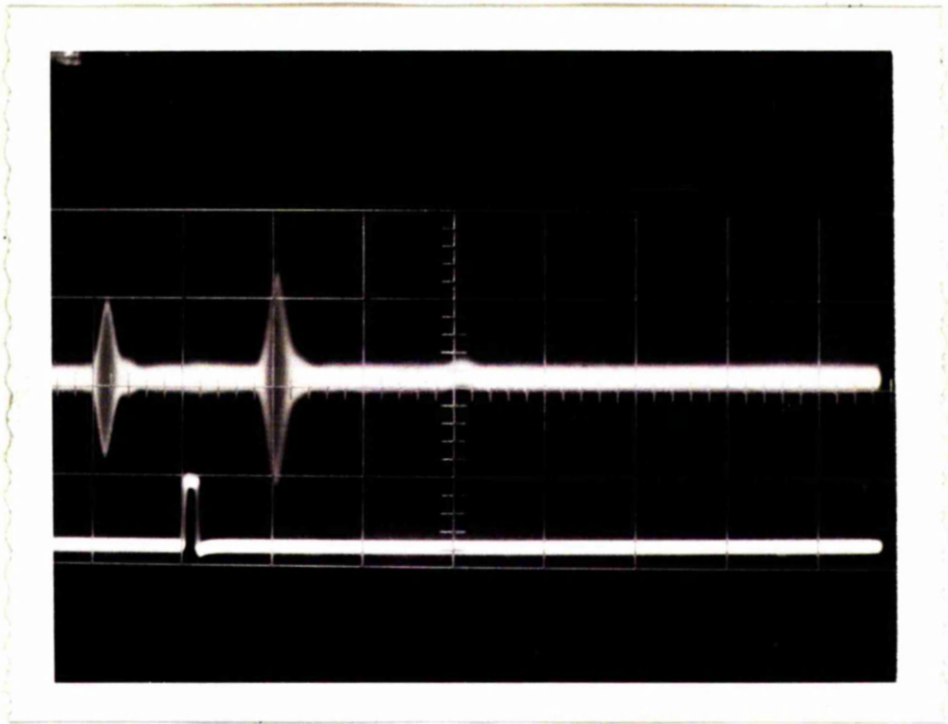


Figure 3.3.2.  $1 \mu\text{sec}/\text{cm.}$ ,  $1 \text{ volt}/\text{cm.}$  Parametric amplification of magnetoelastic waves, magnetoelastic delay  $1.2 \mu\text{sec.}$  Upper trace,  $1.2 \text{ KMc}/\text{s}$ ,  $0.2 \mu\text{sec}$  signal and amplified echo. Lower trace,  $2.4 \text{ KMc}/\text{s}$ ,  $0.2 \mu\text{sec}$  pump pulse. Rod axis is at  $9^\circ$  to the external field.

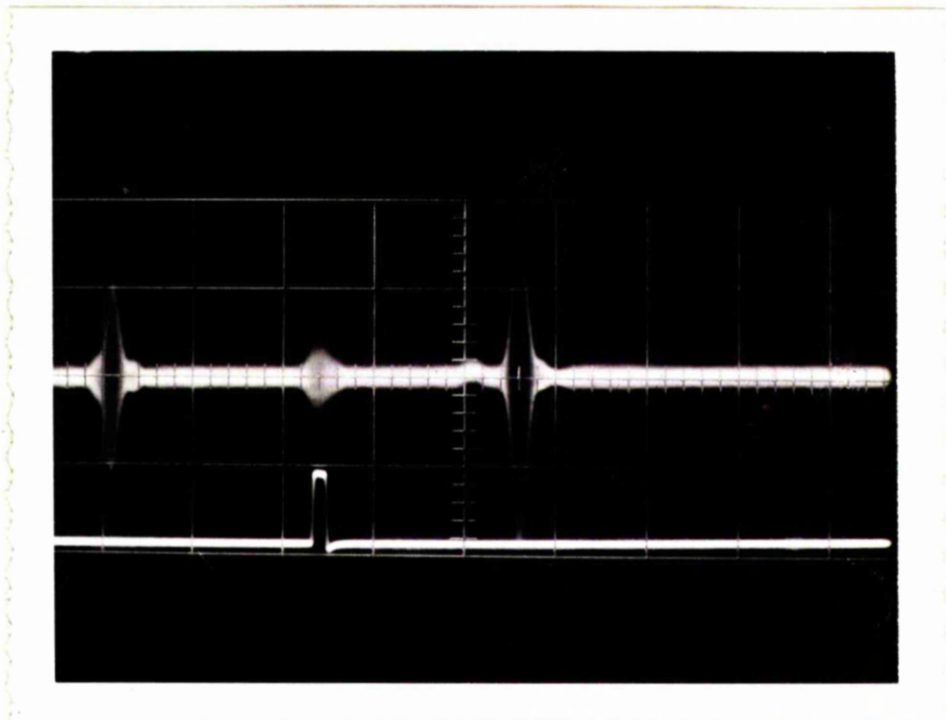


Figure 3.3.3. As in fig 3.3.2. but magnetoelastic delay  $3\mu\text{sec}$ .  
Orientation of rod axis to the external field is  $8^\circ$ .

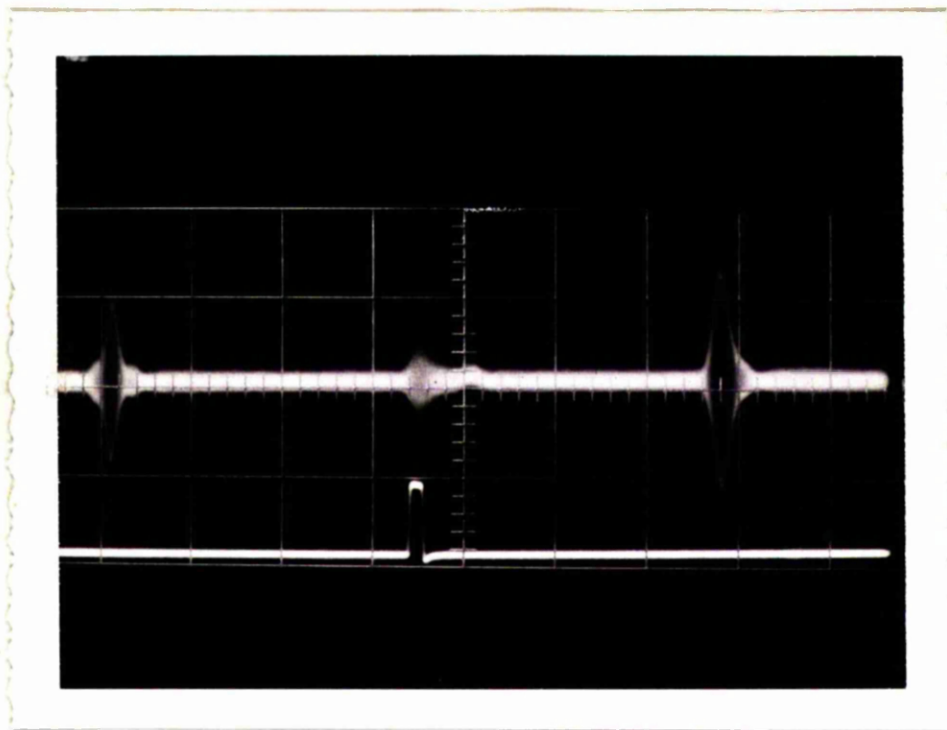


Figure 3.3.4. As in fig. 3.3.2., but magnetoelastic delay  $5\mu$  sec.  
Orientation of rod axis,  $6^\circ$  to the external field.

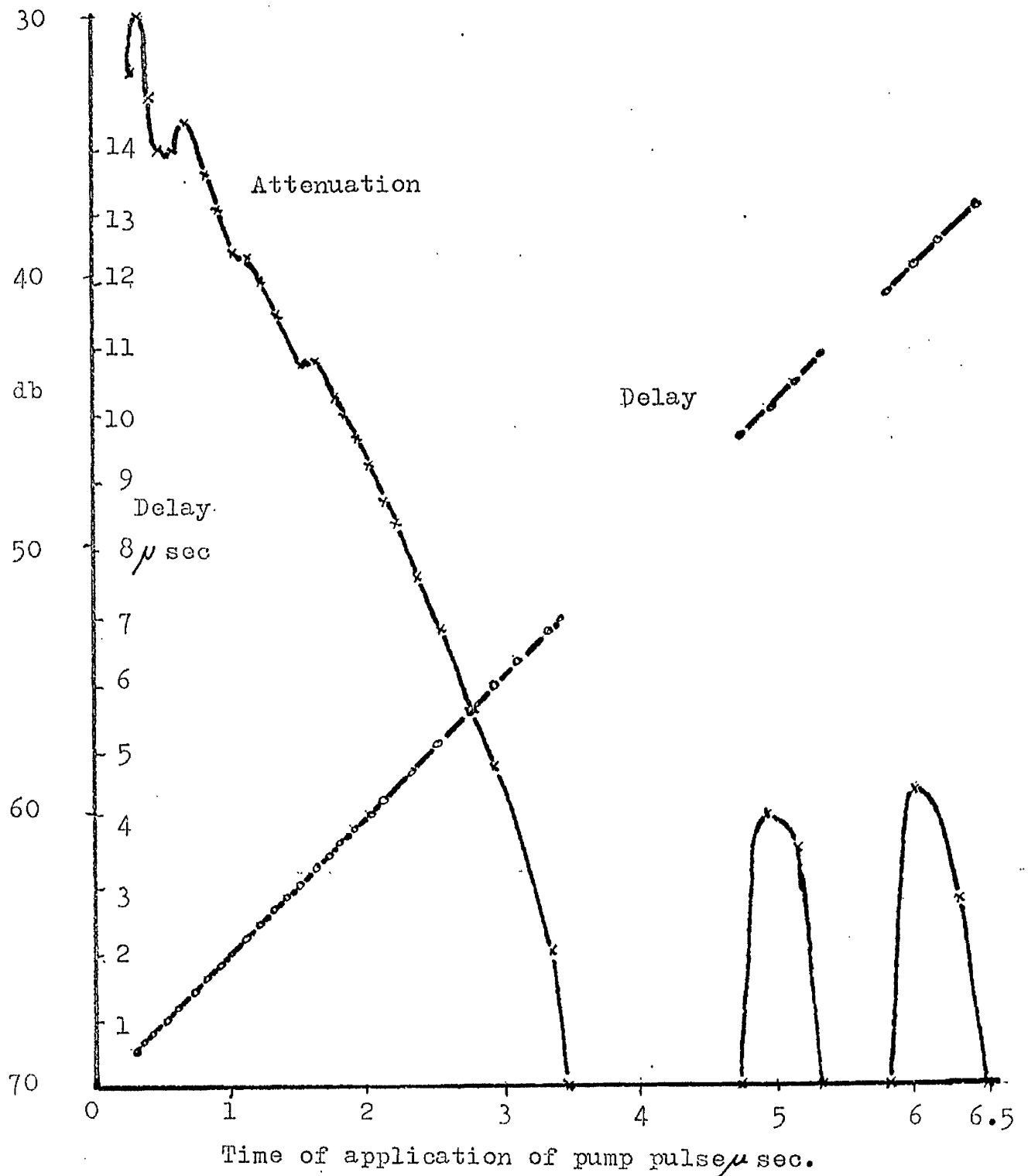
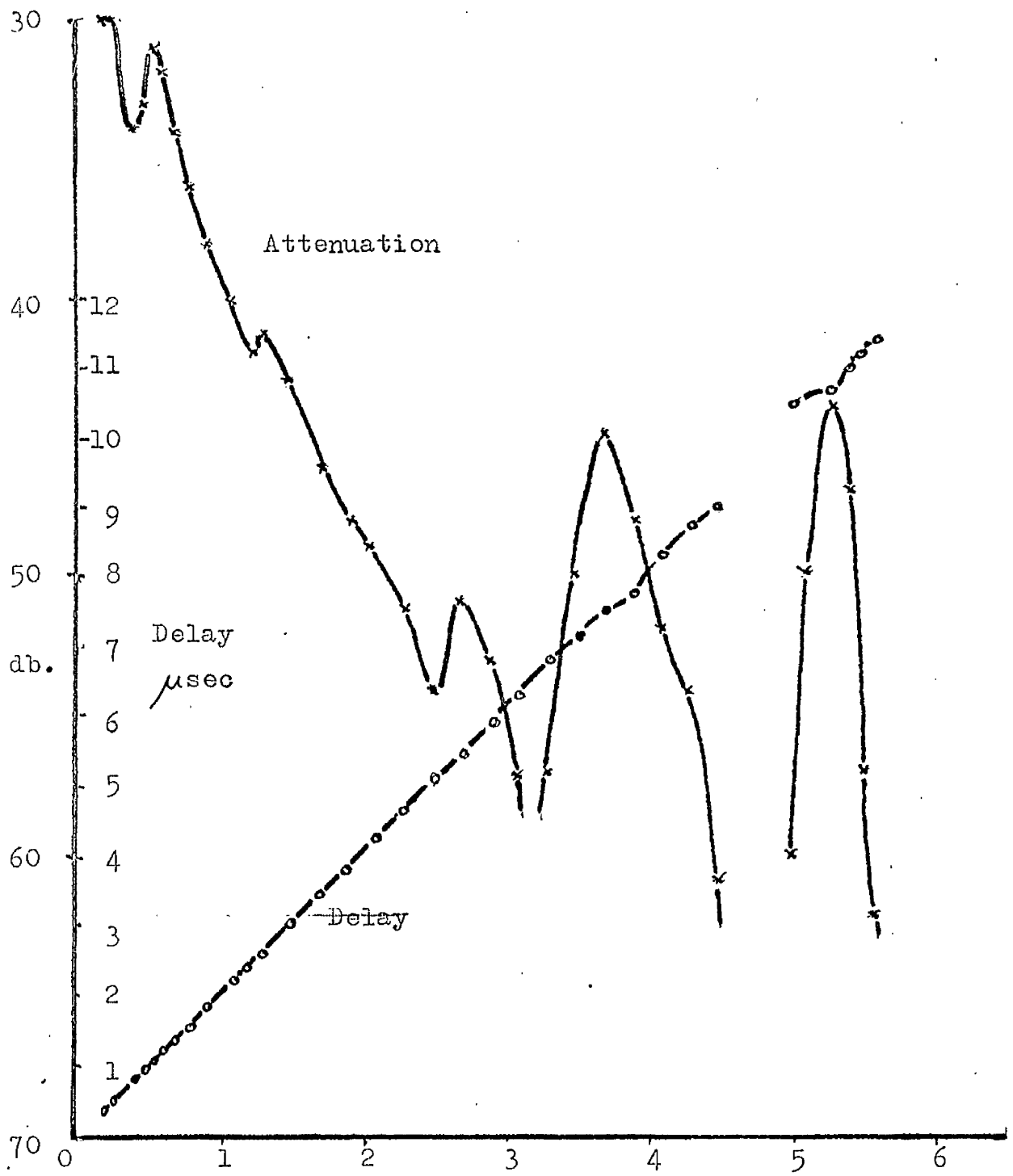


Figure 3.3.5. Plot of attenuation of amplified magneto-elastic pulse, and delay of amplified magnetoelastic pulse against time of application of pump pulse. Rod axially magnetised. magneto-elastic delay  $7.0 \mu\text{sec}$ , attenuation 63 db. Orientation with respect applied magnetic field  $14^\circ$ .



Time of application of pump pulse  $\mu$ sec.

Figure 3.3.6. Plot of attenuation of amplified magnetoelastic pulse, and delay of amplified magnetoelastic pulse against the time of application of the pump pulse. Rod axially magnetised. Magnetoelastic delay  $6.0 \mu$ sec., attenuation 60 db. Orientation of rod to the external field  $18^\circ$ .

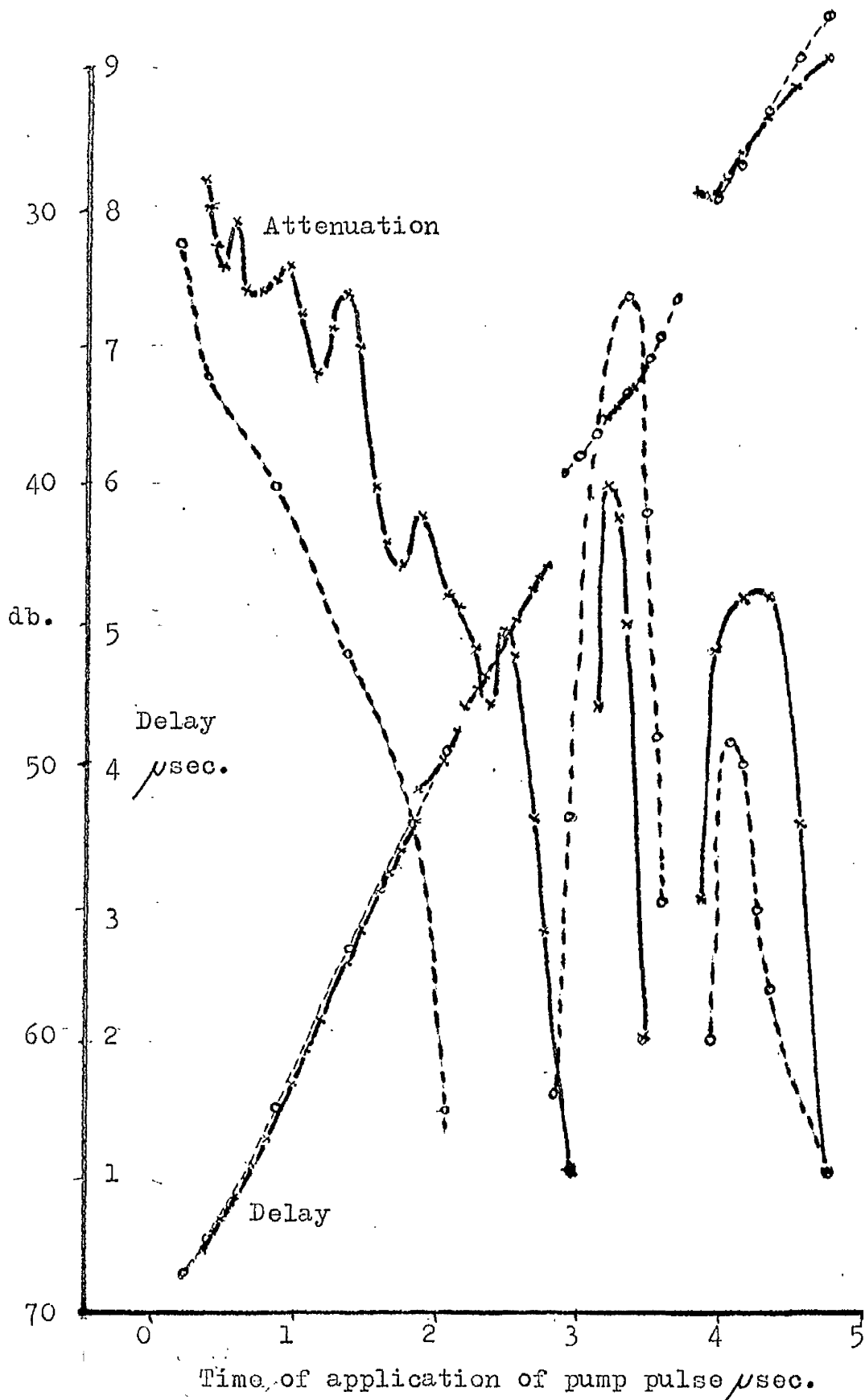


Figure 3.3.7. Plot of attenuation of amplified magnetoelastic pulse, and delay of amplified pulse against time of application of pump pulse. Rod axially magnetised. Magnetoelastic delay  $5 \mu\text{sec.}$ , attenuation 47 db. Orientation of rod to applied field —  $21^\circ$  ---  $6^\circ$ .

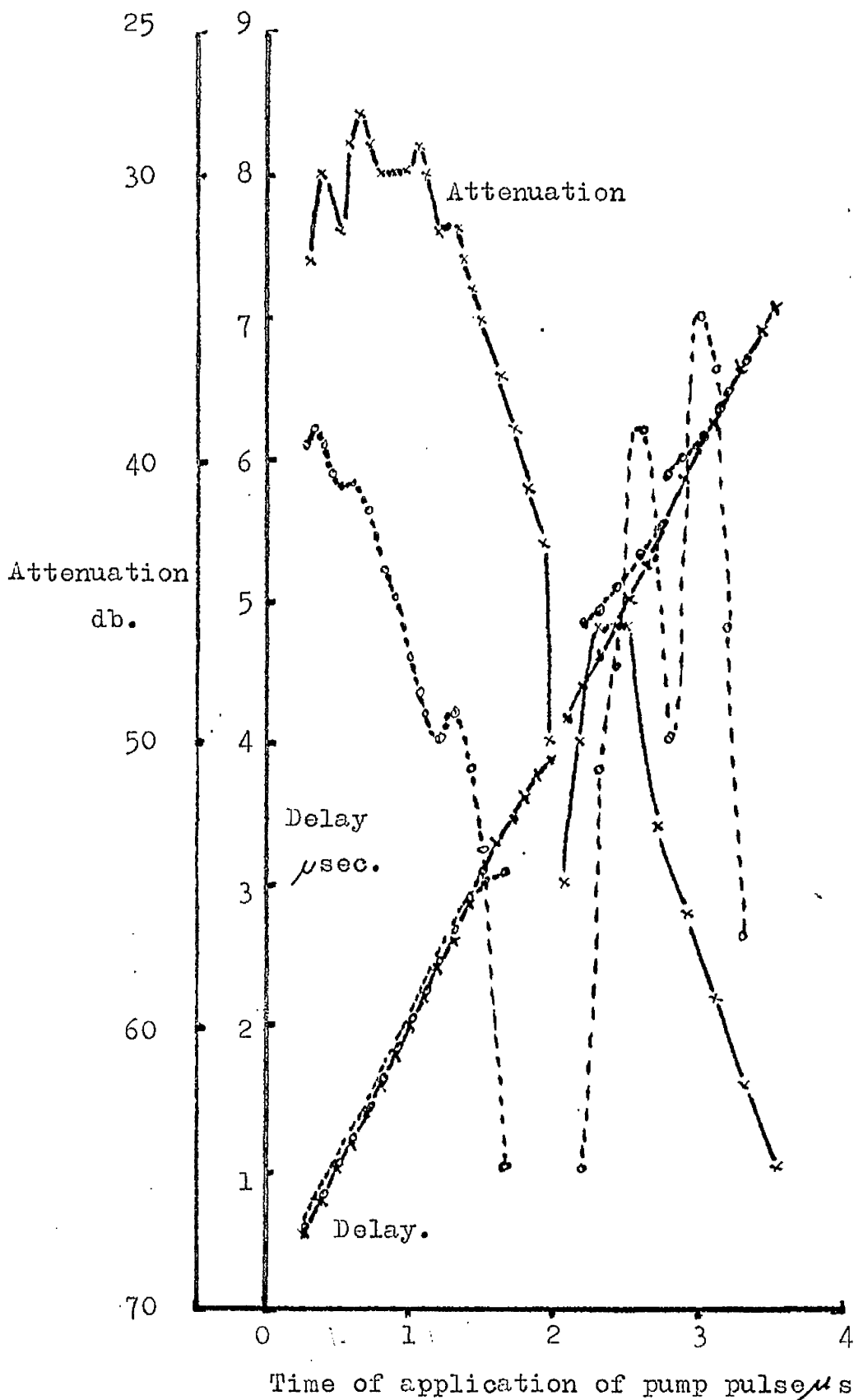


Figure 3.3.8. Plot of attenuation of amplified magnetoelastic pulse, and attenuation of amplified pulse against time of application of pump pulse. Rod axially magnetised. Magnetoelastic delay  $4 \mu$ sec., attenuation 41 db.. Orientation of rod to applied field —  $30^\circ$ , - - -  $8^\circ$ .

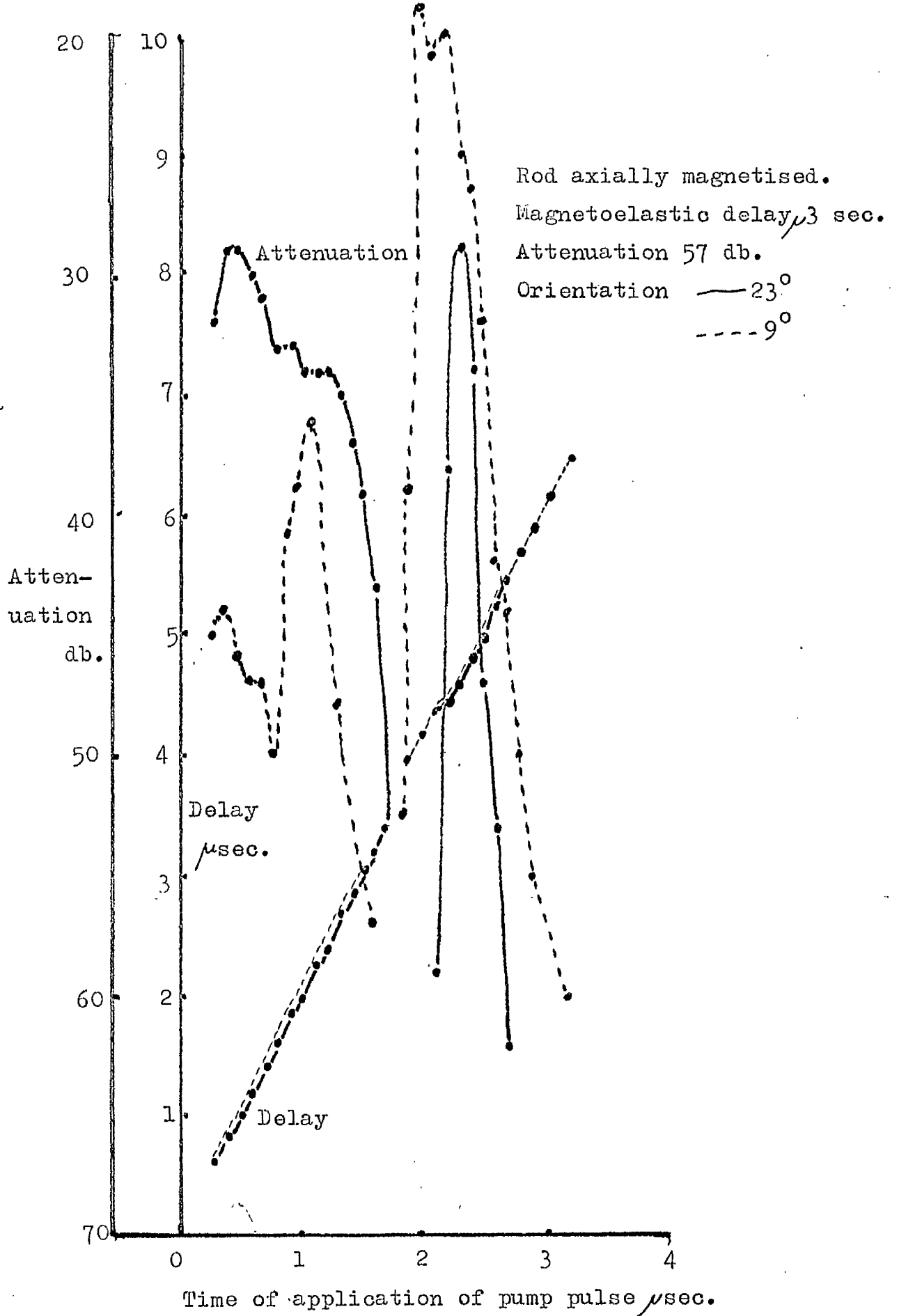


Figure 3.3.9. Plot attenuation of amplified magnetoelastic pulse, and delay of amplified pulse against time of application of pump pulse.

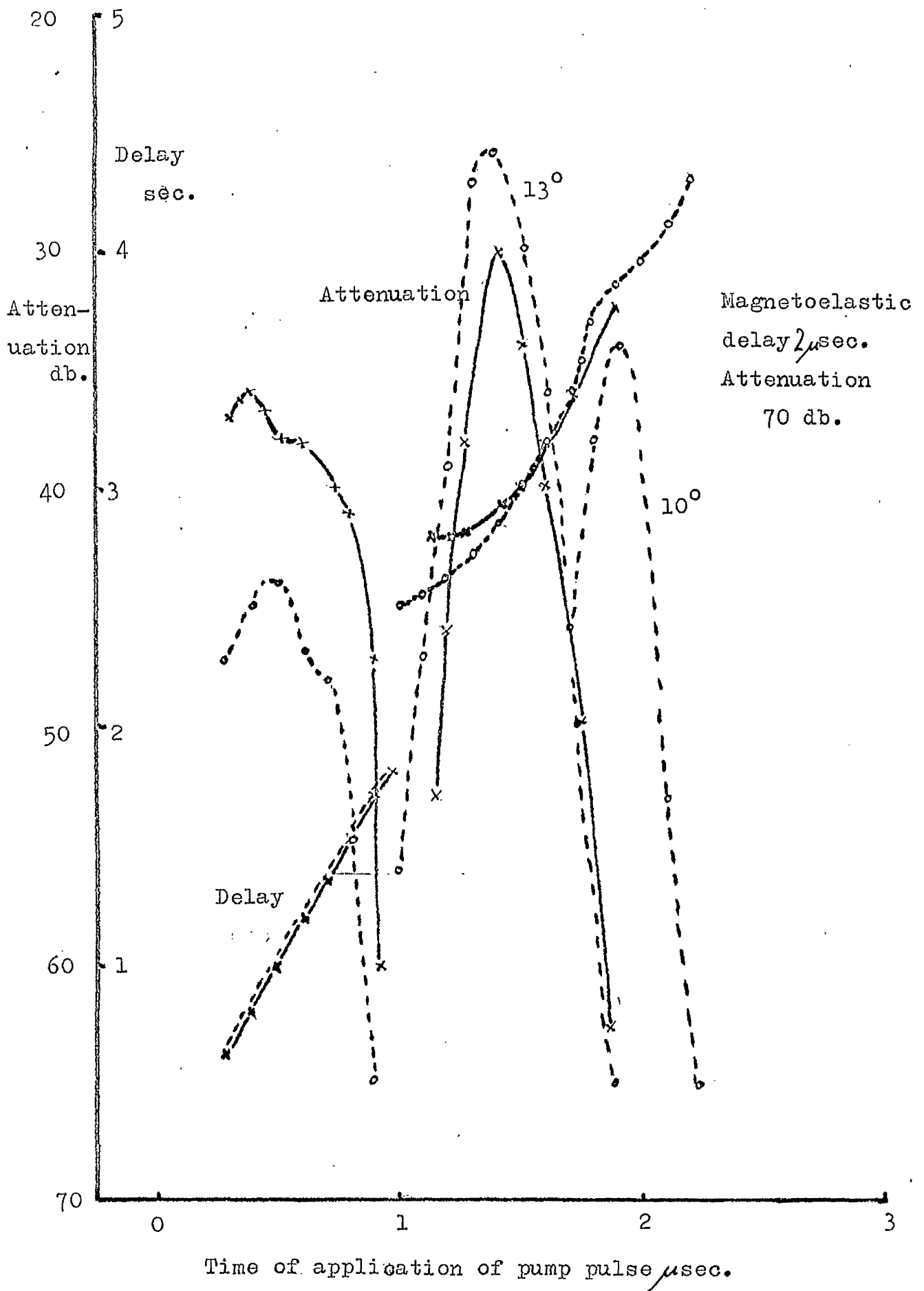


Figure 3.3.10. Plot of attenuation of amplified magnetoelastic pulse, and delay of amplified pulse against time of application of pump pulse. Orientation of rod to applied field —x—19° ---13°

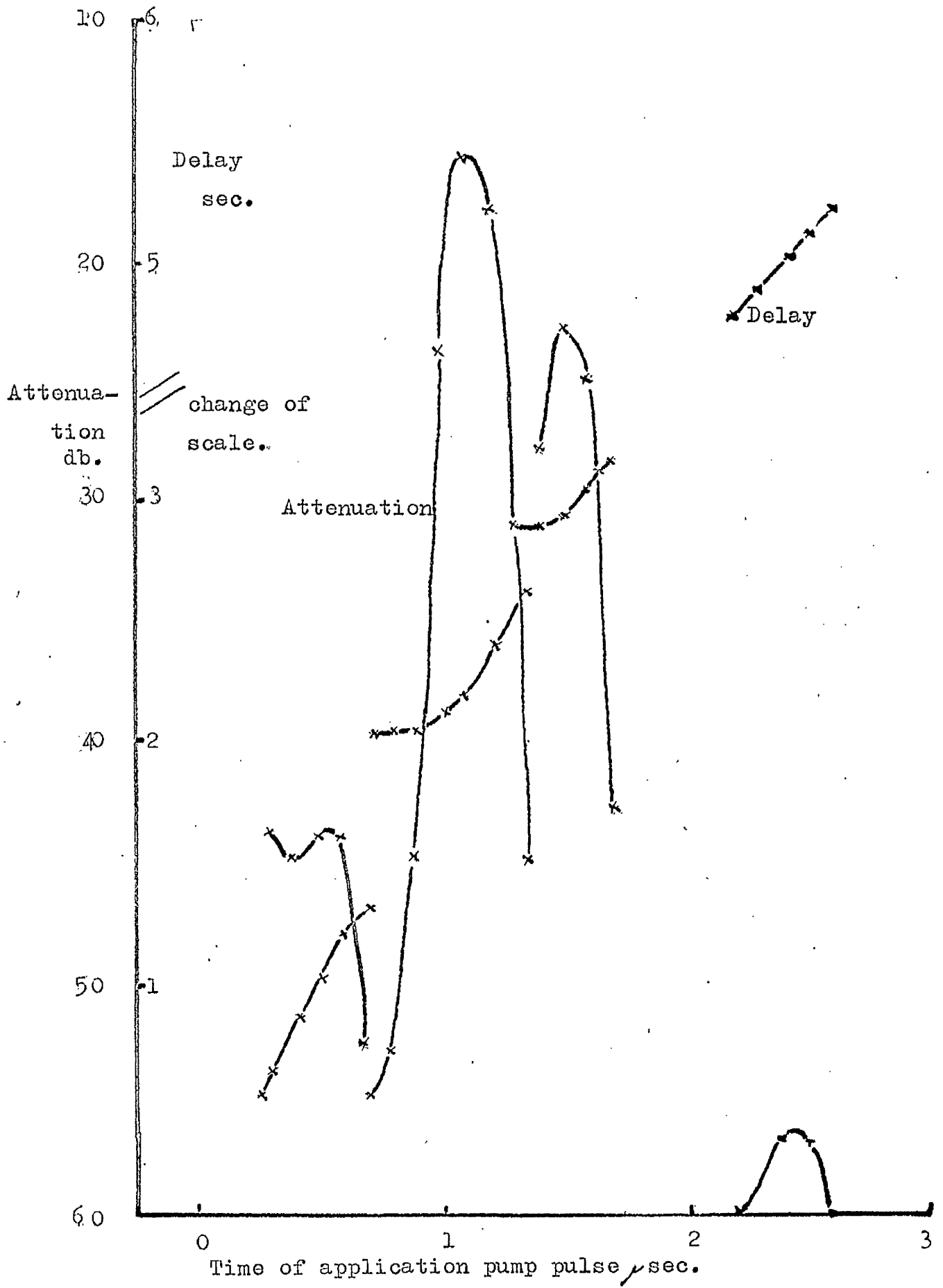


Figure 3.3.11. Plot of attenuation of amplified magnetoelastic pulse, and delay of amplified pulse against time of application of the pump pulse. Magnetoelastic delay  $1.5 \mu\text{sec}$ . Atten. 45db.

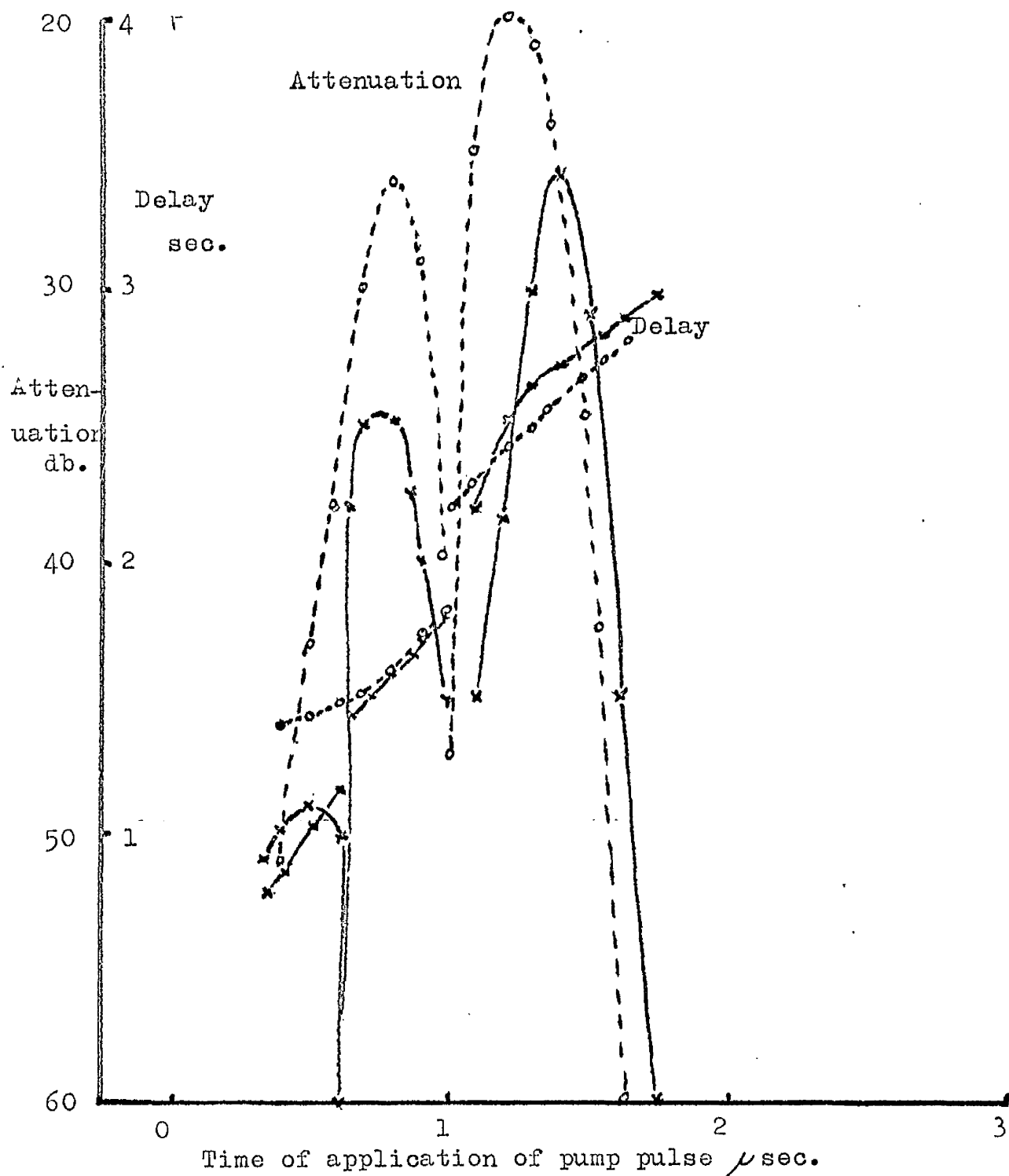


Figure 3.3.12. Plot of attenuation of amplified magnetoelastic pulse, and delay of amplified pulse against time of application of the pump pulse. Magnetoelastic delay  $\mu$ 1.0 sec. Attenuation 38 db. Orientation of rod to applied magnetic field,  $\sim$ x $17^\circ$  --x $10^\circ$ .

pulse. The pump power used to obtain these results was 30 dbm peak, pulse width  $0.2 \mu$  secs., and a signal pulse width of  $0.2 \mu$  secs., peak power -27 dbm.

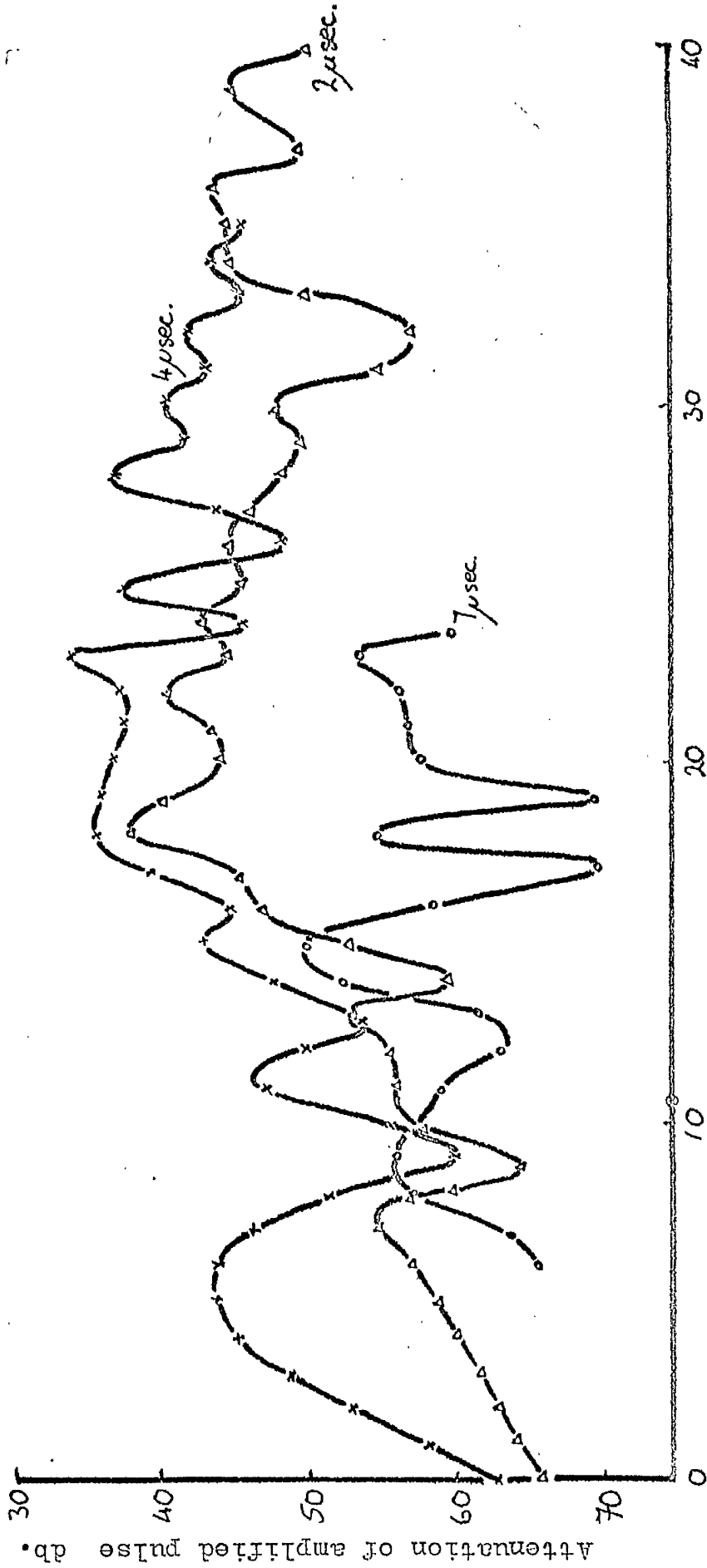
The initial part of the curves, that is, with the time of application of the pump of less than half the delay time of the magneto-elastic pulse, the plot is typical of that obtained for the parametric amplification of magneto-static waves. With increasing field the delay range of this part of the graph decreases, due to the shorter spin wave path, the amplitude also decreases with increasing internal field gradient which results in less efficient excitation of spin waves and possibly a reduction of the coupling between the pump magnetisation and the spin wave. The delay exhibited by the parametrically amplified wave in the region is seen to be  $2 t_p$  where  $t_p$  is the time of application of the pump with respect to the signal.

In the remainder of the plot, with the time of application of the pump greater than half the magneto-elastic delay, there are generally two peaks observable in the amplitude graphs. These can be seen to increase in amplitude with increasing field. Since the path of

the magneto-elastic wave propagating with the rod at an angle to the external field is not known, it is not possible to estimate where in the magneto-elastic path these two peaks occur.

The delay of the amplified echo deviates from  $2\tau$  in this part, the deviations occurring at times corresponding to the short delay slope of the two peaks. The amplification increases with increasing field. The parametric process will be dependent on the difference in wave number of the two components of the magneto-elastic wave and hence will depend on the internal field gradient at that point.

Figure 3.3.13. Shows a plot of amplified pulse amplitude against angle of field with respect to the axis for three different external field values. Note that amplified pulse can be observed in some cases to about  $40^\circ$  of axis. The only definite information to be obtained from these plots is that the threshold for amplification is less with the field at an angle other than to the axis. No increase in the amplitude of the magneto-elastic delayed echo was observed on application of the pump.



Orientation of rod axis to applied magnetic field in  $^{\circ}$

Figure 3.3.13. Plot of attenuation of amplified magnetoelastic echo against

orientation of rod axis to applied magnetic field.

Magnetoelastic delay	$7\mu\text{sec.}$	attenuation	62 db.	pump applied at	$1.9\mu\text{sec.}$
"	"	"	41 db	"	"
"	"	"	70 db	"	"
"	"	"	"	"	"
"	"	"	"	"	"

Figure 3.3.14. Shows a plot of gain against peak pump power. Curve (a) shows the amplification characteristics of a magneto-elastic amplified pulse when the magnetic field and time of application of the pump are optimised for maximum gain. Curve (b) shows the amplification characteristics of a magneto-elastic amplified pulse under non optimum conditions.

Both curves show the same characteristics, linear increase of gain with applied pump power, followed by saturation and turnover. Note that in case (a) net gain occurs with applied pump powers greater than 21.5 dbm or 140 mW.

Figure 3.3.15. Shows a plot of signal power out against signal power in, for different pump levels. All the curves show linear gain followed by saturation and in some cases turnover. The signal input required to saturate, decreases with increasing pump power. The process saturation is a function both of pump and signal powers.

The amplification mechanism is thought to be due to one of those described by Auld,<sup>19</sup> between two branches in the magneto-elastic dispersion, it remains to determine under what conditions each has the lowest threshold.

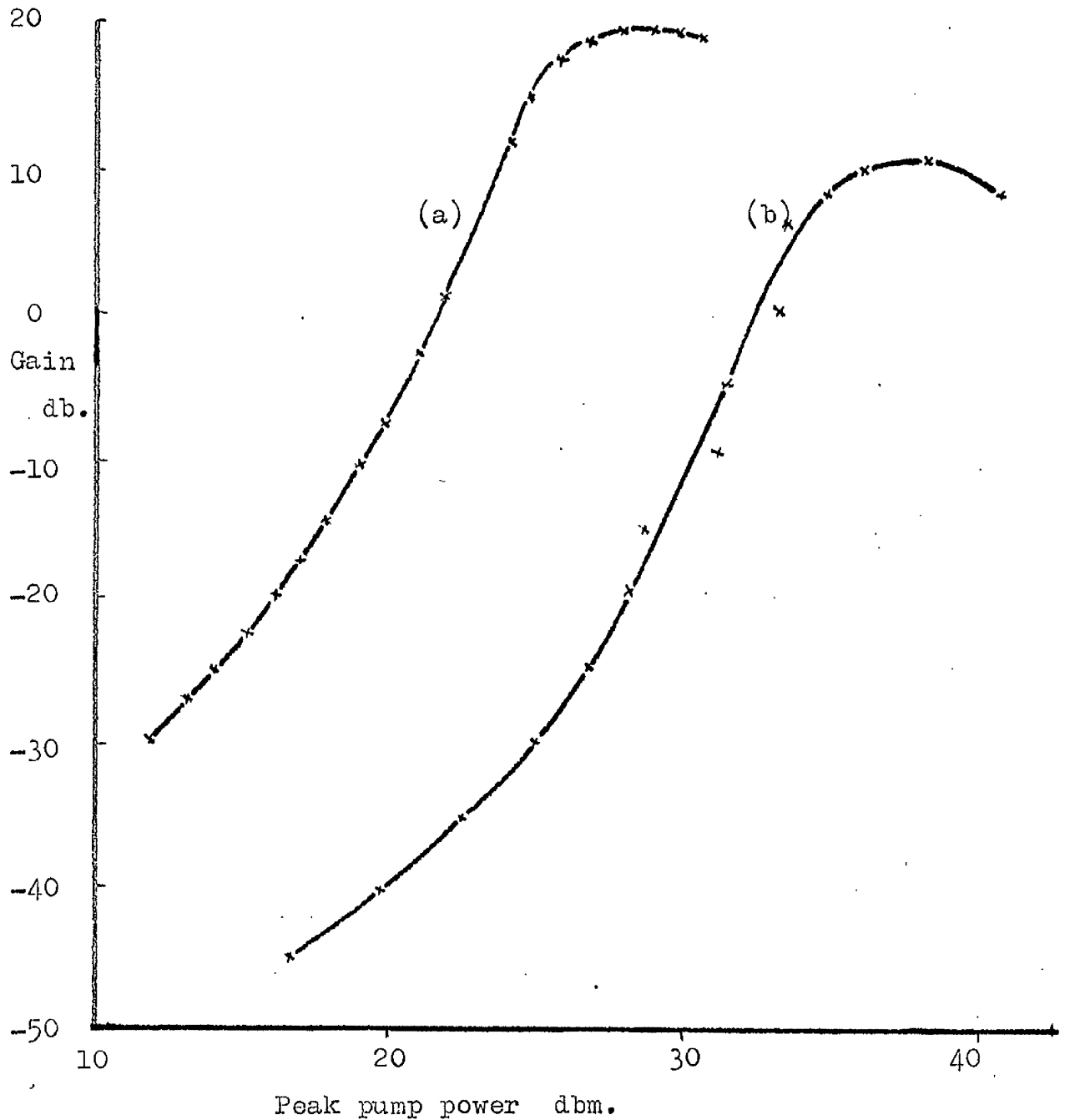


Figure 3.3.14. Plot of gain against peak pump power, magneto-elastic amplification. Signal frequency 1.2 KMc/s., pump frequency 2.4 KMc/s., pulse widths  $0.2 \mu\text{sec.}$ . (a), Signal input power -35 dbm., applied magnetic field 817 oe., orientation of rod axis to the field  $10^\circ$ , delay of amplified pulse  $2.8 \mu\text{sec.}$  (b), Signal power -41 dbm., applied field 825 oe., orientation  $9.2^\circ$ , delay of amplified pulse  $2.2 \mu\text{sec.}$

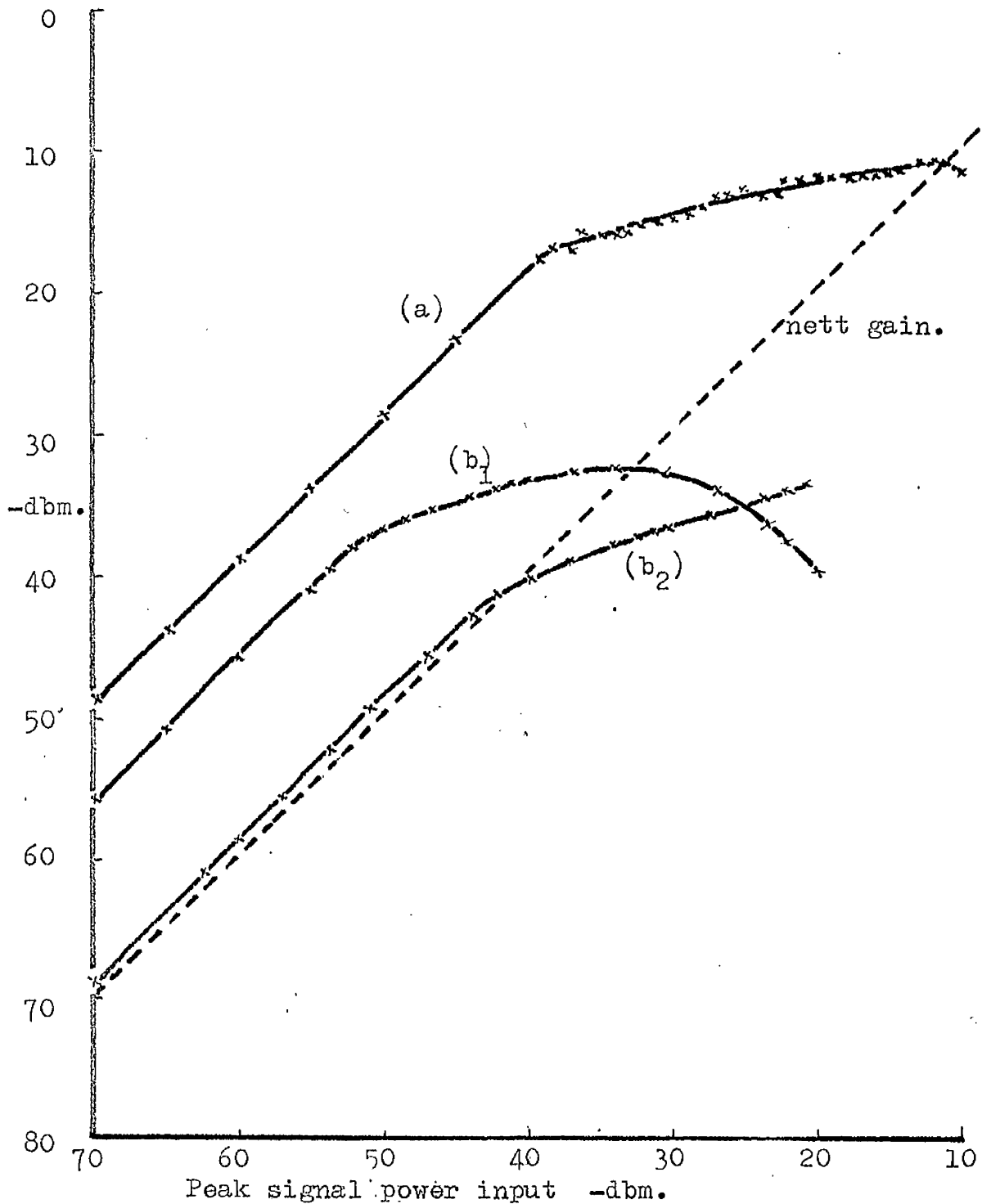


Figure 3.3.15 Plot of signal power output against signal power input, amplification of magnetoelastic waves.

(a) Conditions as in fig. 3.3.14 'a', with pump power constant at 28.1 dbm. (b<sub>1</sub>) As in fig. 3.3.14 'b', with pump power constant at 36.6 dbm. (b<sub>2</sub>) As in fig. 3.3.14 'b' with pump power constant at 32.5 dbm.

Parametric excitation of a delayed pulse by application of two time separated pulses of the same frequency, or w.w. parametric amplification of magneto-static modes, figures 3.4.1, and 3.4.2.

Hahn<sup>24</sup> has demonstrated that an ensemble of oscillators, excited by a sequence of micro-wave pulses can radiate echo pulses. Subsequently Hahn "spin" echoes have been observed using magnetic transitions in electron paramagnets, optical transitions in atoms, cyclotron resonances in gaseous plasmas and magneto-static mode resonances in ferri-magnets. In this section we are concerned with the last type. Results have been reported by Comstock and Raymond<sup>8</sup> at S - band and room temperature in a YIG rod and by Kaplan<sup>7</sup> at x-band and liquid helium temperatures in YIG discs and spheres.

Using the experimental arrangement shown in 1.1.4 a small amplitude 2.4KMc/s signal pulse was applied to  $t=0$ , followed by a larger amplitude 2.4KMc/s pump pulse at  $t=t_p$ , a pulse was observed at  $2t_p$  and amplitude dependent both on the amplitude of the 1st and 2nd pulses. The delayed pulse was observed in the field range 1072 - 1045 oe. A small magneto-static burst was observed at

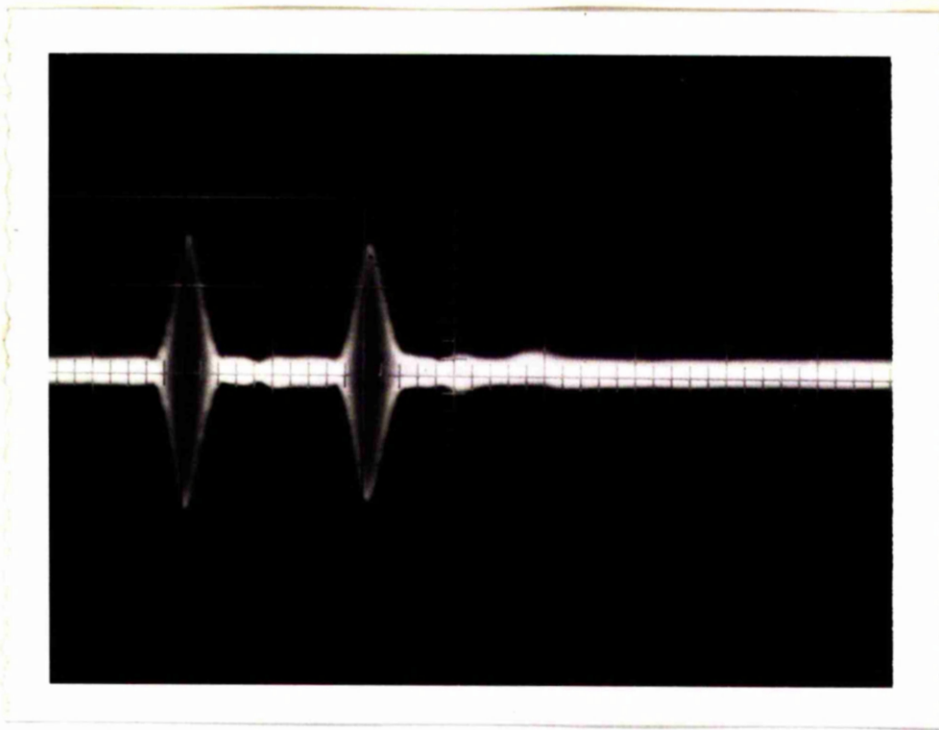


Figure 3.4.1. 1 volt/cm.  $1 \mu\text{sec/cm}$ . Shows time of application of signal and pump pulses for the  $\omega, \omega$ , excitation of a magneto static echo. 2.4 KMc/s, pulse widths  $0.2 \mu\text{sec}$ .

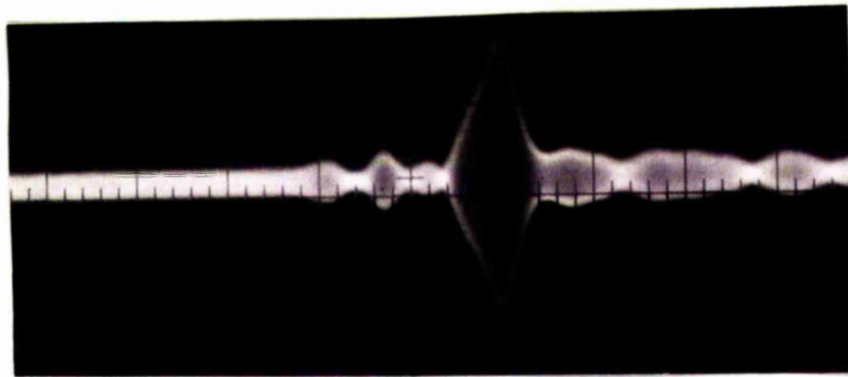


Figure 3.4.2. 1 volt/cm.  $1 \mu\text{sec/cm}$ . Shows  $\omega, \omega$ , magneto-static mode echo excited by the pulses in fig.3.4.1.

1072 oe and the main burst at 1045 oe. The amplitude of the delayed pulse varied considerably with magnetic field, and was a maximum at 1063 oe where the measurements were performed. This was found to be a one port process, since there is a point in the rod where the spin wave length is zero, but in disagreement with Comstock who had observed this as a two port phenomenon.

It was found for example that a delayed echo exists when both first and second pulses had the same amplitude of one milli-watt, and that a delayed pulse could be observed when the large amplitude pulse was applied first followed by a very much smaller second pulse. These suggest a relaxation phenomena of the Hahn spin type, a standing wave being set up bounded by the end face and the turning point.

As the length of the first pulse was increased from  $0.2 \mu$  secs., the delayed pulse amplitude remained relatively constant and its width the same as that of the first pulse. If the second pulse length was increased from  $0.2 \mu$  secs., the delayed pulse amplitude decreased. This is in agreement with the theory of Kaplan, that the pulses must have a large Fourier spectra to excite a plurality of magneto-static modes.

The experimental results are shown in figure 3.4.3. - 3.4.5. Figure 3.4.3. shows a plot of amplitude of delayed pulse against amplitude of first pulse, the amplitude of the second pulse being constant. This curve is reasonably linear but must deviate from this when the first pulse becomes of the same amplitude as the second pulse. Figure 3.4.4. shows a plot of delayed pulse amplitude against the amplitude of the second pulse. The initial slope of this curve is in agreement with the theory of Kaplan, that the amplitude of the echo pulse depends on the radio-frequency magnetic fields of the pulses as  $h_1, h_2^2$ .

Figure 3.4.5. shows the variation of delayed pulse amplitude with time between first and second pulses. The time constant of the decay with delay is  $0.2 \mu$  seconds. The line width is a measure of the relaxation time in a ferrite. The relation between decay time constant and line width being given by  $\Delta H = \frac{2}{\gamma T}^{25}$  where  $\Delta H$  is the line width,  $\gamma$  is the gyro-magnetic ratio and  $T$  is the decay time constant. Substituting values of  $0.2 \mu$  seconds for  $T$ . Then  $\Delta H = 0.56$  oe which is reasonable for a uniform mode line width at  $2.4 \text{KMc/s}$ .

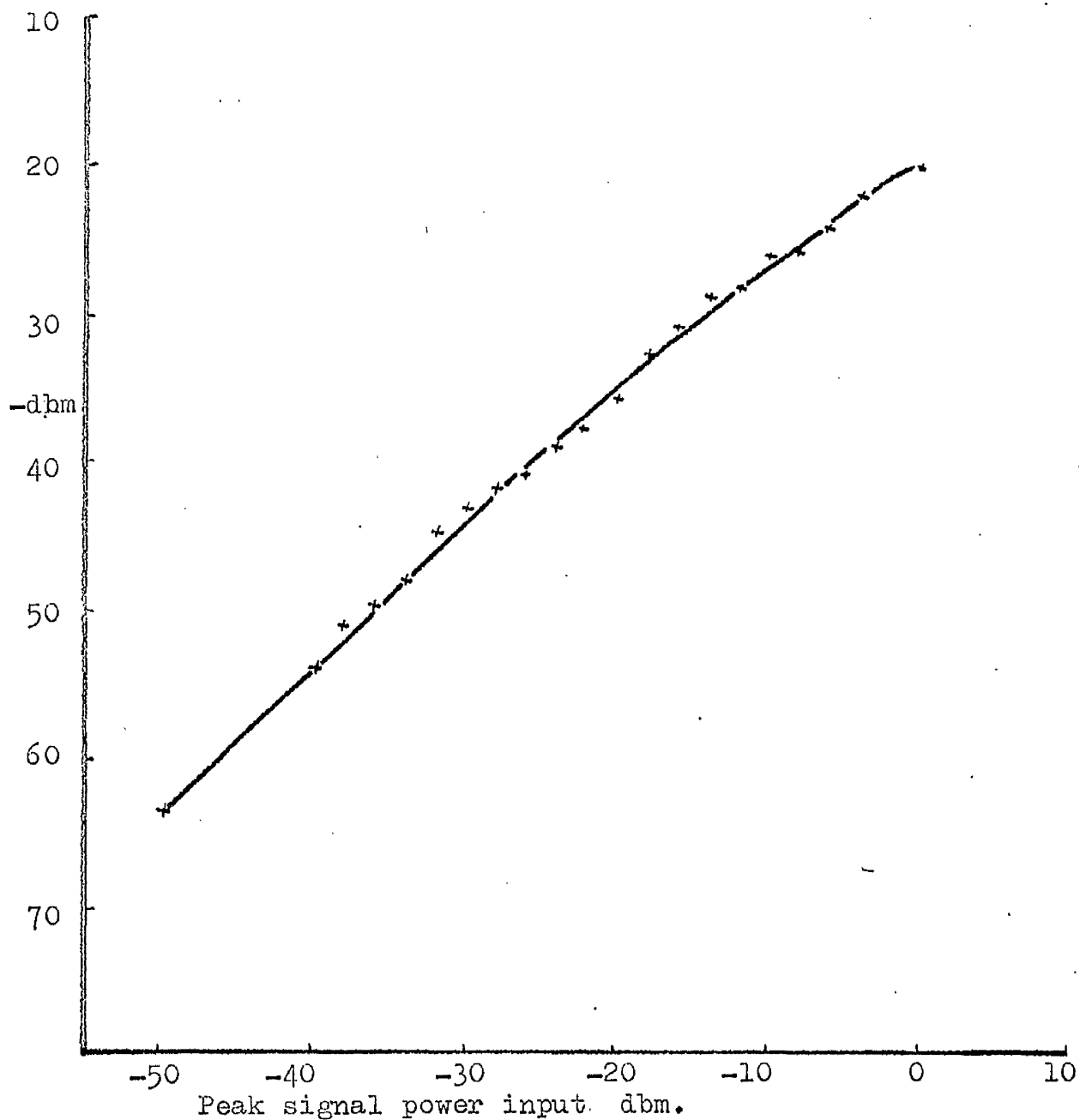


Figure 3.4.3. Plot of amplitude of  $\omega.\omega$ . excited pulse against the amplitude of the first pulse, the amplitude of the second pulse being constant at 21.5 dbm. Pulse widths  $0.2\mu\text{sec}$ . frequency 2.4 KMc/s.

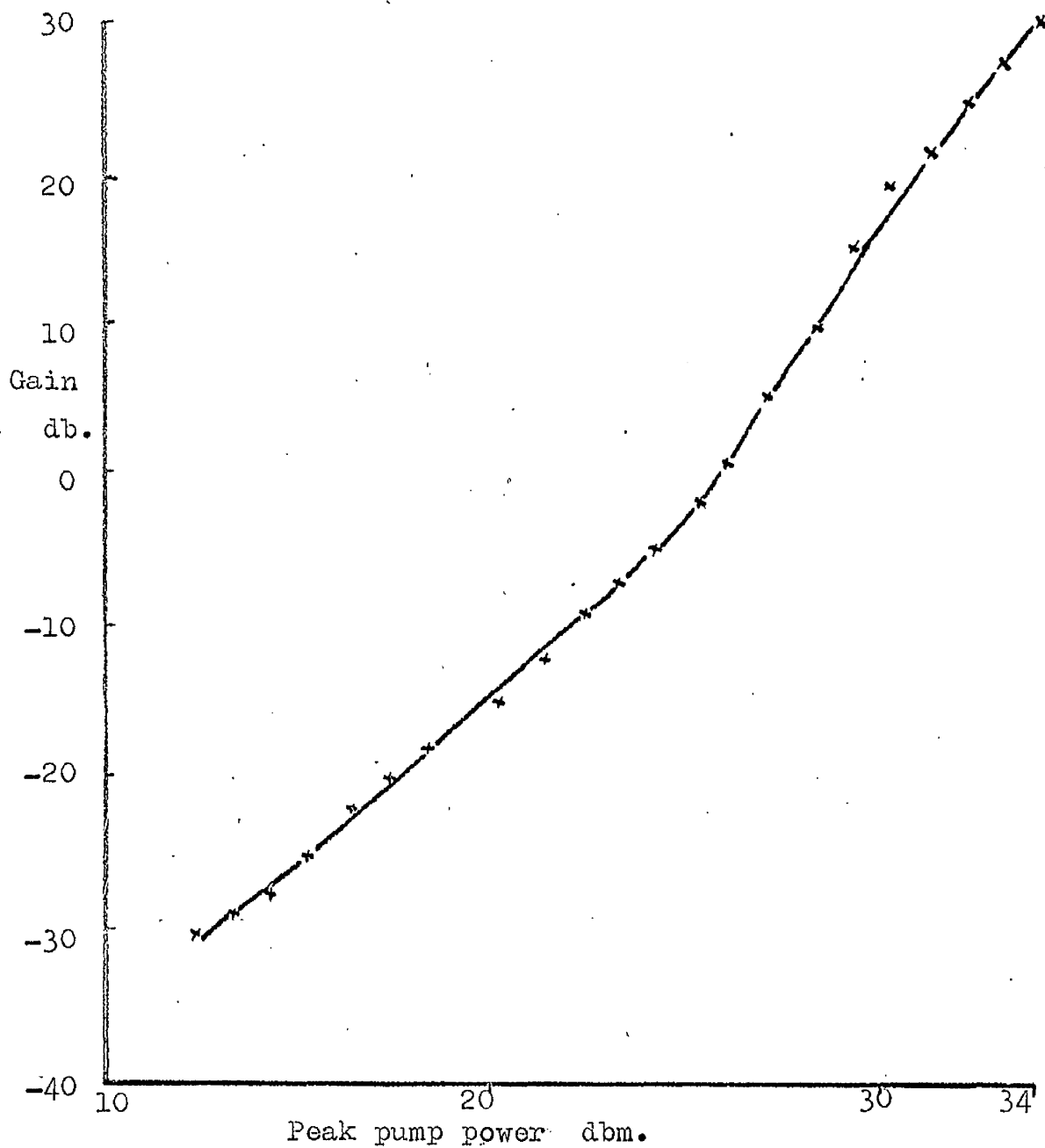


Figure 3.4.4. Plot of gain  $w.w.$  delayed pulse with respect to the first input pulse, against the amplitude of the second input pulse. The amplitude of the first pulse being constant at  $-48.8$  dbm. Pulse widths  $0.2\mu\text{sec}$ . frequency  $2.4$  KMc/s.

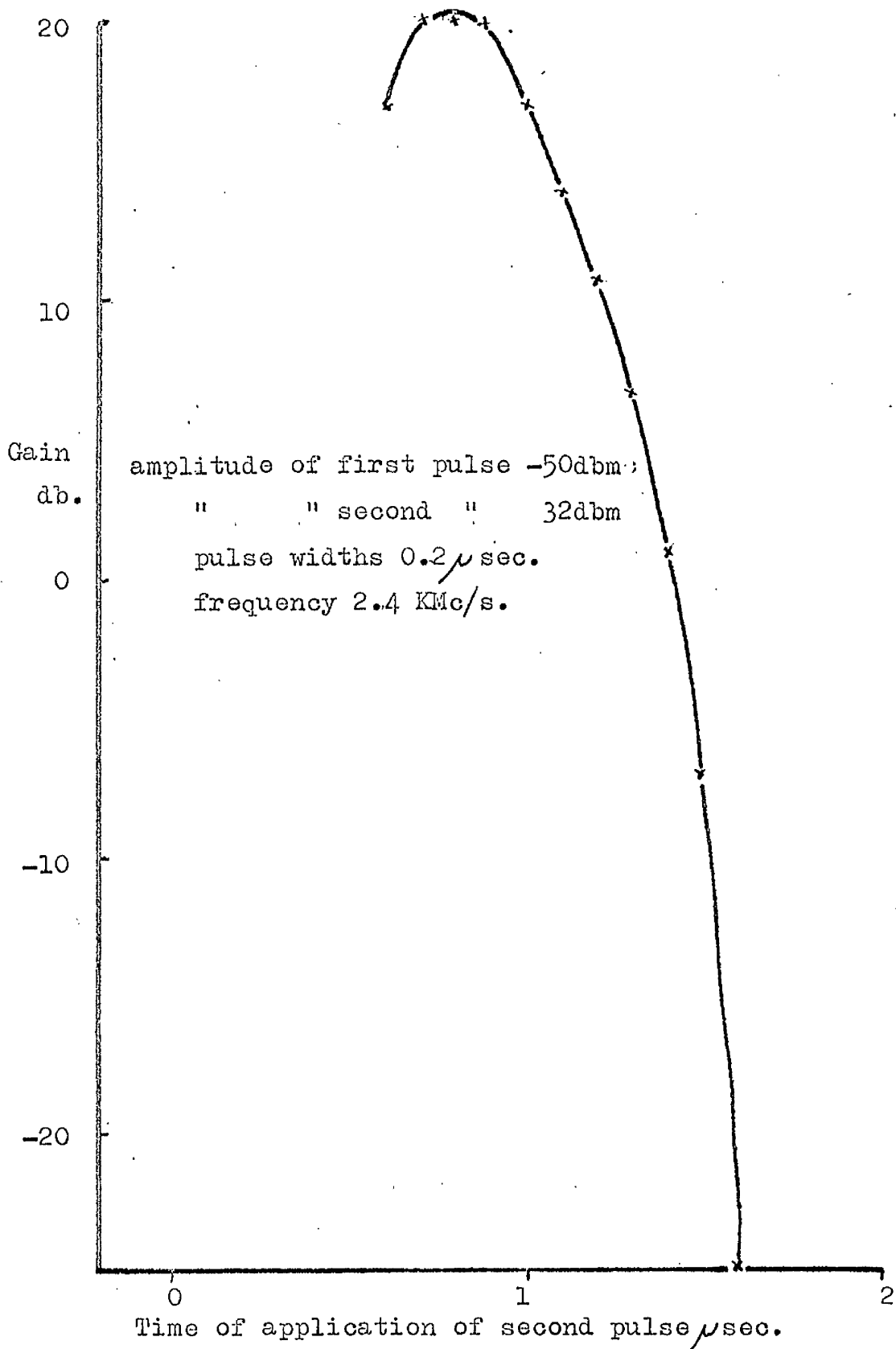


Figure. 3.4.5. Plot of amplitude of delayed pulse with respect to the first signal pulse (gain), against the time of application of the second signal pulse.

The following theory of  $\omega_c$  magneto-static mode echo has been presented by Comstock and Raymond:-

The analysis is based on a model presented by Herrmann and Whitmer.<sup>26</sup>

The spectrum of magneto-static modes has been analysed for general ellipsoids, and in detail for spheres,<sup>27</sup> cylinders<sup>28,29</sup> and disks.<sup>30</sup> The resonant frequencies and spatial distributions of the magnetization and rf magnetic fields for the modes are evaluated by imposing the quasi-static condition on the magnetic field.

$$\underline{H} = \nabla \psi$$

where  $\psi$  is a potential function, and requiring the tangential  $\underline{H}$  and normal  $\underline{B}$  to be continuous at the sample air interfaces. The following analysis of the magneto-static mode echo arising from the nonlinearities in magneto-static modes is sufficiently general to cover all geometries.

The equation of motion for the normalized magnetization in any elliptical precession mode with major axis  $d$  and minor axis  $c$  can be expressed as<sup>31,32</sup>

$$m_i(\vec{r}, t) = i[A_i m_i(\vec{r}, t) + C_i e^{2i\phi} i_{m_i}^*(\vec{r}, t) - \gamma m_i h e^{i\omega_c t} c^t]. \dots (7)$$

where

$$m_i = m_{xi} + im_{yi}$$

$$A_i = \frac{\gamma H}{\omega} \left( \frac{d}{c} + \frac{c}{d} \right)$$

$$C_i = \frac{\gamma H}{2} \left( \frac{d}{c} - \frac{c}{d} \right)$$

and  $\phi_i$  is the angle the major axis of the ellipse makes with respect to the chosen x axis, H is the internal magnetic field and h is the positively rotating rf magnetic field. The linear part of equation (7) can be brought into diagonal form by the Holstein Primakoff transformation defined by

$$b_i(\vec{r}, t) = \lambda_i m_i(\vec{r}, t) + \mu_i m_i(\vec{r}, t).$$

where

$$\lambda_i = \cosh \psi_i / 2$$

$$\cosh \psi_i = A_i / \omega_H$$

$$\mu_i = (\sinh \psi_i / 2) e^{2i\phi_i}$$

$$\sinh \psi_i = C_i / \omega_H$$

$$\omega_i^2 = A_i^2 - C_i^2$$

With no driving field ( $h = 0$ ) the transformed equations of motion are diagonal,

$$b_i(\vec{r}, t) = i \omega_i b_i(\vec{r}, t),$$

where  $\omega_i$  is the resonant frequency of the ith mode.

With a driving field ( $h \neq 0$ ) the transformation yields

$$\dot{b}_i(r, t) = i [\omega_i b_i - \gamma M_z h_{oi} e^{i\omega t} c^t] \dots \dots \dots (8)$$

where

$$h_{oi} = \frac{1}{V} \int_V d^3\vec{r} \lambda_i f_i(\vec{r}) h(\vec{r}),$$

where the normal mode distributions are given by

$$b_i(\vec{r}, t) = a_i(t) f_i(\vec{r}),$$

with the normalization,

$$\frac{1}{V} \int_V d^3\vec{r} f_i(\vec{r}) f_i^*(\vec{r}) = 1.$$

and  $V$  is the sample volume.

The term  $\gamma m_z h_{oi}$  acting on each normal mode is influenced by the total  $z$  component of magnetization, i.e., by the sum over all  $m_{zi}$ . As an approximation we replace  $m_z$  by its spatial average, which can be shown to be,<sup>27</sup>

$$\bar{m}_z = \sum_i \bar{m}_{zi} = 1 - \frac{1}{2} \sum_i \frac{\bar{A}_i}{\omega_i} a_i a_i^* \dots \dots \dots (9)$$

where

$$\bar{A}_i = \frac{\omega_i}{V} \int_V d^3\vec{r} (\lambda_i^2 + |\mu_i|^2) |f_i|^2.$$

the above approximation will be more valid for the lower order magneto-static modes which do not have a large spatial variation in  $m_z$ . After equation (9) is substituted into the equation of motion, equation (8) and using the orthogonality of the  $f_i$ , the results is

$$\dot{a}_i = i\omega_i a_i - \gamma \left( 1 - \frac{1}{2} \sum_m \frac{\bar{A}_m}{\omega_m} a_m a_m^* \right) h_{ti} e^{i\omega_c t}, \quad (10)$$

where

$$h_{ti} = \frac{1}{V} \int_V d^3r f_i \cdot h_{oi}$$

It is now assumed that the magneto-static mode spectrum is centered about a frequency  $\omega_c$

$$\omega_i = \omega_c + \Delta\omega_i,$$

where  $\Delta\omega_i \ll \omega_i$ . Also, the applied microwave pulses with amplitudes  $h$  are assumed to have duration  $t_p$  which are much less than  $\frac{1}{\Delta\omega}$ . During the time of a pulse the modes are all excited to resonance and the mode amplitudes are assumed to be given by the approximation of slowly varying coefficients,<sup>26</sup>

$$a_i = B_i e^{i\omega_c t} + B_i^* e^{-i\omega_c t}$$

the above solution when combined with equation (10)

yields

$$\dot{B}_i = -i\gamma \left( 1 - \frac{1}{2} \sum_m \frac{\bar{A}_m}{\omega_m} B_m B_m^* \right) h_{ti} e^{i\omega_c t}$$

The mode of amplitudes at the end of a pulse can be found by expanding  $B_i$  in terms of  $h_{ti} t_p$  resulting in

$$B_i(t_0 + t_p) = B_i(t_0) - i\gamma \left[ 1 - \frac{1}{2} \sum_m \frac{\bar{A}_m}{\omega_m} B_m(t_0) B_m^*(t_0) \right] h_{ti} t_p.$$

The initial mode amplitude distribution following the first pulse is taken as

$$a(0) = \sum_i a_i(0) = M_i B_{i0} e^{i\omega_i t} + B_{i0}^* e^{-\omega_i t}$$

and the mode amplitudes following the second pulse are then given by

$$B_i(\tau + t_{p2}) = B_{i0} e^{i\Delta\omega_i \tau} - i\gamma \left[ 1 - \frac{1}{2} \sum_m \frac{\bar{A}_m}{\omega_m} B_{m0} B_{m0}^* \right] h_{ti2} t_{p2}$$

Parametric excitation of magneto-static mode echo by  
Subsidiary Absorption.

It has been predicted by Hermann and Whitmer<sup>26</sup> and confirmed by Comstock,<sup>8</sup> that a Hahn - type echo can be observed when the frequency of the second pulse is twice the frequency of the first, which is a result of parametric mixing between excitation at  $\omega$  and  $2\omega$  in the non-linear oscillators. It has been shown by Comstock that the magneto-static mode echo is the result of selective parametric excitation of certain modes by subsidiary absorption. We distinguish between the parametric amplification of magneto-static travelling waves, and the parametric amplification of the magneto-static delayed echo in this case, by, in the first case the fields used are above the magneto-static burst so that a turning point exists in the rod, hence spin waves are cut off in the middle region of the rod, therefore this is a one port phenomena. In the latter case the field is such that no turning point exists in the rod, so that this is a two port effect. Figure 3.5.1.

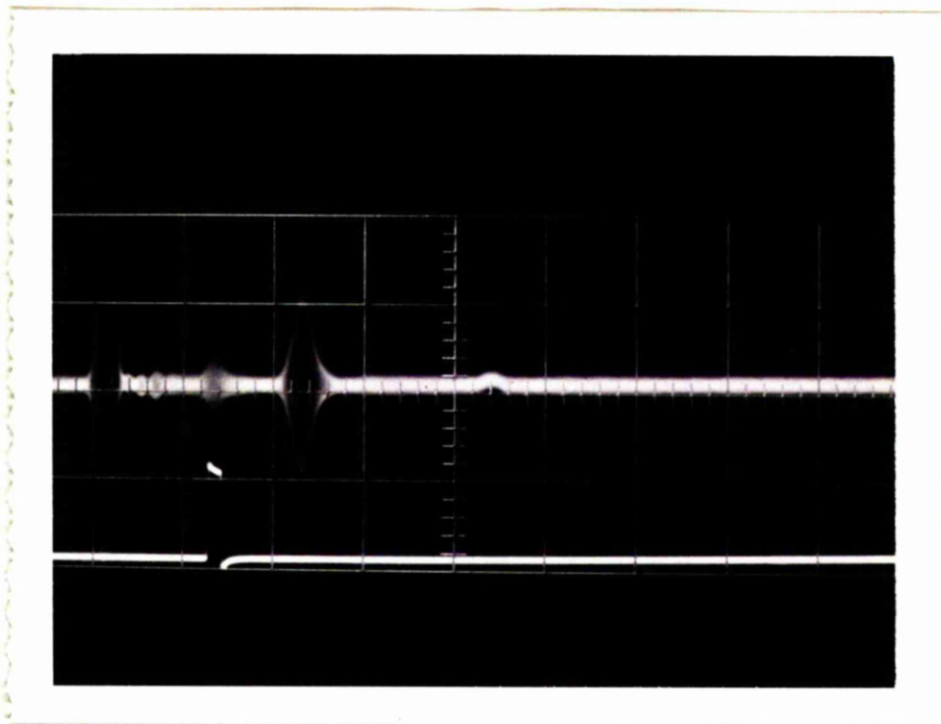


Figure 3.5.1. Excitation of magnetostatic delayed echo by Subsidiary Absorption. Upper trace , input and delayed pulses. Lower trace shows the time of application of the pump pulse. Signal frequency 1.2 KMc/s. pulse width  $0.2\mu\text{sec}$ . Pump frequency 2.4 KMc/s. pulse width  $0.2\mu\text{sec}$ . Scales:- 1 volt/cm.  $1\mu\text{sec/cm}$ .

In these experiments the delayed pulse is observed in the field range 470 oe to 360 oe. The signal frequency used was 1.2KMc/s, pulse width 0.2  $\mu$  seconds and a pump frequency of 2.4KMc/s, pulse width 0.2  $\mu$  seconds. The isolation between signal input and put-put line in the two port case was 36db. The delayed echo was always observed with a delay, with respect to the signal pulse of twice the time of application of the pump pulse. It should be noted that, due to the low signal frequency used, the ends of the rod are not magnetically saturated. The delayed pulse was observed with the same amplitude and delay, both one port and two port which suggests that this process is due to a standing wave mode interaction and occurs throughout the whole of the rod. The amplitude of the delayed pulse varied greatly with field change due, probably to a variation of the density of modes available with change in field. At 2.4KMc/s the subsidiary absorption with the lowest threshold is coincident with the main absorption,<sup>33</sup> however subsidiary absorption is possible though not so efficiently at the field used in this experiment.

Figure 3.5.2. Shows a plot of attenuation of the delayed pulse against peak pump power. Note that the attenuation is high, 60-100db., due to the low efficiency of the subsidiary absorption mechanism in this experiment. Comstock reported a notch in the trailing edge of the pump pulse. No such observation was made in this case, even when the pump pulse width was increased to 1  $\mu$  second, due to a low value of subsidiary absorption.

Figure 3.5.3. Shows a plot of signal power against delayed pulse power. Note that  $P_{out}(db) = -59.5 + \frac{4}{5} P_{in} db$ . This is unusual and suggests that although saturation is not apparent there are some active second order nonlinearities in the process. Figure 3.5.4. Shows a plot of attenuation of the delayed pulse against time of application of the pump pulse.

The following theory has been presented by Comstock.<sup>8</sup> For the subsidiary absorption, the modes are not excited directly by the driving field of the second pulse, but parametrically, i.e., by a decrease in their damping constants. In order to understand the way in which the parametrically excited modes can produce an echo, we use

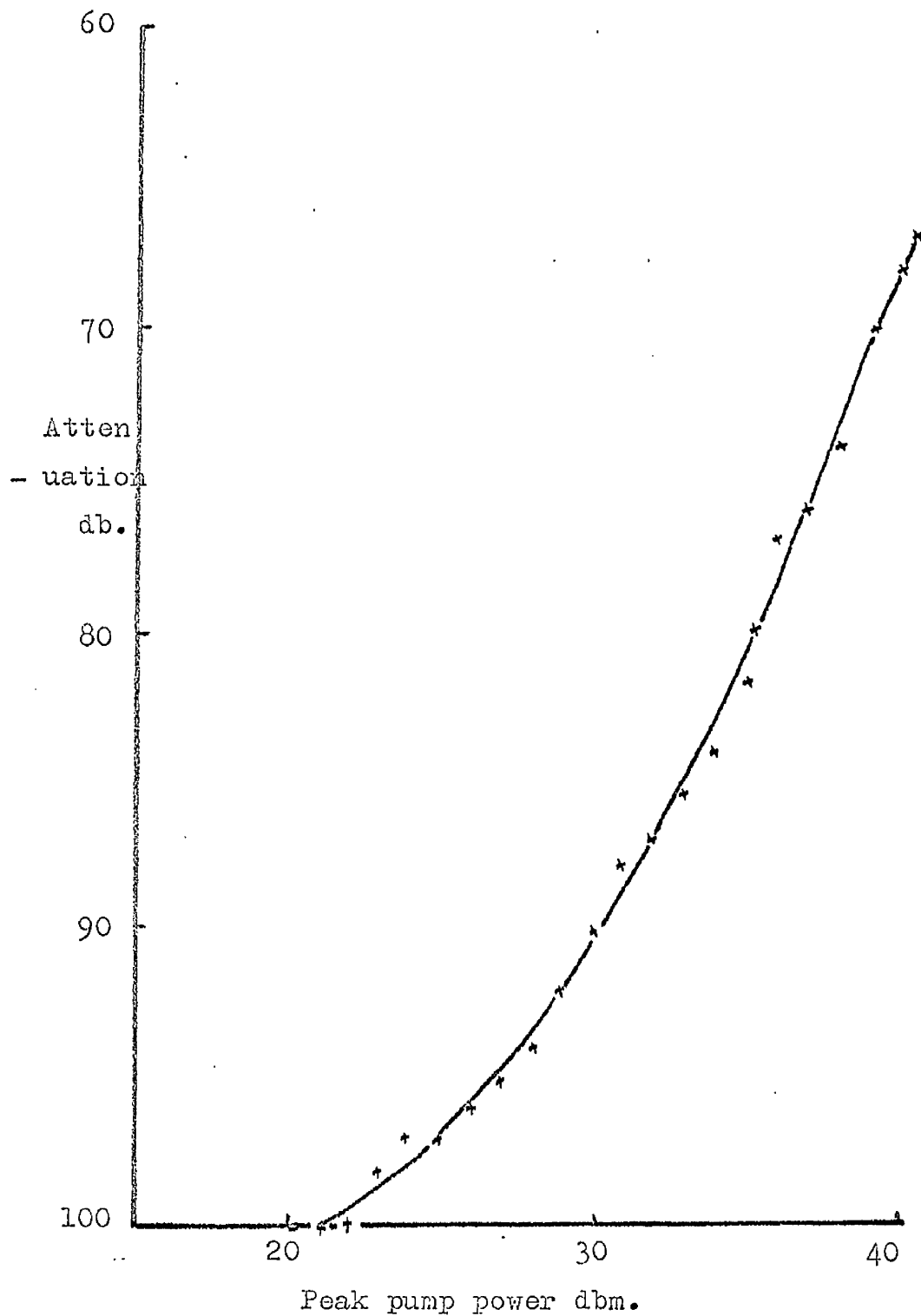


Figure 3.5.2. Plot of attenuation of delayed pulse due to Subsidiary Absorbtion, against peak pump power. Signal power constant at 26.5 dbm. Signal frequency 1.2 KMc/s, pulse width  $0.2\mu$ sec.. Pump frequency 2.4 KMc/s, pulse width  $0.2\mu$  sec Applied magnetic field 380 oe.

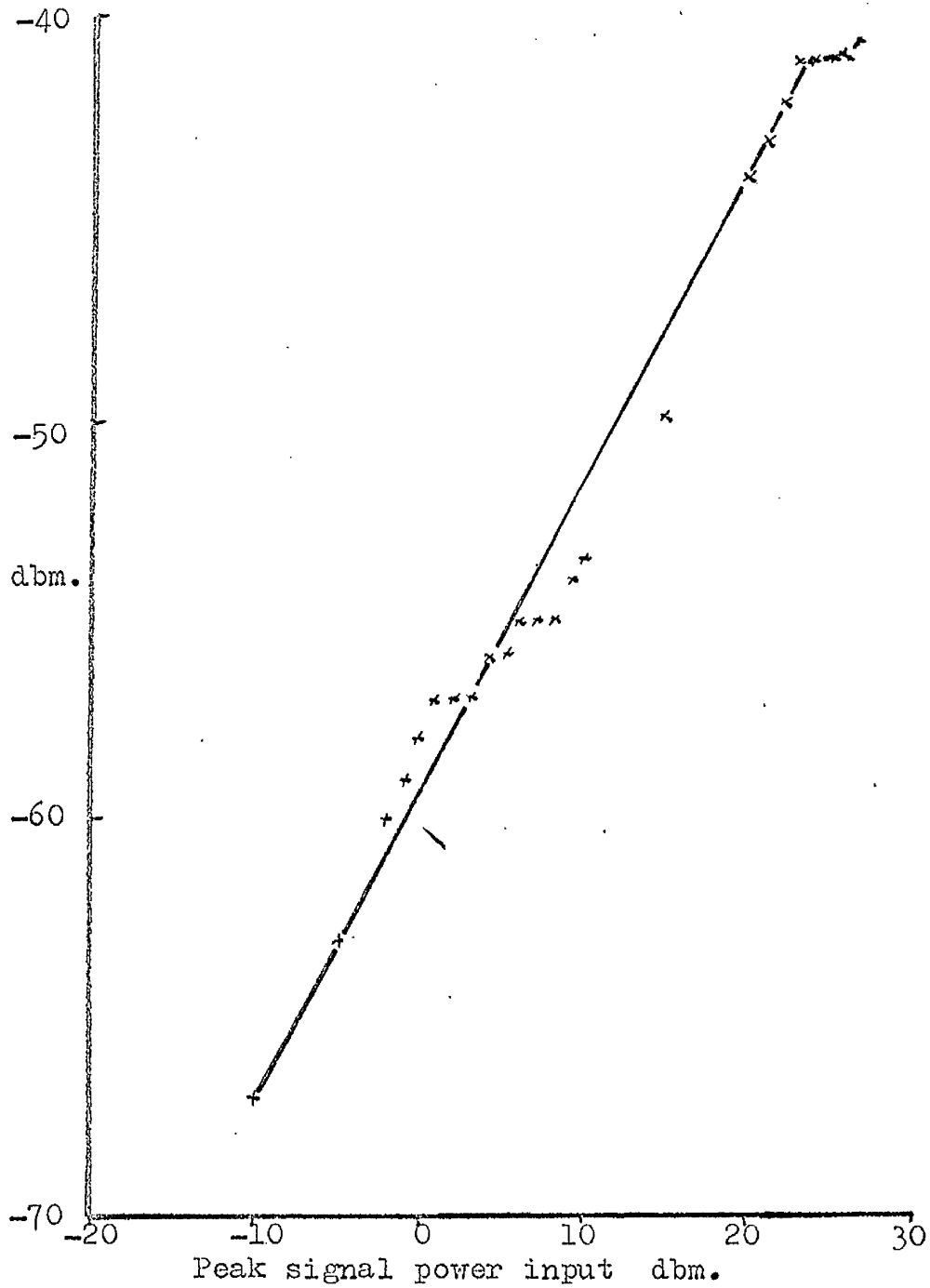


Figure 3.5.3. Plot of signal power output for delayed pulse due to subsidiary absorption, against signal power input. Pump power constant at 40.4 dbm.

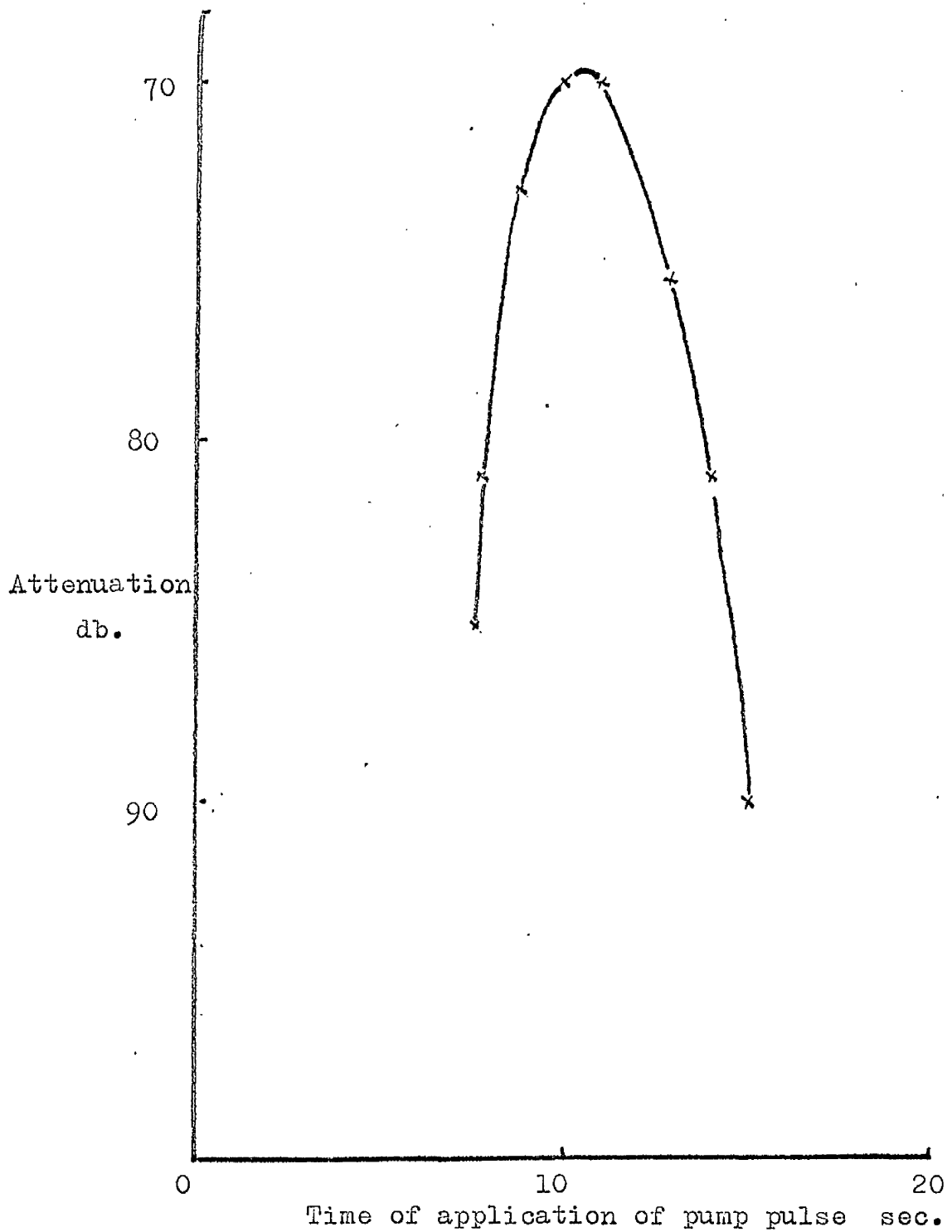


Figure 3.5.4. Plot of attenuation of delayed pulse against time of application of pump pulse . Peak pump power 40.4dbm Signal input power 10dbm. Signal and pump pulse widths 0.2 $\mu$ sec.

the model for the  $\omega$ .  $\omega$ . echo discussed previously by Kaplan.<sup>7</sup> In this model the time dependent part of the mode eigen function is represented by a phasor rotating at the mode resonant frequency. In a frame rotating at the average resonant frequency ( $\omega_a$ ). the phasors representing the 'fast' modes, i.e., those with resonant frequency higher than average, slip ahead of the stationary average mode phasor - while the 'slow' mode phasors slip behind. Between pulses one and two the phasors distribute themselves inside a circular boundary. The subsidiary absorption selects for amplification from the entire manifold of magneto-static modes only those satisfying the necessary phase requirements for degenerate parametric excitation. The phase requirement can be illustrated in the case of plane waves (amplitude  $b_k$ ) by Suhl's<sup>22</sup> theory of the subsidiary absorption in ellipoids, in which the amplitude of a plane wave is given by

$$-i b_k = \rho_k b_0 b_{-k}^* \exp[i(\omega - 2\omega_k)t].$$

where  $b_0$  is the amplitude of the uniform mode at angular frequency  $\omega$  and  $\rho_k$  depends on the angle of propagation to the d.c. field, and static magnetisation. A trial solution to the above equation is given by.

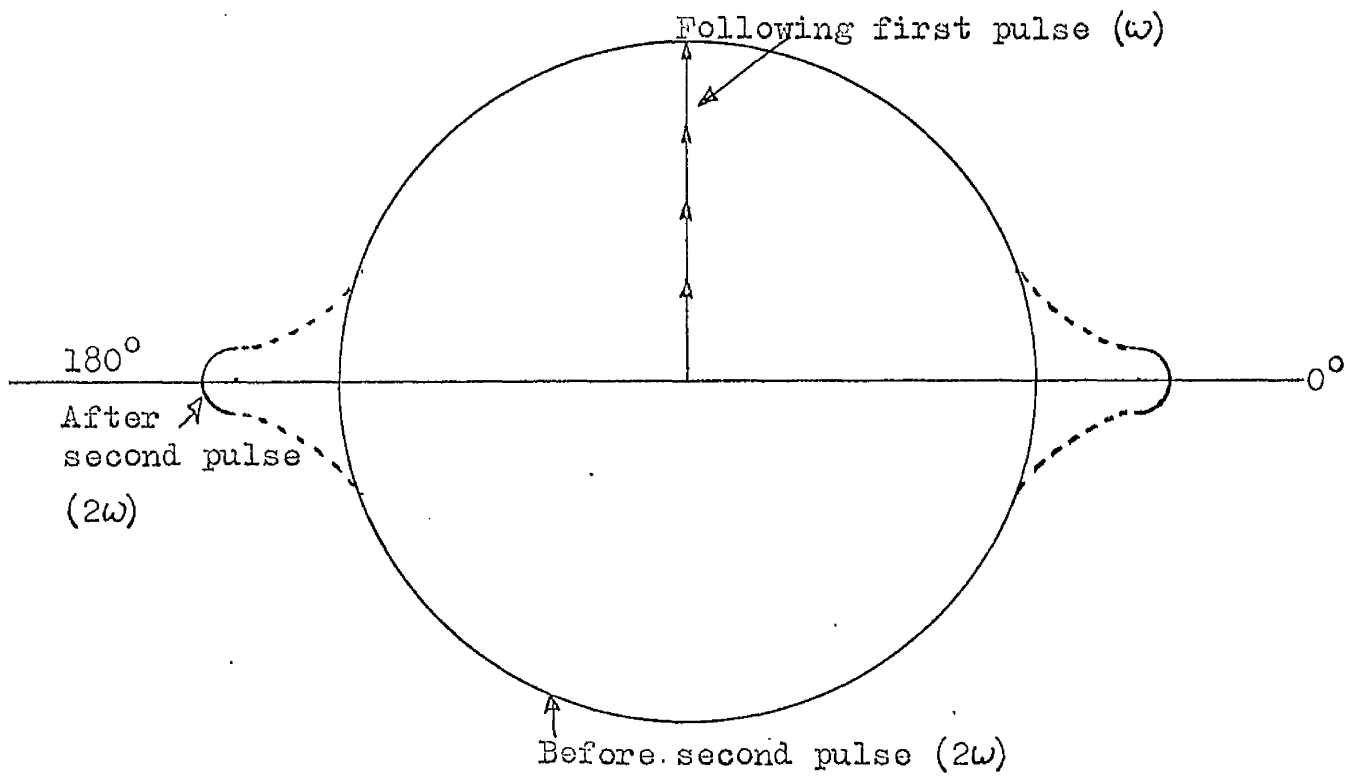


Figure 3.5.5. Diagram showing phasor boundary. Dashed shows the effect of the subsidiary absorption after the time of the second pulse.

$$b_k = \bar{b}_k \exp i[(\omega - 2\omega_k)t + \phi_k].$$

When the trial solution is substituted in the differential equation it is found that the only modes excited are those with phase angles  $\phi_k$  equal to  $0^\circ$  or  $180^\circ$ . Similar phase requirements can be shown also to exist for  $k = 0$  magnetic-static modes. The effect of the subsidiary absorption after the time of the second pulse is to distort the circular boundary discussed above into a shape with protuberances near  $0^\circ$  and  $180^\circ$  figure 3.5.5. A detailed calculation of the shape of the phasor boundary following the second pulse is difficult because of the varying growth rates of the parametrically excited modes. For narrow enough pulses the manifold of modes are all excited to resonance by the first pulse, so following that pulse all the phasors are along one axis as shown. Following a drift time  $\tau$  after the second pulse, the protuberances coalesce along the  $0^\circ$  axis, producing an echo of the first pulse in the same way as for the elliptical phasor boundary which produces the  $\omega$ .  $\omega$ . echo. The growth constant of the magneto-static modes, i.e.,  $b_k \exp \alpha_k t$ , for the above threshold, is proportional to

$b_{o2}$ , the amplitude of the uniform mode excited by the second pulse. The echo amplitude for  $\alpha_k t_2 \ll 1$  is then proportional to  $b_{k1} b_{o2}$ .

### Conclusions.

It has been shown that, micro-wave energy in a single crystal ferrimagnet, in the form of, cut-off propagating magneto-static modes, elastic, and magneto-elastic waves, and nonpropagating magneto-static modes, can experience a parametric interaction in the presence of a pump pulse of twice the frequency, and that a magneto-static mode echo can be parametrically excited by application of two time separated pulses of the same frequency.

These phenomena are discussed in order of decreasing field.

An elastic regime, in which the d.c. field requires adjustment close to the value for normal elastic echoes. The delay times correspond to those of elastic shear wave propagation. The pump pulse timing must have a special relationship with the signal pulse. This is inherently a one or two port phenomena, net gain not observed.

A magneto-elastic regime, in which a lower d.c. field is used, the delay times and the timing of the pump pulse, relative to the signal pulse, for maximum amplification varies with the d.c. field. The rod must

be oriented at an angle between  $8^\circ$  and  $20^\circ$  from the field direction for maximum amplification although parametrically excited pulses can be observed when the rod axis is parallel to the direction of the external field. Parametric amplification of noise at the signal frequency is observed when a pump at twice the signal frequency is applied with no signal pulse. This seems to take place at the signal turning point in the rod. Net gain was observed. With the internal field profile of a bare rod, magneto-elastic delay lines are intrinsically one port.

A magneto-static propagating mode, where the d.c. field has been reduced to a point where the magneto-elastic waves have very long delay, but two port transmission of magneto-static waves through the rod has not yet appeared. Delay of the parametrically excited pulse is dependent only on the timing of the pump pulse, net gain was not observed, this phenomena extends into the magneto-elastic region.

A magneto-static one port mode echo, parametrically excited by application of two time separated pulses of the same frequency, occurs in the same field range as

above, this is one port phenomena, net gain is available. This process is more efficient than magneto-elastic amplification but not so suitable for further development, due to the non-degeneracy of the signal and pump.

A non-propagating magneto-static range where the parametric interaction is thought to be due to subsidiary absorption of the pump frequency. This is a two port phenomena.

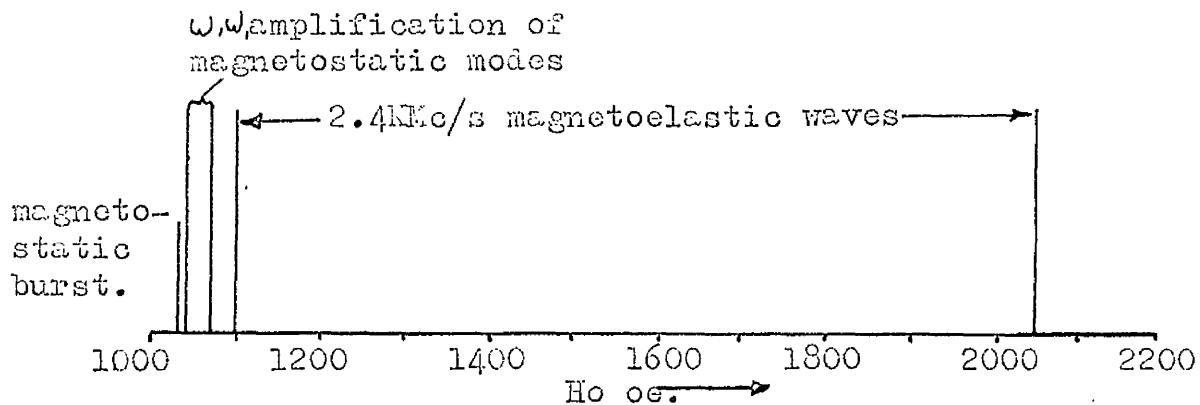
The experimental internal field determination, demonstrates that the experimental method is capable of producing results which give very good agreement with theory providing the rod length is large compared with its other dimensions.

The parametric amplification of noise which seems to occur at the signal frequency turning point in the rod, suggests a different mechanism, than that for parametric amplification of magneto-elastic waves which has a minimum threshold at the cross over point.

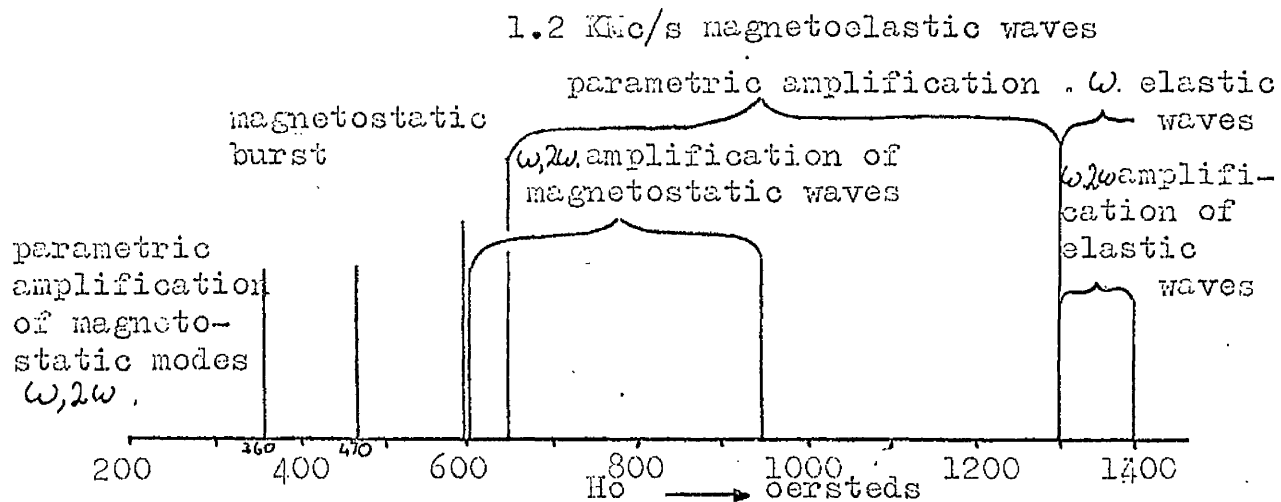
There is no generally accepted mechanism for the parametric amplification of magnet-elastic waves. The main difficulty being in determining the lowest threshold

of these mechanisms outlined by Auld, for different fields, frequencies, and angles of the rod with respect to the field direction. An other difficulty is that the magneto-elastic path, in the rod when oriented at an angle to the field, is not exactly known.

Although this thesis demonstrates all the parametric process, which occur in bare single crystal YIG rods, to date. Figure 4.1.1. There still remains a formidable amount of work, both experimental and theoretical before the phenomena described are fully understood.



Signal frequency 2.4 KMc/s. rod axially magnetised



Signal frequency 1.2 KMc/s. Pump frequency 2.4 KMc/s.

Rod axially magnetised.

Figure 4.1.1. Summary of delayed echoes observed in an axially magnetised YIG rod.

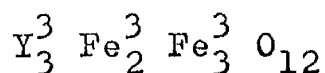
## Appendix:-

A Summary of the Properties of Yttrium Iron Garnet.<sup>34</sup>

The Crystal Structure of Garnets.

The unit cell contains eight formula units of  $M_3Fe_5O_{12}$ , where M is a Transition Metal for example Yttrium. The cubic unit cell length is approximately  $12.5\text{\AA}$ . In the array of 96 oxygen ions, three types of interstices are occupied by metal cations. They are, the smallest, tetrahedral or 'a' site, surrounded by four oxygen ions located at the corners of a tetrahedron. These are sixteen of these sites. The next in size are the octahedral or 'd' site, of which there are 24, each surrounded by six oxygen ions located at the corners of an octahedron. The largest of the interstices, the dodecahedral or 'c' sites, have eight oxygen ions located at corners of a polyhedron with 12 faces and 18 edges. The 24 sites of this type are usually occupied by Yttrium or rare-earth ions.

In the unit cell the 40 ferric ions fill the 'a' and 'd' sites and the 24  $Y^3$  ions enter into the 'c' sites.



c   a   d                    sites

### Magnetic Properties:-

There is a very strong negative interaction between the  $\text{Fe}^3$  ions on the 'a' and 'd' sites which induces all the ions in each sublattice to enter into parallel alignment and the 'a' and 'd' sublattices into anti-parallel alignment with each other. Since, per formula unit ( $\text{Y}_3\text{Fe}_5\text{O}_{12}$ ) there are two octahedral and three tetrahedral ferric ions, there will be a net magnetic moment equivalent to one ferric ion ( $5\mu_B$ ) from these two sublattices.

Large single crystals of YIG with few structural defects can be grown from the melt. Single crystal YIG has a low line-width,  $\Delta H$  of less than 0.5 oe. at L-band and room temperatures. The saturation magnetisation,  $4\pi M_s$  of YIG at room temperatures is 1760 oe. YIG has low magnetic anisotropy,  $\frac{K_1}{M_s} = 41$  oe.,  $\frac{K_2}{M_s} = 0$ , and a phenomenological exchange constant of  $D = 5 \times 10^{-9}$  oe. cms.<sup>2</sup>. The Curie temperature of YIG is 550°K.

In a garnet, magneto-elastic effects arise from the coupling between magnetic spins and the elastic vibrations of the host lattice in which the spins are

embedded. The magneto-elastic coupling constant  $b_2$  for YIG is  $= 6.2 \times 10^6$  erg/cm.<sup>3</sup>. The acoustic loss can be less than 1 db/sec. at L-band and room temperatures. The acoustic shear wave velocity is  $3.85 \times 10^5$  cm./second.

## References:-

1. H. Matthews, Physical Review Letters, Volume 12, Number 12, 23rd March 1964.
2. R.W. Damon and H. van de Vaart, Applied Physics Letters, Volume 6, Number 8, 15th April 1965.
3. R.W. Damon and H. van de Vaart, Applied Physics Letters, Volume 6, Number 10, 15th May 1965.
4. R.W. Damon, H. van de Vaart and M.I. Grace, Electronics Letters, Volume 1, Number 5, July 1965.
5. R.A. Sparks and E.L. Higgins, Applied Physics Letters, Volume 7, Number 2, 15th July 1965.
6. L.F. Donaghey and F.A. Olson, Electronics Letters, Volume 1, Number 6, August 1965.
7. D.E. Kaplan, Physical Review Letters, Volume 14, Number 8, 22nd February 1965.
8. R.L. Comstock and J.J. Raymond, to be published in Journal of Applied Physics.
9. W. Strauss, Journal of Applied Physics, Volume 35, page 1022, 1964.
10. E. Schlomann, Journal of Applied Physics, Volume 35, Number 1, January 1964.
11. B.A. Auld and W. Strauss, Journal of Applied Physics, Volume 37,

12. R.I. Joseph and E. Schlomann, Journal of Applied Physics, Volume 36, Number 5, May 1965.
13. J.F. Dillon, S. Geshwins and V. Jaccarino, Physical Review, Volume 100, page 759, 1957.
14. J.H. Collins and G.G. Neilson, Electronics Letters, Volume 2, Number 4, April 1966.
15. M.R.B. Dunsmore, Electrical Engineering Department, The University of Glasgow, private communication.
16. T. Kochane, E. Schlomann and R.I. Joseph, Journal of Applied Physics, Volume 36, page 1267, 1965.
17. R.C. Addison and B.A. Auld, Paper LI., 12th Annual Conference on Magnetism and Magnetic Materials, Washington, D.C. November 15-18th, 1966.
18. J.H. Collins, Report on visit to United States Laboratories, December 1965, Department of Electrical Engineering, the University of Glasgow,
19. B.A. Auld, Journal of Applied Physics, Volume 36, Number 3, part 1, March 1965.
20. E.K. Kirchner, Paper L4, 12th Annual Conference on Magnetism and Magnetic Materials, Washington D.C. November 15-18th 1966.
21. R.W. Damon and H. van de Vaart, Proc. I.E.E.E., April 1965.

22. H. Suhl, Journal of Phys. Chem. Solids, Volume 1, pp. 209-227, 1957.
23. J.H. Collins, private communication.
24. E.L. Hahn, Physical Review, 80, 588, (1950).
25. Lax and Button, 'Micro-wave Ferrites and Ferri-magnetics' section 4-5. Lincoln Laboratory Publications, McGraw-Hill Book Co. Inc.
26. G.F. Herrmann and R.F. Whitner, Physical Review, 43, 122 (1966).
27. P.C. Fletcher and R.O. Bell, Journal of Applied Physics, Volume 30, page 687, 1959.
28. P.C. Fletcher and C. Kittel, Physical Review, 120, 2004, (1960).
29. R.I. Joseph and E. Schlomann, Raytheon Tech. memo, T-249, Research Division, Raytheon Co., Waltham, Mass., (1960).
30. R.W. Damon and H. van de Vaart, Journal of Applied Physics, Volume 36, page 3453, 1965.
31. E. Schlomann, Tech. Report R-48. Research Division Raytheon Co., Waltham, Mass., (1965).
32. P.L. Richards, Micro-wave Laboratory Report No. 875, Stanford University, Stanford, California (1962).

33. Lax and Button, Micro-wave Ferrites and Ferrimagnetics, section 12-13, Lincoln Laboratory Publication, McGraw-Hill Book Co. Inc.
34. Properties of Ferrimagnetic Material for Micro-wave Application, Bell Telephone Laboratories, Technical Report Number ML-TDR-64-224.